UNIVERSITÉ DE SHERBROOKE
Faculté de génie
Département de génie mécanique

DYNAMIC MODELING AND OPTIMAL CONTROL OF AN EJECTOR BASED REFRIGERATION SYSTEM

MODÉLISATION DYNAMIQUE ET COMMANDE OPTIMALE D'UN
SYSTÈME DE RÉFRIGÉRATION À BASE D'ÉJECTEUR

Thèse de doctorat
Spécialité : Génie Mécanique

ELHAMEH NARIMANI

Sherbrooke (Québec) Canada

November 2019

I dedicate this thesis to my mother and sister, Mahin and Shima

and to the memory of my late father, Reza.

MEMBRES DU JURY

Mikhail SORIN, Prof.
Directeur

Philippe MICHEAU, Prof.
Co-Directeur

Alexandre GIRARD , Prof.
Rapporteur et Évaluateur

Bernard MARCOS, Prof.
Évaluateur

Brice LE LOSTEC, PhD
Évaluateur

ABSTRACT

Recently, the ejector-based refrigeration system (ERS) has been widely used in the cooling industry as an appropriate alternative to the compressor-based cooling systems. However, the advantages of ERS such as the reliable operation and low operation and maintenance costs are overshadowed by its low efficiency and design complexity. In this context, this thesis presents the efforts to develop a control model enabling the ERS to operate in its optimal operational conditions. The extensive experimental studies of ERS revealed that at a fixed condenser inlet condition ($T_{c,i}$), there exists an optimal primary stream mass flow rate (generating pressure) that simultaneously maximizes the compression ratio (Cr) and exergy efficiency (η_{II}) and minimizes the evaporating pressure (P_e). Then, the steady state models of the heat exchangers were developed and used to investigate the influence of the increase in generating pressure on the coefficient of performance (COP) of the system and it showed that increasing the generating pressure reduces the COP, linearly. In order to predict the choking regime of the ejector and explain the reasons of observed physical phenomenon, the 1D model of a fixed geometry ejector installed within an R245fa ERS was developed. The developed model demonstrated that the ejector operates in the subcritical mode when the generating pressure is below the Cr optimum point, while it operates in critical mode at or above the optimum generating pressure. Next, a dynamic model of the ERS was built to evaluate the ERS transient response to an increase in the primary stream mass flow rate. Since the ERS dynamics is mainly dominated by the thermal dynamics of the heat exchangers, the dynamic models of the heat exchangers were developed using the moving boundary approach and connected to the developed models of the ejector and steady state models of the pump and expansion valve to build a single dynamic model of the system. The built dynamic model of an ERS was used to estimate the time response of the system in the absence of accurate experimental data of the system's dynamics. Finally, a control model was designed to drive an ERS towards its optimal operation condition. A self-optimizing,

model-free control strategy known as Extremum seeking control (ESC) was adopted to minimize P_e in a fixed condenser thermal fluid inlet condition. The innovative ESC model named batch phasor ESC (BPESC) was proposed based on estimating the gradient by evaluating the phasor of the output, P_e, in batch time. The simulation results indicated that the designed BPESC model can seek and find the optimum P_e with good performance in terms of predicting the steady state optimal values and the convergence rates.

Keywords: Ejector based refrigeration system, dynamic modeling, control strategy, Extremum seeking control, discrete time, batch phasor extremum seeking control

RÉSUMÉ

Récemment, le système de réfrigération à éjecteur (SRE) a été largement utilisé dans l'industrie du refroidissement en tant que solution de remplacement appropriée aux systèmes de refroidissement à compresseur. Cependant, les avantages du SRE, tels que le fonctionnement fiable et les faibles couts d'exploitation et de maintenance, sont éclipsés par son faible rendement et sa complexité de conception. Dans ce contexte, ce projet de recherche de doctorat a détaillé les efforts déployés pour développer une stratégie de commande permettant au système de fonctionner dans ses conditions opérationnelles optimales. Les études expérimentales approfondies du SRE ont révélé que, dans une condition d'entrée de condensateur constante ($T_{c,i}$), il existe un débit massique optimal du flux primaire (générant une pression) qui maximise simultanément le taux de compression (Cr) et l'efficacité exergétique (η_{II}), et minimise la pression d'évaporation (P_e). Ensuite, les modèles à l'état d'équilibre des échangeurs de chaleur ont été développés et utilisés pour étudier l'influence de l'augmentation de la pression générée sur le coefficient de performance (COP) du système et il en ressort que l'augmentation de la pression génératrice réduit le COP de manière linéaire. Afin de prédire le régime d'étouffement de l'éjecteur et d'expliquer les raisons du phénomène physique observé, le modèle 1D d'un éjecteur à géométrie fixe installé dans un système SRE R245fa a été développé. Le modèle développé a démontré que l'éjecteur fonctionne en mode sous-critique lorsque la pression génératrice est inférieure au point optimal de Cr, alors qu'il fonctionne en mode critique à une pression égale ou supérieure à la pression génératrice optimale. Ensuite, un modèle dynamique du SRE a été développé pour étudier la réponse transitoire du SRE lors d'une augmentation du débit massique du flux primaire. Puisque la dynamique du SRE est principalement dominée par la dynamique thermique des échangeurs de chaleur, les modèles dynamiques des échangeurs de chaleur ont été développés à l'aide de l'approche des limites mobiles et connectés aux modèles développés de l'éjecteur et des modèles à l'état stationnaire de la

pompe et de la vanne un seul modèle dynamique du système. En l'absence de données expérimentales précises sur la dynamique d'un système SRE, le modèle dynamique développé du SRE a été simulé numériquement pour étudier sa réponse temporelle. Enfin, une stratégie de commande extrêmale (ESC) a été élaboré pour régler automatiquement le SRE à ses conditions de fonctionnement optimales, c'est-à-dire pour trouver la vitesse de la pompe qui minimise la pression P_e dans des conditions d'entrée de condenseur fixes. Afin de proposer une ESC implémentable en temps discret sur une installation réelle sujette à un bruit de mesure important et un traitement hors-ligne par trame, une nouvelle commande extrémale basée sur une approche par phaseur avec une procédure de traitement de signal par trame (BPESC) a été développée et simulée avec le modèle numérique. Les résultats de la simulation ont indiqué que le modèle BPESC peut trouver la vitesse optimale de la pompe avec de bonnes performances en termes de précision et de vitesse de convergence.

Mots clés: Système de réfrigération à éjecteur, modélisation dynamique, stratégie de commande, commande extrêmale, temps discret, phaseur, optimisation

Acknowledgments

I would like to offer my sincere gratitude to my supervisor, Prof. Mikhail Sorin and my co-supervisor, Prof. Philippe Micheau, for his great wisdom, expert guidance, extensive encouragement and constructive criticism during my PhD at the University of Sherbrooke.

I am very grateful to all of those who I have had the pleasure to work with during this research project. I would like to thank Dr. Hakim Nesreddine for his assistance with laboratory work, for extended discussions during preparation of journal papers, and for his willingness to help in every possible way.

I would like to thank all my friends in Canada: Yulia, Alireza, Ghofrane, Bahar and Samaneh for their love, laughter, encouragement, and understanding.

TABLE OF CONTENTS

LIST OF TABLES

LIST OF FIGURES

CHAPTER 1 INTRODUCTION

1.1. General Background

Industrial developments and the significant increase in the population and higher living standards have resulted in a growing demand of energy, and consequently the energy shortage and higher prices, as well as the global environmental issues. These issues force researchers to seek the renewable energy alternatives and approaches of utilizing low grade energies.

A remarkable portion of the energy in the residential and industrial sectors are consumed by heating, ventilation, and air conditioning (HVAC) systems and it is predicted that by mid-century countries would use more energy for cooling than heating. Indeed, the mounting demand for thermal comfort will give rise to a rapid increase in cooling system use and, consequently, electricity demand due to air-conditioning in the buildings. Application of the thermal refrigeration systems using low-grade heat would substantially reduce the energy consumption in the cooling sector.

Amongst the available technologies for the thermal refrigeration systems, the heat-driven ejector refrigeration system (ERS) is considered as a promising technology due to its reliable operation and limited maintenance needs. Furthermore, ERS is an interesting alternative to the traditional compressor-based technologies which produces the cooling effect by harvesting the waste heat from industrial processes or using renewable energy, such as solar radiation and geothermal energy. In addition, ERS has some other important advantages, including using no-moving parts in the ejector in comparison with the compressor in conventional refrigeration systems which make them vibration-free, having low initial and operational costs with long lifetime, and providing the possibility of using sustainable refrigerants [1]. According to ASHRAE, 1979 [2] the steam jet refrigerator or ejector driven

refrigeration system (ERS) is first introduced by Le Blanc and Parson in 1901. However, due its low efficiency and severe degradation in performance when operating under non-idealized design conditions, ERS was not able to penetrate the market.

In fact, an ERS is made up of six components: vapor generator, ejector, condenser, evaporator, electronic expansion valve and a liquid pump. In the generator, at a constant pressure, the heat is absorbed from the external source (low grade heat source) to generate a high-pressure vapor, which is sent to ejector. The ejector also known as injector, jet pump, thermo-compressor, allows a high-pressure primary stream to accelerate and induce a low-pressure secondary stream into the primary stream path. The two streams mix through the mixing chamber and then the pressure recovery occurs in the diffuser, which enables the ejector to function as a compressor or a pump. In the condenser, the refrigerant rejects the absorbed heat (in the both evaporator and generator) and energy provided by the pump (usually negligible) to the external medium. The subcooled stream leaving the condenser is divided into two streams (primary and secondary streams). The pressure of the primary stream increases to the generating pressure using the pump and then enters the generator, whilst the secondary flow passes through an expansion valve where its pressure is reduced to the evaporating pressure. Then, it enters the evaporator, evaporates by absorbing the heat from the cooled medium and produces the cooling effect. The superheated stream leaving the evaporator is entrained by ejector [3].

However, as it was previously mentioned the ERS has some drawbacks that hold back the wide applications of such systems in the cooling industry. First, it has a low coefficient of performance (COP) in comparison with the conventional compressor-based refrigeration systems. Second, ERS is more complicated than the conventional refrigerator in terms of availability of more components in the cycle, which can cause more complexity in analyzing its behavior and designing a control model. Furthermore, the performance of ERS is severely sensitive to the instability in the low-grade heat resource [4]. Thus, the comprehensive numerical and experimental studies of ERS are required in order to improve its energy efficiency and define the optimal operation conditions.

There are many studies in the literature investigating the impacts of different factors on the performance of both the conventional and ejector-based refrigeration systems. However, despite the tremendous work in the area of ejectors, there is still a huge gap in the studies adopting the systemic approaches to develop the dynamic and control models for ERSs.

Hence, this PhD research project aligns with this objective to fill the literature gap in this regard. The current document will present the results of an extensive study on the development of a control model for an ERS. First, the optimal operation conditions of an ERS was investigated in terms of performance indicators including COP, Compression ratio (Cr) and the exergy efficiency (η_{II}) using the experimental studies. It was found out that there is an optimum generating pressure in a fixed condenser inlet condition which could simultaneously maximize the Cr and η_{II} and minimize the evaporating pressure (P_e).

The new 1D thermodynamic model of the ejector was developed to explain the reasons of this phenomenon in the ejector. The unique feature of this model was related to the method it used to recognize choking regime inside the ejector. The developed model demonstrated that the ejector operates in either the critical or the sub-critical conditions using the secondary mass flux comparison with its maximum value in the hypothetical throat. Furthermore, the steady state model of the heat exchangers was developed to determine the impact of increasing the generating pressure on the COP and η_{II}.

Then, the dynamic model of the ERS based on the moving boundary approach of heat exchangers was developed and validated with experimental data. The equations of the developed dynamic model of ERS was solved in MATLAB. At the end, a novel scheme of Extremum seeking control strategy (ESC) named batch phasor ESC was proposed to develop a control model for an ERS. The systems' dynamics was included in in the batch phasor ESC using developed dynamic model of the ERS.

1.2. Objectives and Scopes

Regarding the need for improving the efficiency of ERS by designing an optimal control model, the present study aimed mainly at responding the following question:

How to develop a control strategy to optimize the performance of ERS?

To achieve the main objective of this study explained by the research question, the following steps should be followed:

- Performing the experimental analyses of an ERS to identify the optimal operation conditions
- Developing the numerical steady state models of the ejector and heat exchangers within an ERS to predict the optimal operation conditions of ERS
- Developing of a dynamic model of an ERS based on th moving boundary approach of the heat exchangers
- Designing a control model using Extremum Seeking Control strategy (ESC) to optimize the performance of the ERS

1.3. Statement of originality

To the best of authors' knowledge, this study is one of the first studies introducing an optimal control model for an ERS. The first dynamic model of ERS was also developed in this work. Furthermore, the novel Extremum seeking control named as batch phasor Extremum seeking control was proposed in this PhD research project which can be easily applied on the other systems with large and even variable phase lags. The author believes the control and dynamic models presented herein, along with findings of the experimental studies of the ERS, would form a comprehensive guideline for designing the more efficient ERSs.

1.4. Organization of the Dissertation

The present thesis consisted of 7 chapters:

- CHAPTER 1 provides an outline of the thesis with a brief description of the contents of each chapter

- CHAPTER 2 discusses a literature review of the main characteristics of the single-phase ejector in an ERS including the modeling and optimal operational conditions, principles of the dynamic modeling of the heat exchangers and its applications in designing the dynamic models of HVAC systems and principles of the Extremum seeking Control (ESC) in designing control models for the various HVAC systems.
- CHAPTER 3 (conference article) presents a paper which was published in a conference proceeding. In this paper, the steady state moving boundary models of the plate heat exchangers were developed based on ε-NTU approach. The developed model was used to investigate the impact of the primary stream (generating) pressure on the COP and η_{II} of an ERS. The model outputs were verified using the experimental data provided by Laboratoire des technologies de l'énergie (LTE) of Hydro-Quebec.
- CHAPTER 4 (1st journal article) includes a journal article, which was published during this doctoral study. It presents a numerical model of a single-phase ejector installed in an ERS. First, the experimental data obtained from the ERS set-up installed in LTE of Hydro-Quebec was analyzed to investigate the impact of generating pressure on Cr and evaporating pressure (P_e). It was observed that there is an optimum value of the generating pressure in a fixed condenser condition that simultaneously maximizes Cr and minimizes P_e. Then, a 1-D model of the ejector was developed which was able to predict the occurrence of the optimal Cr in the mentioned operational conditions.
- CHAPTER 5 (2nd journal article) presents a published journal article in which a novel dynamic model of the ERS was developed based on the moving boundary approach of the plate heat exchangers. The transient response of the model to the step change of the pump speed was validated using the experimental data provided by LTE of Hydro-Quebec.
- CHAPTER 6 (3rd journal article) This chapter is a submitted journal article which represents the development of an Extremum Seeking control model

(ESC) for the ERS to achieve the minimum P_e in the fixed condenser condition. The new scheme of ESC named batch phasor ESC was introduced in this chapter to find the optimal pump speed minimizing P_e in an adaptive, model-free manner.

- CHAPTER 7 presents a summary of the conclusions obtained from the experimental studies carried out in LTE and numerical studies. Furthermore, some recommendations for the future work are presented to develop the more comprehensive documentation on the subject, with fewer limitations.
- CHAPTER 8 includes Appendixes. Appendixes A-C show the flowcharts of the developed steady state models of three heat exchangers in the chapter 3. Appendixes D & E represent the equations of the developed dynamic models of the condenser and evaporator in chapter 5, respectively.

The references are listed at the end of this document. All the chapters from 4 to 6 include "Avant-Propos" section, which explains abstract, the status of the articles and their contribution to this thesis in French.

CHAPTER 2 LITERATURE REVIEW

This chapter deals with a comprehensive literature review on the preceding studies investigating the refrigeration systems as well as HVAC systems. In three parts, the former work will be reviewed. In the first part, work related to the numerical and experimental studies of the ejector in the refrigeration systems as well as effective parameters of its performance will be investigated. The second part will focus on the dynamic modeling of the HVAC systems. The literature investigating the control models for HVAC systems will be outlined in the third part.

2.1. Principle of an Ejector's operation

Recently, the interest in renewable and carbon free energy resources has grown among which the industrial waste heat has caught more attention due to its emission-free characteristics. The major sources of industrial waste heat are outlined in Table 2-1 [5]. Based on the report published by Thekdi and Nimbalkar [5], 20-50% of input energy to various energy systems are lost through stacks, vents and flares.

Table 2-1. Temperature range and characteristics for industrial waste heat sources

Waste Heat Source	Temperature Range °F	Temperature Range °C	Cleanliness
Furnace or heating system exhaust gases	600 – 2000	316 – 1100	Varies
Gas (combustion) turbine exhaust gases	900 – 1100	480 – 600	Clean
Reciprocating engines			
Jacket cooling water	190 – 200	90 – 100	Clean
Exhaust gases (for gas fuels)	900 – 1100	480 – 600	Mostly clean
Hot surfaces	150 – 600	65 – 316	Clean
Compressor after or inter cooler water	100 – 180	38 – 82	Clean
Hot products	200 – 2500	100 – 1370	Mostly clean
Steam vents or leaks	250 – 600	120 – 316	Mostly clean
Condensate	150 – 500	65 – 260	Clean
Emission control devices – thermal oxidizers, etc.	150 – 1500	65 – 816	Mostly clean

The industrial waste heat losses can be converted and recovered in some other processes like heat-driven refrigeration systems. Ejector refrigeration technology is one of those processes, which can capture the value of waste heat by cooling industrial hot streams. As this cooling system utilizes the waste heat instead of electricity produced by fossil fuel, it can reduce greenhouse gases (GHG) emissions. Ejector is an efficient device in this kind of cooling systems due to its reliability, long lifespan and low operating and maintenance costs. However, its drawbacks including low efficiency, design complexity and the fluctuations of operation particularly in off-design conditions have limited the industrial use of ejector refrigeration system. The schematic representation of an ejector-based refrigeration system (ERS) is shown in Figure 2-1.

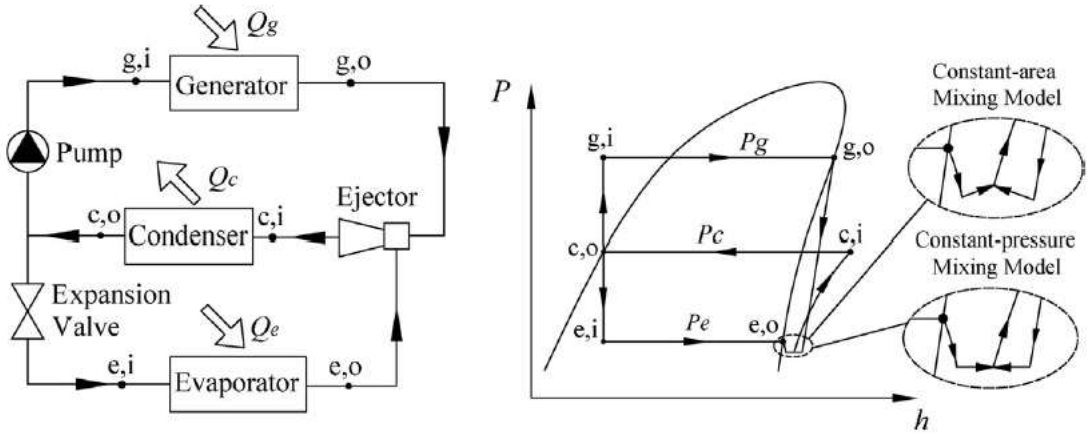

Figure 2-1: Schematic representation of the ERS and P-h diagram [1]

The ERS performance is strongly influenced by the flow behavior inside the ejector. Figure 2-2 indicates the schematic view of a typical ejector. In fact, the ejector is a flow device and has a simple structure consisted of four parts: a nozzle, a suction chamber, a mixing chamber and a diffuser. As the primary stream accelerates through the converging-diverging motive nozzle, its speed increases to the sonic speed and leaves with supersonic speed. Then, a low-pressure region is developed due to the expansion in the primary nozzle, which induces the secondary stream from the evaporator. The secondary stream also accelerates to its sonic speed and chokes at some point inside the primary nozzle (close to the outlet of the motive nozzle). The primary and secondary flows are mixed somewhere between in the primary nozzle of the ejector (based on constant-pressure mixing theory [6]) and constant-area

section(based on constant-area mixing theory [6]). A pressure recovery process occurs as the mixed stream crosses a stationary shock wave and fans out through the diffuser.

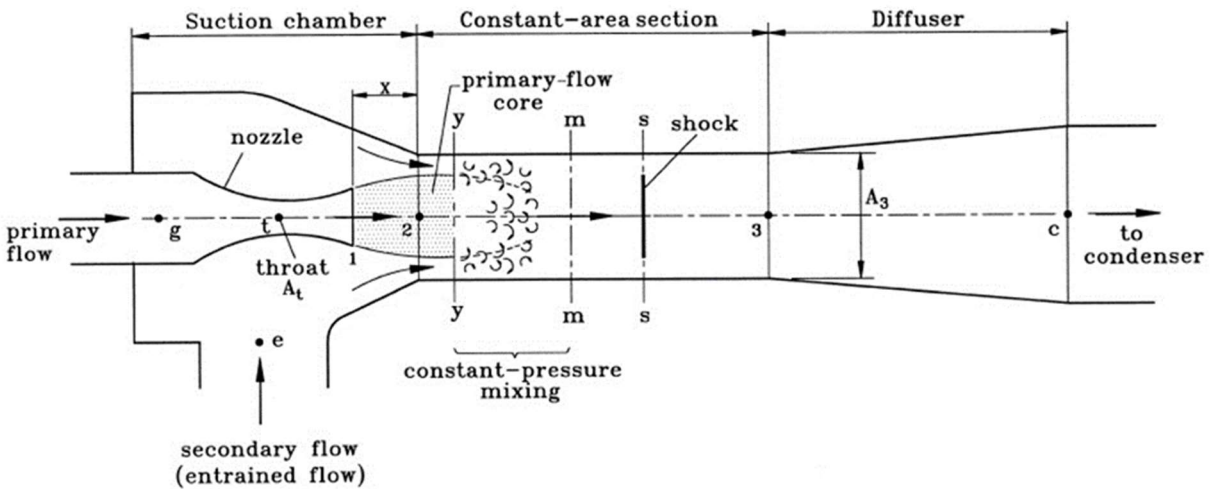

Figure 2-2: Schematic diagram of the ejector

The performance of an ejector is defined by means of the global indicators:

$$Er\ or\ \omega = \frac{\text{mass flow rate of the secondary flow}}{\text{mass flow rate of the primary flow}} = \frac{\dot{m}_s}{\dot{m}_p} \tag{2-1}$$

$$Cr = \frac{\text{static pressure at diffuser exit}}{\text{static pressure at secondary inlet}} = \frac{P_c}{P_e} \tag{2-2}$$

where Er and Cr entrainment ratio and compression ratio, respectively. Another performance indicator of the ERS is coefficient of performance (COP) which is defined as follows:

$$COP = \frac{\text{heat absorbed in the evaporator}}{\text{thermal energy required at the generator} + \text{pump work}} \approx \frac{\dot{m}_s \Delta h_{evaporator}}{\dot{m}_p \Delta h_{generator}} = Er \frac{\Delta h_{evaporator}}{\Delta h_{generator}} \tag{2-3}$$

It should be noted that the pump work is usually negligible. The ejector is considered as the heart of ERS where the irreversible transformations take place. Therefore, studying its features and modeling approaches would be beneficial for designing an optimal control

strategy. There exist abundant studies in the literature investigating the ejector and parameters influencing its performance. Some review papers were published to summarize the research efforts in the field of ejector [3][1]. There are other review articles studying the developments in the mathematical modeling and design of the jet ejectors [7][8]. Regarding the importance of the ejector modeling, many numerical and the complementary experimental work were conducted to explain impacts of different parameters on the ejector performance. Generally, the available numerical and experimental ejector studies assumed three zones for flow regime inside the ejector:

a) Nozzle section where the primary stream accelerates to its supersonic speed and consequently generates a low-pressure region at the nozzle exit plane and produces the entrainment effect to entrain the secondary fluid [8].
b) Mixing zone where the mixing of two streams has been explained with two feasible theories of constant-area mixing and constant-pressure mixing theories first proposed by Keenan et al. [6]. Huang et. al. [9] conducted a study based on the design of a "constant-pressure constant-area ejector and showed a good improvement in simulation results compared with the former models.
c) Diffuser section: the normal shock wave will usually occur before the supersonic fluid mixture enters the diffuser.

The mixed flow passes through the diffuser, and the velocity decreases to zero and the pressure increases high enough to cause discharge.

The large number of mathematical models of ejectors are one dimensional (1-D) steady state explicit equations evaluating state and operation parameters along the ejector and using the similar assumptions [10][11][12]:

- one dimension, adiabatic and steady state flow inside the ejector
- negligible kinetic energy at the inlet planes of the primary nozzle and the suction chamber and at the diffuser exit
- mass flux maximization criterion for both primary and secondary nozzles

Most of the studies in this field have used the ideal gas assumptions for their modeling, which inevitably results in the errors comparing with the reality. To remove the analytical error resulted from ideal gas assumption, Rogdakis and Alexis [13] and Chen et al. [14] used

the real gas relations in their simulations, which led to an improvement in the accuracy of their models. The ejector performance with fixed primary and secondary flows pressures can be explained in three operational zones shown in Figure 2-3 as explained by Huang et al model [9].

- Double-choking mode ($P_c \leq P_{Critical}$): the primary and secondary streams are both choked and the entrainment ratio Er is constant, i.e. $Er = Er_{Critical}$
- Single-choking mode ($P_{Critical} < P_c < P_{co}$): only the primary flow is choked, and the entrainment ratio Er changes with the backpressure P_c
- Back-flow mode ($P_c \geq P_{co}$): both the primary and secondary flows remain unchoked and the secondary flow is reversed.

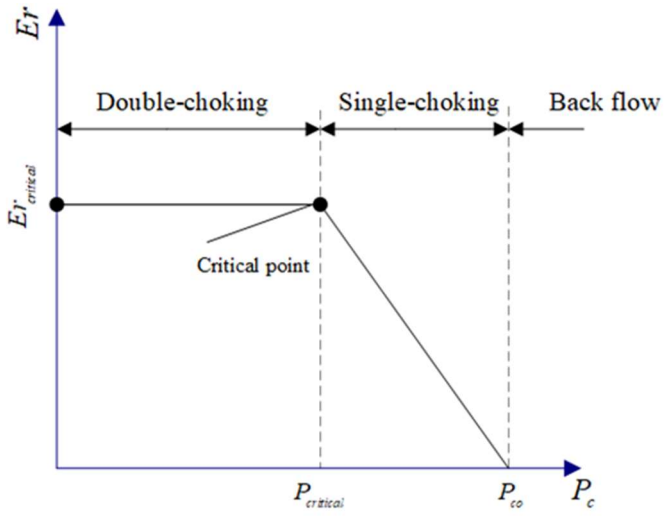

Figure 2-3: Operational modes of an ejector [10]

There exist three main factors mainly influence the performance of ejector and consequently the performance of an ERS including properties of working fluid, ejector geometry and operation conditions which have been widely investigated in the literature.

- **Working fluid:**

The product of the latent heat and mass flow rate of the refrigerant defines the system capacity. Thus, the higher latent heat for a given capacity, the lower mass flow rate, the less pumping energy and pipes' size, and generally the less overall cost is required to run the cycle. In addition, the environmentally friendly and inexpensive refrigerants are preferable

working fluids in the refrigeration systems. According to a research carried out by Chen et al. [15] the working fluids of the refrigeration systems can be categorized into three groups based on the slope of the vapor saturation curve on the Temperature-entropy diagram (dT/ds): dry, isentropic and wet fluids. The Temperature-entropy diagram of three groups of refrigerants are shown in Figure 2-4.

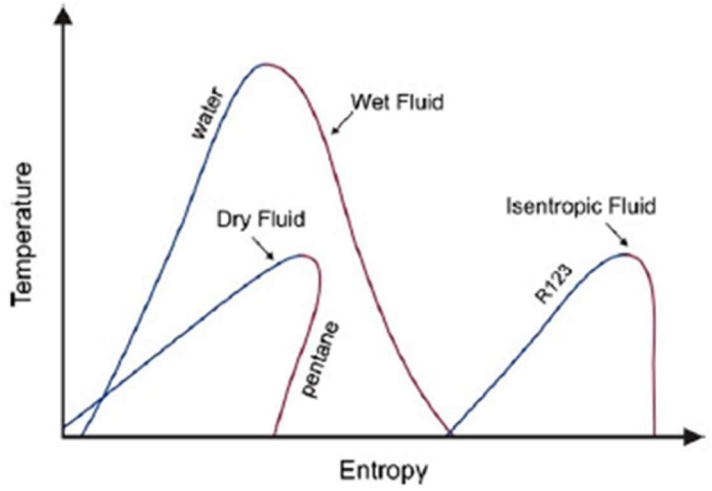

Figure 2-4: Temperature-entropy charts for the three types of working fluids [15]

Dry and isentropic vapor fluids do not experience any phase change during the expansion process passing through the primary nozzle, while small droplets may be formed at the nozzle exit for a wet working fluid, which can be eliminated by superheating of inlet streams. Cizungu et al. [16] conducted a simulation for an ejector refrigerator with four various refrigerants, including R123, R134a, R152a, and R717 using the same ejector. Simulation results revealed that R134a and R512a are suitable for heat source temperature ranged from 70 °C to 85°C, while ammonia is suitable for heat source temperature more than 90 °C. The similar studies also investigated the application of various refrigerants in the refrigeration systems [17][18][19]. Cizungu et al. [17] concluded that for the same ejector geometry using the environmentally friendly working fluids such as R123, R134a, R152a and R717 (ammonia), the entrainment ratio and the system efficiency (COP) depend mainly on the ejector geometry and the compression ratio. It was also shown by Roman and Hernandez [18] that the best performance of the ejector-based refrigeration system corresponded to the system with propane as a working fluid, since it has the highest coefficient of performance

and its ejector has the maximum entrainment ratio value, the least area ratio value and the highest efficiency value.

Furthermore, the authors of reference [19] demonstrated a short overview of the development process and results of a small cooling capacity (1.5 kW) solar driven cooling system using a variable geometry ejector. Based on their analysis, R600a was selected as a most efficient working fluid.

- **Ejector geometry:**

Ejector geometry including the area ratio (AR) which is defined as the area of the constant-area part in the mixing chamber divided by the nozzle throat area, primary nozzle throat diameter, nozzle exit position (NXP) and constant-area section length also effect the efficiency of ejector and the cycle performance. Chen et al [20] presented an ejector model to determine the optimum performance and to obtain the designed area ratio of an ejector in a refrigeration system. Yapıcı et al [21] studied the performance of the ejector refrigeration system using ejectors with cylindrical mixing chamber for various values of area ratio. Thongtip and Aphornratana [22] experimentally studied the impact of the primary nozzle throat diameter on the ejector performance in an R141b ejector refrigerator. They found out that use of the bigger nozzle throat, operated with lower generator temperature, is preferable and the primary nozzle exit Mach number should be as high as possible and be designed to be consistent with the heat source's temperature for implementing the nozzle at the designed conditions.

The Nozzle Exit Position (NXP), at the front or back of the mixing chamber can influence both the entrainment ratio and pressure ratio of the ejectors. Some experimental studies as well as numerical CFD simulations indicated that moving the nozzle exit into the mixing chamber reduces the COP and cooling capacity [7] [23][24][25]. Pianthong et al [26] showed that the constant area section length has no impact on the entrainment ratio.

- **Operational conditions:**

It was suggested by several experimental and theoretical studies that performance of an ERS in terms of COP, Er and Cr are strongly affected by operating conditions of the evaporator, generator and condenser in the cycle.

Thongtip and Aphornratana [22] showed that in an R141b ERS with fixed generator temperature, the suction pressure (evaporator pressure) approximately remains constant with increasing the condenser pressure to a threshold. Then, with the further increase in the condenser pressure beyond the threshold, the evaporator pressure increases linearly (Figure 2-5). Other experimental and theoretical studies using the fixed geometry ejectors suggested that for ejectors with similar area ratios, in a given evaporator temperature, a rise in the boiler temperature would reduce COP and the cycle must operate at a higher condenser temperature. On the other hand, in a fixed boiler temperature, an increase in the evaporator temperature would raise the COP, while the condenser should work at a higher temperature, which is shown in Figure 2-6 [9] [23][27][28][29]. Figure 2-6 also illustrates that decreasing the backpressure of the ejector would result in a rise in COP as well as Er. Then, Er or COP will remain constant with further decreasing the backpressure to below a critical backpressure of the ejector. This phenomenon is closely related to the choking regime inside the ejector. The secondary flow usually reaches the sonic speed somewhere inside the nozzle section of the ejector. Increasing the back pressure of the ejector beyond its critical value will lead to the disappearance of chocking for the secondary flow, a rapid fall in the entrainment ratio and finally it will cause the ejector to stop from working.

Thongtip and Aphornratana [27] showed that there is an optimum primary fluid mass flow for a particular geometry of the ejector, which can produce the lowest evaporator temperature (or lowest suction pressure) for a specified condenser pressure. They mentioned that at this point the ejector is able to operate at a higher critical condenser pressure (Figure 2-7) [27].

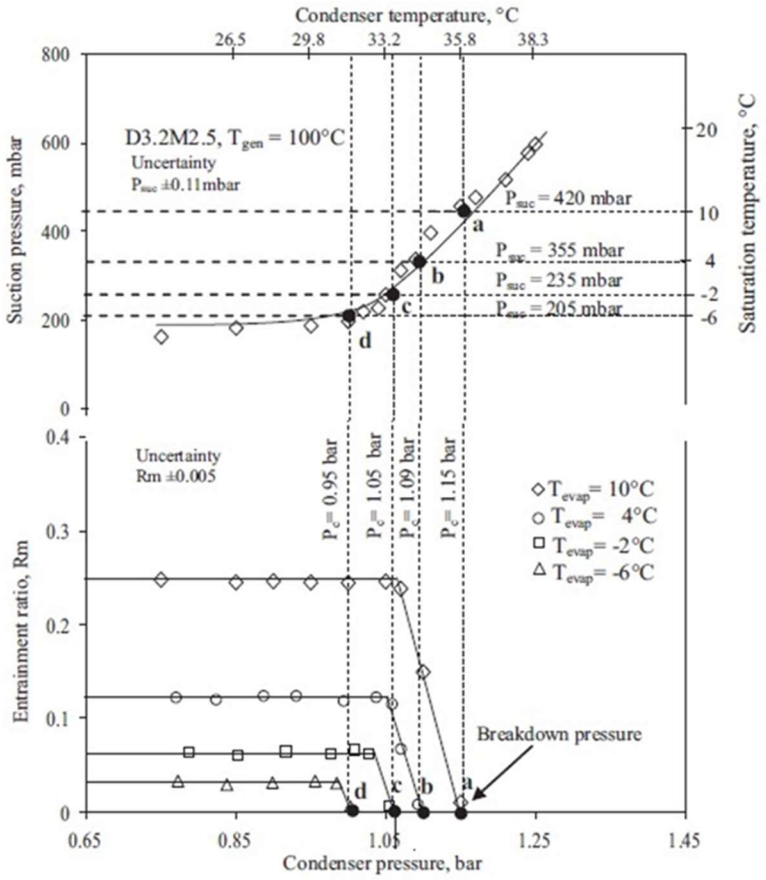

Figure 2-5: Variation of the suction pressure against condenser pressure[22]

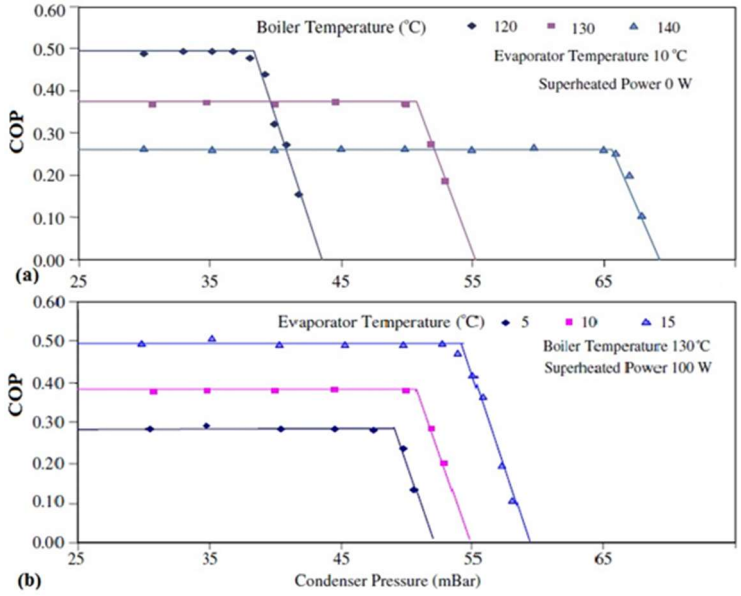

Figure 2-6: Variation of COP with condenser pressure a) at different boiler temperatures b) at different evaporator temperatures [23]

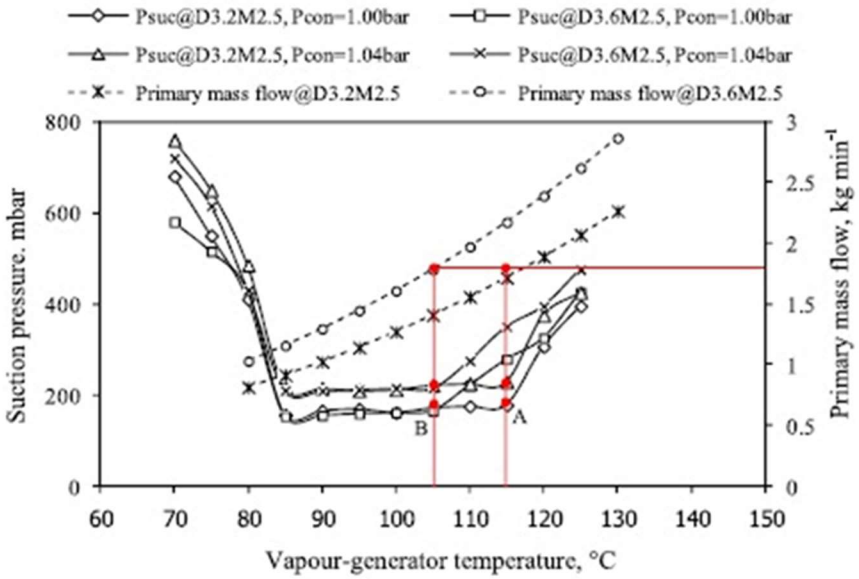

Figure 2-7: Variation of the suction pressure and primary fluid mass flow rate with the vapor-generator temperature [27]

Huang et al. [29] gathered this information in a map called ejector performance map based on which the pressure of actuating vapor (primary flow), either in design or field operation should be adjusted as close as possible to the critical back pressure to achieve the highest efficiency (Figure 2-8).

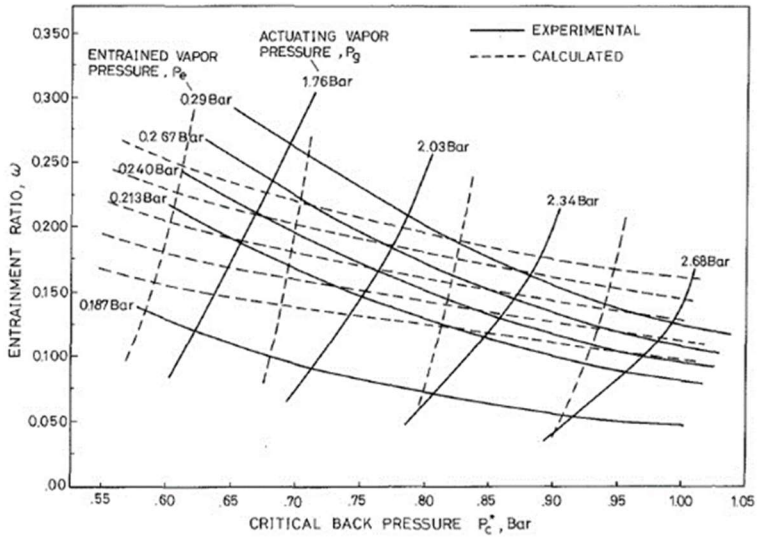

Figure 2-8: Measured and experimental ejector performance map[29]

Despite the considerable effort made in the literature to study the performance of ejector, there is still a gap in studies investigating the ejector operation in full interaction with other system components under various conditions. Hamzaoui et al. [30] is one of pioneers in this field whom investigated the interaction between the different governing parameters and their combined effect on the ERS performance in an extensive experimental study.

2.2. Principles of the dynamic modeling

As it was shown previously many literatures performed thermodynamic analyses and steady state simulations of ERS. However, the thermodynamic study cannot directly reflect the effect of structural and operating parameters on the performance of the system. Furthermore, since the steady state simulations study the static parameters such as COP, they are unable to explain the parameters variation over the time. Dynamic modeling is an efficient approach for various purposes such as analyzing and optimizing the system performance, designing a control strategy; controlling the tuning and commissioning; and detecting the faults. It should be taken into account that each of the tasks requires a different modeling approach with various levels of accuracy. Building a dynamic modeling of ERSs is a challenging task, which should make the balance between accuracy and complexity. It was assumed by many studies [31][32] that selecting appropriate heat exchanger models is the important factor to develop a dynamic model of a vapor compression system due to the complexity of the evaporating and condensing processes in the heat exchangers. In order to build a dynamic model, first it is required to decide which parameters would have the dynamic effects and which ones can be assumed as the quasi-steady parameters.

The main issue associated with the construction of dynamic models of vapor compression systems is related to modeling instabilities caused by transients' starts (start-stop), the transition regions in the two-phase flow and variations in thermal load. The dynamic models of vapor compression systems can be categorized into two main classes: inductive and deductive models as mentioned by Koury et al [33].

The inductive models are developed using a mathematical relation between the entry and exit variables of the system where the necessary parameters can be extracted from the

adequate experiments. The empirical dynamic models, which belong to the inductive model category, are quite useful due to the simple and easy model establishment and the quick identification from data. However, their application is limited to the system derived from, with their particular conditions. The examples of this approach can be found in the literature. For instance, Leducq et al. [34] developed a simple non-linear model of a vapor compression cycle to design a predictive optimal control algorithm of the system. Li et al. [35] obtained the parameters of the empirical dynamic model of a variable speed refrigeration system using the experimental data. A model of a vapor compression refrigeration system with a variable-speed compressor based on a black-box modelling technique was presented by Navarro-Esbrı et al. [36]. They used neural networks to predict the performance of the system with low cost data requirement in terms of input variables and training data. In another work conducted by Romero et al. [37] a black-box model to accurately predict the chilled water temperature dynamic response of a vapor compression chiller was proposed.

On the other hand, the deductive models, which are based on the conservation equations of mass, momentum and energy derived from physics laws, are preferred by many researchers since they provide a greater insight into the physical processes occurring under fluctuating conditions. Thus, it is believed that deductive models can be more efficient than inductive models to develop some advanced control strategies that can potentially improve control performance. Some examples of the deductive dynamic models reported in the literature are mentioned in the following section. Wang [38] developed a dynamic model of centrifugal chiller to simulate the dynamics of a seawater-cooled chilling system controlled by EMCS on-line strategies. A dynamic model for a direct expansion (DX) water-cooled air-conditioning system was presented by Shiming [39] in which the model was used to study the influence of refrigerant mass flow rate, evaporation pressure as well as air side state on the system performance. In another study conducted by Browne and Bansal [40] a simple dynamic model for vapor compression liquid chillers with modulating and on/off control was developed. The model applied the thermal capacitance approach for specific state variables to account for the dynamics of the chiller and ancillaries.

Lei and Zaheeruddin [41] built a lumped-parameter dynamic model of a water chiller refrigeration system based on the component models including evaporator, compressor,

condenser and a thermostatic expansion valve (TEV) and investigated the impact of control inputs such as compressor operational frequency and TEV opening fraction on the output performance of the system with the built dynamic model. Llopis et al. [42] presented a dynamic mathematical model of a shell and tube condenser operating in a vapor compression refrigeration plant.

Pfafferott and Schmitz [43] developed a Modelica based dynamic model of the CO2-refrigeration systems in which the predicted pressure parameters showed a fair agreement with the experiment while the mass flow rates differed considerably when the system was subjected to the disturbances of compressor speed step. Shi et al [44] developed the dynamic model of a transcritical CO2 supermarket refrigeration system in Dymola to study the performance of the system in the absence of experimental data.

Yao et al. [45] derived a state-space model for the vapor compression chiller by using the lumped parameter method without considering the phase change process in the condenser and evaporator thus, it was unable to simulate the dynamic responses of refrigerant states in the evaporator and condenser when subjected to ambient disturbances. Moving boundary model makes a correlative approach to describe the transient behavior of the two-phase flow heat exchanger in refrigeration system.

As Bendapudi and Braun [46] mentioned there exists two most common approaches to model heat exchangers including either discretization using the finite volume method or the implementation of a moving boundary model which both are in the deductive models category. Some studies [47] [48][49] compared the trade-off between more accurate finite volume models and computationally less expensive moving boundary models and found out that with a sufficient number of finite volumes, both approaches can achieve similar accuracies.

Therefore, as the computational effort can be crucial in dynamic optimization, the moving boundary approach has been widely used by preceding studies [50] [51] [52] [53] [54] [55] [56] [57] [58] [59] in dynamic modeling of vapor compression systems and heat pumps. The moving boundary approach (MB) divides the heat exchanger into several regions (i.e. control volumes) corresponding to the different refrigerant phases. The model parameters are

obtained based on the laws of conservation. Capturing the moving of the control volume boundary, the MB approach can precisely simulate the dynamic behavior of the heat exchangers.

Yao et al. [50] developed a dynamic model of a variable capacity refrigeration system based on moving boundary method which mainly focused on how to switch different MB models depend on the appearance and disappearance of phase regions. Bonilla et al. [51] built moving boundary models for evaporator and condenser which support dynamic switching between all possible flow configurations, and the simulation results were validated by experimental data. Kim et al. [52] showed a more reliable moving boundary model for heat exchangers the two-phase control volume of the heat exchanger based on which, the mean void fraction was the key parameter to calculate the fluid physical property. It was proposed by Xu and Fang [60] that the mean void fraction can be written as a function of the fluid pressure, the inlet specific enthalpy (inlet vapor quality) and the outlet specific enthalpy (outlet vapor quality) of the control volume. In the next study of Zhang and Zhang [54] implied the mean void fraction time derivative in the mass and energy equations for the evaporator, which is widely used in recent dynamic simulations [56][61].

The vapor compression systems with ejector is more complicated than the conventional vapor compression systems in terms of the system coupling and solver. Zheng et al. [61] developed a dynamic model of a transcritical CO2 ejector expansion refrigeration cycle (EERC) using mathematical models for gas cooler, evaporator and separator formulated by applying the mass and energy conservation equations.

2.3. Principles of control models

Residential and industrial air conditioning/refrigeration (AC & R) systems have extremely large start-up times and rarely operate at the steady state conditions. They are constantly trying to compensate for changes in set points and external conditions. It is evident that effective control strategies are required to drive such systems to their optimal operational conditions. There are a significant number of studies investigated various control strategies for different objective function to control AC &R systems. The considerable amount of

literature has dealt with the control and optimization of AC &R systems operation based on models obtained under nominal and/or calibrated conditions

Rasmussen and Alleyne developed an advanced multi-input multi-output (MIMO) control technique to control a conventional compressor-based refrigeration system for multiple objective functions of maximizing COP, exchanging efficiency for capacity when needed, controlling not only the temperature, but also humidity, and so on. They used a gain-scheduled control approach based on local models and local controllers [62]. He et al. [63] suggested a new lumped-parameter model for describing the dynamics of vapor compression cycles and studied dominating dynamic characteristics of the cycle around an operating point and concluded that single-input single-output (SISO) control technique cannot efficiently control this system.

In another study conducted by Marcinichen et al. [64] the use of a dual SISO control strategy for the simultaneous control of compressor speed and expansion valve opening was investigated and the control strategy was devised to achieve a maximum coefficient of performance (COP) within a defined values of cooling capacity. In addition, some other linear control techniques including decoupling multivariable control [65], model predictive control [66] [67], LQG control [68] [69] and robust H∞ control [70][71] [72] were used in literature to generate control models for vapor compression refrigeration systems.

Jain [73] presented a multivariable feedforward-plus-feedback control strategy to achieve the optimal cycle calculated in an offline condition. In another study carried out by Jain and Alleyne a model predictive controller (MPC) based on dynamic destroyed exergy was used to control a vapor compression refrigeration cycle [74].

However, the efficiency of model-based control strategies can be dramatically compromised in practical applications due to significant variations in the actual system characteristics and measurement errors. Recently, a class of self-optimizing controllers called “extremum seeking” has received a great deal of attention in the control literature. Extremum seeking control is mainly a form of an adaptive control where the steady-state input-output characteristic is optimized, without requiring any explicit knowledge about this input-output characteristic except that it has an extremum. Unlike the other control strategies such as

MPC, Extremum seeking control optimizes the system without any reference value. It has caught a great interest in the field of optimal control since extremum seeking is model free and it has proven to be both robust and effective in many different application domains. Equally being model free, there are clear limitations to what can be achieved. Perhaps paradoxically, although being model free, extremum seeking is a gradient based optimization technique and needs the efficient approaches to estimate the gradient. It means that although the extremum seeking control does not require any dynamic model of the system, the limited knowledge of the system and the efficient numerical techniques are still required to evaluate the gradient of the map . The gradient in vicinity of the optimum point of map is approximately zero.

ESC is ideal for a few reasons:

- The control model is not based on a numerical model of the system, therefore, the simplifying assumptions in developing the system's model would not affect the accuracy of the control model.
- Unlike the other control strategies such as MPC and IMC needing the predetermined reference values, ESC is a self-optimizing control model which is not designed to peruse any reference value. As a result, the accuracy of ESC is not deteriorated by inaccuracy in the optimization method used to define the reference value of the controlled parameter.
- In order to reconstruct the state, ESC needs fewer sensors compared to MPC and IMC, and therefore the system requires less frequent maintenance for fine tuning.
- ESC observes only output of the performance index (for example, Efficiency, cost, and so on) and seeks the optimal state based on only the output signal. Then it is necessary to stabilize the system, but not necessary to know the system and the performance index forms.

However, ESC suffers from a limitation which is the requirement of a multiple time-scale separation between the system dynamics, the perturbation frequency, and the adaptation rate so as to avoid interactions and possible instabilities. This causes the convergence of ESC to be extremely slow.

The first notable work in this field was done by LeBlanc in 1922 [75] and also mentioned in reference [76] in which the gradient is estimated by a dither-demodulating scheme [77]. In his paper, LeBlanc explained a mechanism to transfer power from an overhead electrical transmission line to a tram car using an ingenious non-contact solution. To maintain an efficient power transfer in what is essentially a linear, air-core, transformer/capacitor arrangement with variable inductance, due to the changing air-gap, he indicated the need to adjust a (tram based) inductance (the input) to maintain a resonant circuit, or maximum power (the output). Leblanc explained a control mechanism of maintaining the desirable maximum power transfer using a method lately was known an extremum seeking solution.

Then, Some research was done in Russia in extremum seeking control field during the World War II by Kazakevich [78] [79]. Draper and Li [80] published the first English literature in extremum seeking field and detailed its performance. This paper addressed the optimization of an internal combustion engine in which the approach was perused to choose the ignition timing (the input) to achieve maximum power output. Ever since this publication, the internal combustion engines have remained a renowned application domain for extremum seeking.

Extremum seeking, like all other forms of adaptive control, was a popular research topic in the 1950s and 1960s and appeared in the literature by many different names such as extremum regulation suggested by Morosanov [81] and Ostrovskii [82], automatic optimization implied by Meerkov [83][84], optimalizing control system [85], and hill-climbing systems [86] to name but a few.

Many studies over the next three decades after the first appearance of Extremum seeking control (1970-2000), mainly focused on finding the optimal value of a static mapping and the stability issues were ignored. The first proof of extremum seeking stability based on Lyapunov stability analysis was published by Luxat and Lees [87] for a very special scheme in 1971. Despite the slow progress on the theory at the time, the practice and industrial applications of extremum seeking grew rapidly, as Astrom and Wittenmark [88] mentioned in their book in 1995 that extremum seeking was one of the most promising adaptive control methods.

The first rigorous proof of stability was published by Krstić and Wang [89] and its non-local stability was proofed by Tan et al. [90]. These publications sparked the renewed interests in the application of the extremum seeking control in various fields. In fact, its ability to automatically discover inputs optimizing a performance metric without requiring a model of the system distinguishes it from other nonlinear control techniques.

A block diagram of a typical Extremum seeking control (ESC) shown by Liu and Krstic [91] is illustrated in Figure 2-9.

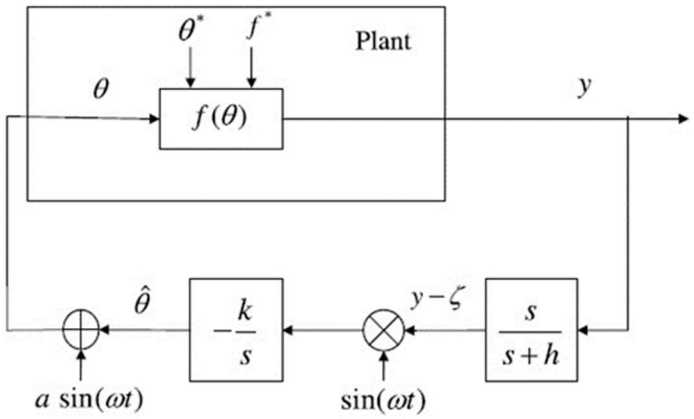

Figure 2-9: block diagram of ESC strategy for a static map [91]

In this approach the gradient is estimated by a dither-demodulating scheme. A sinusoidal perturbation of sin (ωt) additively enters the map. Then, the measured output $y = f(\theta)$ passes through a washout filter and is multiplied by the same perturbation signal, sin(ωt), to estimate the derivative (scalar gradient) $f'(\theta)$ at the input of the integrator. Afterwards, the estimation of $\hat{\theta}$ will be updated in the direction of driving the gradient to zero. For k > 0 the ESC scheme drives $\hat{\theta}$ toward the nearest local minimum of $f(\theta)$, whereas for k <0 the scheme converges toward the nearest maximum. Most of the extremum seeking algorithms until 1990 used the periodic excitation to explore the steady state map. Stochastic excitation started to become popular in the 1990s which can be found in some work like references [92][93][94]. Mainly there are two approaches of extremum seeking control in the literature:

- using a continuous signal to excite the steady state map and approximate the implicit gradient as described by Ariyur and Krstic [77]

- using a (repeated) sequence of constant probing inputs that exploit the numerical optimization methods as shown by Tee1 and Popovic [95]

Extremum seeking has been used in various fields such as compressor/thermoacoustic/jet engine instability control [96][97][98][99][100][101], electromechanical valve [102], internal combustion engines [85] [99][103][104] [105][106], flow control problems [107][108][109][110], flocking and formation control[111][112][113], human exercise machines [114], optimizing neural network/fuzzy logic controllers [115][116], maximum gain control in optical amplifiers[117], process control [118][119][120], weigh feeder control systems [121], tunable thermo-acoustic cooler [122] and so forth.

ESC has been widely used in HVAC system in the recent years due to its robust and usually fast transient performance in comparison with typical static optimization approaches. In a study carried out by Li et al. [123] an extremum-seeking control (ESC) based on self-optimizing strategy is proposed to minimize the energy consumption, with the feedback of chilled water supply command rather than the temperature and humidity measurements. In another study, Li et al. [124] applied an extremum seeking control scheme for energy efficient operation of chilled-water system, and used a Modelica based dynamic model to demonstrate the effectiveness of the proposed control strategy.

Burns et al. [125] used a model-free extremum seeking algorithm to adjust the set points of the compressor discharge temperature to optimize energy efficiency. They showed that the relationship between compressor discharge temperature and power consumption is convex (which is a requirement for this class of real-time optimization), and applied time-varying extremum seeking to drive these set points to values that minimize the power. Burns and Laughman [126] designed an energy optimizing extremum seeking controller for vapor compression systems (VCS) that automatically discovers sets of inputs that minimizes the energy consumption while the machine is in operation. This controller optimizes an input-output map (from VCS inputs to electrical energy consumed) in real-time without relying on a dynamic model of a system. Koeln and Alleyne [127] applied Extremum seeking control in a vapor compression system to find an optimal subcooling that maximizes the efficiency. For the air-source transcritical CO2 heat-pump water heater, the discharge pressure set point is taken as the input to the ESC controller, while the system COP is taken as the performance

index in a study conducted by Hu et al. [128]. To evaluate the proposed ESC strategy, they developed a Modelica based dynamic simulation model.

Having reviewed the literature, in three steps, I concluded that the Moving Boundary approach is the most efficient method to build a dynamic model of an ERS. Furthermore, based on the experimental findings of the optimal operational conditions of the ERS, the Extremum Seeking Control (ESC) is chosen as a control strategy to develop an optimal controller of an ERS in this PhD research project.

2.4. Nomenclature

Table 2-2. Nomenclature

Symbols	Definition
P	Pressure, [kPa]
$\dot{m}$	Mass flow rate, [kg s^{-1}]
T	Temperature, [°C]
S	Entropy, [kJ kg^{-1}°C]
h	Enthalpy, [kJKg^{-1}]
subscripts	
c	Condenser
e	Evaporator
g	Generator
s	Secondary
p	Primary
i	Inlet
o	Outlet
Greek characters	
ω	Entrainment ratio
Abbreviation	
Cr	Compression ratio
COP	Coefficient of performance
ERS	Ejector refrigeration system
Er	Entrainment ratio
ESC	Extremum seeking control
NXP	Nozzle exit position
VCS	Vapor compression system
1-D	One dimensional
CFD	Computational fluid dynamics

CHAPTER 3 Numerical Study of the Influence of the Primary Stream Pressure on the Performance of the Ejector Refrigeration System Based on Heat Exchanger Modeling

Avant-propos

Auteurs et affiliation:

Elhameh Narimani: étudiant au doctorat, faculté de génie, département de génie mécanique, Université de Sherbrooke

Mikhail Sorin: professeur, faculté de génie, département de génie mécanique, Université de Sherbrooke.

Philippe Micheau: professeur, faculté de génie, département de génie mécanique, Université de Sherbrooke.

Hakim Nesreddine: PhD, Chercheur-Chargé de projet, Laboratoire des technologies de l'énergie, Shawinigan (Québec), Canada

Date d'acceptation : 9 Septembre 2018

État de l'acceptation : acceptée

Revue: Proceedings of ICEESD 2019- International Conference on Energy, Environment and Sustainable Development

Titre français: Étude numérique de l'influence de la pression du courant primaire sur la performance du système de réfrigération à éjecteur sur la base de la modélisation d'échangeur de chaleur

Contribution au document:

Ce chapitre a étudié l'influence de l'augmentation du débit massique primaire sur la performance d'un système de réfrigération à éjecteurs en termes de COP et d'efficacité exergétique (η_{II}) grâce à la modélisation statique des échangeurs de chaleur.

Résumé en français:

Des modèles numériques pour les échangeurs de chaleur dans le système de réfrigération à éjecteurs (SRE) ont été développés et validés avec des données expérimentales. Les modèles ont été basé sur le modèle des échangeurs de chaleur à plusieurs passes en utilisant la méthode des limites variables, qui permet d'estimer la longueur des zones, les températures de sortie des deux côtés et les charges thermiques à divers points expérimentaux. Les modèles développés ont été utilisés pour étudier l'influence de la pression primaire sur la performance d'un système R245fa en fonction de son coefficient de performance (COP) et de son efficacité exergétique (η_{II}). Il a été illustré numériquement et a prouvé expérimentalement que l'augmentation de la pression d'écoulement primaire réduit légèrement le COP tandis que l'efficacité exergétique passe par un maximum avant de diminuer.

3.1. Abstract

Numerical models of the heat exchangers in ejector refrigeration system (ERS) were developed and validated with the experimental data. The models were based on the switched heat exchangers model using the moving boundary method, which were capable of estimating the zones' lengths, the outlet temperatures of both sides and the heat loads at various experimental points. The developed models were utilized to investigate the influence of the primary flow pressure on the performance of an R245fa ERS based on its coefficient of performance (COP) and exergy efficiency (η_{II}) . It was illustrated numerically and proved

experimentally that increasing the primary flow pressure slightly reduces the COP while the exergy efficiency goes through a maximum before decreasing.

Keywords: Coefficient of performance, ejector refrigeration system, exergy efficiency, heat exchangers modeling, moving boundary method.

3.2. Introduction

The ejector refrigeration cycles are recently used in many engineering applications due to their advantages compared with conventional refrigeration systems: the structural simplicity, low capital cost, the ability to use the inexpensive and free low-grade heat resources like waste heat from various industries and solar energy, to name a few. However, the main drawback of the ejector-based refrigeration cycle is related to its low performance. As a result, it is required to improve the performance of such systems.

Considerable efforts have been made in the literature to investigate the various refrigeration systems numerically and experimentally. It was suggested by several experimental and theoretical studies that performance of the ERS are strongly dependent on the operating conditions of the ejector, evaporator, generator and condenser in the cycle. The most recent findings can be found in the studies conducted by Aphornratana et al. [129], Huang et al. [29] Eames et al. [130], Thongtip and Aphornratana [22] and Chen et al. [131].

Heat exchangers are considered as crucial components in the ERS modeling. Heat exchangers modeling approaches can be mainly categorized into three groups: 1) single node model or lumped parameter model[132] 2) multi-node model or distributed parameter model[133], and 3) zone model or moving boundary model [134][135] [136][137]. The moving boundary model is widely used to model heat exchangers in transient and steady state conditions due to its high accuracy and low computation time. This model splits a heat exchanger into several regions (based on the number of phases) or Control Volumes (CVs) in which the lumped thermodynamic properties are averaged.

The boundaries of the regions may move between CVs. Despite the high accuracy of the finite volume or finite difference models, the lumped parameter or moving-boundary method

is much faster which is shown by Grald and MacArthur [59].The moving-boundary method is considered as an appropriate approach to model the heat exchangers for control purposes. Although the tremendous work performed in this area, some improvements are still required in the moving boundary method. For instance, the significant number of available models assumes the fixed number of zones or the fixed lengths for the zones.

In this work, the numerical investigation of the three heat exchangers used in an ERS was conducted. To develop the steady-state models of the heat exchangers, the ε-NTU model in combination with the moving boundary method was applied. A simple method was presented to evaluate the length of the different zones in the heat exchangers and the simulation results showed a good agreement with experimental data. The developed models could predict the thermal loads and outlet temperatures of the both sides with the errors up to 8.55 % and 6.46 %, respectively.

3.3. Modeling

The ejector refrigeration cycle includes six components: the generator, condenser, evaporator, ejector, electronic expansion valve and pump. Figure 3-1 shows the schematic view of a typical ejector refrigeration system. The values of all the model parameters applied in this study are obtained by employing an R245fa ejector driven refrigeration plant located at LTE center of Hydro-Quebec. EES software was applied to solve the developed equations.

The zone model or moving boundary model [134] [135] is widely used to model the heat exchangers in transient and steady state conditions. In the present study, the moving boundary model is applied to model the heat exchangers. The values of the thermal loads in the evaporating, preheating, condensing and desuperheating regions of the generator, evaporator and condenser can be evaluated using the heat exchangers' pressure and inlet temperatures of the both sides and with comparing those values with their equivalent values calculated by ε-NTU method. The solution algorithms applied to model the heat exchangers are demonstrated in Appendixes A-C.

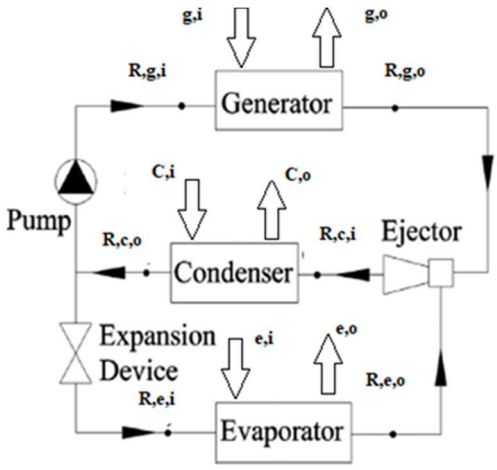

Figure 3-1: Schematic representation of an ejector refrigeration circle

The relation introduced by Gnielinski [138][139][140] was used to evaluate the convective heat transfer coefficients in single-phase regions. The heat transfer coefficients of the evaporation zones (in the generator and evaporator) are calculated using the correlation introduced by Yan and Lin [136]. Furthermore, the heat transfer coefficient of the condensation zone of the condenser is estimated by Yan et al. correlation [136].

Figure 3-(2-4) depict the heat transfer diagrams and the thermal plans along the heat exchangers.

It was assumed that the heat transfer areas in the three heat exchangers are divided into three zones in the generator and the condenser while the evaporator is represented by two zones. The heat transfer area of each region is a portion of the total heat transfer area of the corresponding heat exchanger defined by dimensionless length factors. All the equations are listed in Table 3-1.

For instance, in the generator, length factors of the preheating (η_{ph}) and evaporating (η_{ev}) zones are calculated in the iterative solutions based on which the heat transfer rates in the evaporation zones ($\dot{Q}_{ev}$) and preheating $\left(\dot{Q}_{ph}\right)$ are evaluated using Eqs (3-2) and (3-4). The i_{fg} represents the vaporization enthalpy of the refrigerant at the generator and condenser pressures. In each iteration, the evaluated values of $\dot{Q}_{ev}$ and $\dot{Q}_{ph}$ are compared to their real values calculated by Eqs. (3-3) and (3-5) and the estimated values of η_{ph} and η_{ev} are renewed until convergence is reached. The same method is used for the condenser and evaporator.

Table 3-1: Governing equations in the heat exchangers

Generator	Equations	No.
Superheating Zone	$\dot{C}_{r,g,sh} = (\dot{m}Cp)_{r,g,sh}$	(3-1)
	$\dot{C}_{g,sh} = (\dot{m}Cp)_{g,sh}$	
	$\dot{C}_{\min,sh} = \min(\dot{C}_{r,g,sh}, \dot{C}_{g,sh})$	
	$\dot{C}_{\max,sh} = \max(\dot{C}_{r,g,sh}, \dot{C}_{g,sh})$	
	$C_{sh} = \dfrac{\dot{C}_{\min,sh}}{\dot{C}_{\max,sh}}$	
	$A_{sh} = \eta_{sh} A_g$	
	$UA_{sh} = U_{sh} A_{sh}$	
	$NTU_{sh} = UA_{sh} / \dot{C}_{\min,sh}$	
	$\varepsilon_{sh} = f_{he}(NTU_{sh}, C_{sh})$	
	$\dot{Q}_{sh} = \varepsilon_{sh} \dot{C}_{\min,sh} (T_{g,i} - T_{r,g,sat})$	
	$T_{g,mid,sh} = T_{g,i} - \dot{Q}_{sh} / \dot{C}_{g,sh}$	
	$T_{r,g,o} = \dot{Q}_{sh} / \dot{C}_{r,g,sh} + T_{r,g,sat}$	
Evaporation Zone	$\dot{C}_{r,g,ev} = (\dot{m}Cp)_{r,g,ev}$	(3-2)
	$\dot{C}_{g,ev} = (\dot{m}Cp)_{g,ev}$	
	$C_{ev} = \{ phase \quad change \} = 0$	
	$A_{ev} = \eta_{ev} A_g$	
	$UA_{ev} = U_{ev} A_{ev}$	
	$NTU_{ev} = UA_{ev} / \dot{C}_{g,ev}$	
	$\varepsilon_{ev} = f_{he}(NTU_{ev})$	
	$\dot{Q}_{ev} = \varepsilon_{ev} \dot{C}_{g,ev} (T_{g,mid,sh} - T_{r,g,sat})$	
	$T_{g,mid,ph} = T_{g,mid,sh} - \dot{Q}_{ev} / \dot{C}_{g,ev}$	
	$\dot{Q}_{ev,cal} = \dot{m}_{r,g} i_{fg}$	(3-3)
Preheating zone	$\dot{C}_{r,g,ph} = (\dot{m}Cp)_{r,g,ph}$	(3-4)
	$\dot{C}_{g,ph} = (\dot{m}Cp)_{g,ph}$	
	$\dot{C}_{\min,ph} = \min(\dot{C}_{r,g,ph}, \dot{C}_{g,ph})$	
	$\dot{C}_{\max,ph} = \max(\dot{C}_{r,g,ph}, \dot{C}_{g,ph})$	
	$C_{ph} = \dfrac{\dot{C}_{\min,ph}}{\dot{C}_{\max,ph}}$	
	$A_{ph} = \eta_{ph} A_g$	
	$UA_{ph} = U_{ph} A_{ph}$	
	$NTU_{ph} = UA_{ph} / \dot{C}_{\min,ph}$	
	$\varepsilon_{ph} = f_{he}(NTU_{ph}, C_{ph})$	
	$\dot{Q}_{ph} = \varepsilon_{ph} \dot{C}_{\min,ph} (T_{g,mid,ph} - T_{r,g,i})$	
	$T_{g,o} = T_{g,mid,ph} - \dot{Q}_{ph} / \dot{C}_{g,ph}$	
	$\dot{Q}_{ph,cal} = \dot{C}_{r,g,ph} (T_{r,g,sat} - T_{r,g,i})$	(3-5)
	$\dot{Q}_g = \dot{Q}_{ph} + \dot{Q}_{sh} + \dot{Q}_{ev}$	(3-6)
Condenser	**Equations**	**No.**
Subcooling Zone	$\dot{C}_{r,c,sb} = (\dot{m}Cp)_{r,c,sb}$	(3-7)
	$\dot{C}_{c,sb} = (\dot{m}Cp)_{c,sb}$	
	$\dot{C}_{\min,sb} = \min(\dot{C}_{r,c,sb}, \dot{C}_{c,sb})$	
	$\dot{C}_{\max,sb} = \max(\dot{C}_{r,c,sb}, \dot{C}_{c,sb})$	
	$C_{sb} = \dfrac{\dot{C}_{\min,sb}}{\dot{C}_{\max,sb}}$	
	$A_{sb} = \eta_{sb} A_c$	
	$UA_{sb} = U_{sb} A_{sb}$	
	$NTU_{sb} = UA_{sb} / \dot{C}_{\min,sb}$	
	$\varepsilon_{sb} = f_{he}(NTU_{sb}, C_{sb})$	
	$\dot{Q}_{sb} = \varepsilon_{sb} \dot{C}_{\min,sb} (T_{r,c,sat} - T_{c,i})$	
	$T_{c,mid,sb} = T_{c,i} + \dfrac{\dot{Q}_{sb}}{\dot{C}_{c,sb}}$	
	$T_{r,c,o} = T_{r,c,sat} - \dfrac{\dot{Q}_{sb}}{\dot{C}_{r,c,sb}}$	
Condensation Zone	$\dot{C}_{r,c,cond} = (\dot{m}Cp)_{r,c,cond}$	(3-8)
	$\dot{C}_{c,cond} = (\dot{m}Cp)_{c,cond}$	
	$C_{cond} = \{ phase \quad change \} = 0$	
	$A_{cond} = \eta_{cond} A_c$	
	$UA_{cond} = U_{cond} A_{cond}$	
	$NTU_{cond} = UA_{cond} / \dot{C}_{c,cond}$	
	$\varepsilon_{cond} = f_{he}(NTU_{cond})$	
	$\dot{Q}_{cond} = \varepsilon_{cond} \dot{C}_{c,cond} (T_{r,c,sat} - T_{c,mid,sb})$	
	$T_{c,mid,des} = T_{c,mid,sb} + \dfrac{\dot{Q}_{cond}}{\dot{C}_{c,cond}}$	

$$\dot{Q}_{cond,cal} = \dot{m}_{r,c} i_{fg} \quad (3\text{-}9)$$

desuperheating Zone	$\dot{C}_{r,c,des} = (\dot{m}Cp)_{r,c,des}$	(3-10)
	$\dot{C}_{c,des} = (\dot{m}Cp)_{c,des}$	
	$\dot{C}_{\min,des} = \min(\dot{C}_{r,c,des}, \dot{C}_{c,des})$	
	$\dot{C}_{\max,des} = \max(\dot{C}_{r,c,des}, \dot{C}_{c,des})$	
	$C_{des} = \dfrac{\dot{C}_{\min,des}}{\dot{C}_{\max,des}}$	
	$A_{des} = \eta_{des} A_c$	
	$UA_{des} = U_{des} A_{des}$	
	$\varepsilon_{des} = f_{he}(NTU_{des}, C_{des})$	
	$\dot{Q}_{des} = \varepsilon_{des} \dot{C}_{\min,des} (T_{r,c,i} - T_{c,mid,des})$	
	$T_{c,o} = T_{c,mid,des} + \dot{Q}_{des} / \dot{C}_{c,des}$	
	$\dot{Q}_{des,cal} = \dot{C}_{r,c,des} (T_{r,c,sat} - T_{r,c,i})$	(3-11)
	$\dot{Q}_c = \dot{Q}_{sb} + \dot{Q}_{cond} + \dot{Q}_{des}$	(3-12)

Evaporator	Equations	No.
Superheating Zone	$\dot{C}_{r,e,sh} = (\dot{m}Cp)_{r,e,sh}$	(3-13)
	$\dot{C}_{e,sh} = (\dot{m}Cp)_{e,sh}$	
	$\dot{C}_{\min,sh} = \min(\dot{C}_{r,e,sh}, \dot{C}_{e,sh})$	
	$\dot{C}_{\max,sh} = \max(\dot{C}_{r,e,sh}, \dot{C}_{e,sh})$	
	$C_{sh} = \dfrac{\dot{C}_{\min,sh}}{\dot{C}_{\max,sh}}$	
	$A_{sh} = \eta_{sh} A_e$	
	$UA_{sh} = U_{sh} A_{sh}$	
	$NTU_{sh} = UA_{sh} / \dot{C}_{\min,sh}$	
	$\varepsilon_{sh} = f_{he}(NTU_{sh}, C_{sh})$	
	$\dot{Q}_{sh} = \varepsilon_{sh} \dot{C}_{\min,sh} (T_{e,i} - T_{r,e,sat})$	
	$T_{e,mid} = T_{e,i} - \dot{Q}_{sh} / \dot{C}_{e,sh}$	
	$T_{r,e,o} = \dot{Q}_{sh} / \dot{C}_{r,e,sh} + T_{r,e,sat}$	
Evaporation Zone	$\dot{C}_{r,e,ev} = (\dot{m}Cp)_{r,e,ev}$	(3-14)
	$\dot{C}_{e,ev} = (\dot{m}Cp)_{e,ev}$	
	$C_{ev} = \{phase \quad change\} = 0$	
	$A_{ev} = \eta_{ev} A_e$	
	$UA_{ev} = U_{ev} A_{ev}$	
	$NTU_{ev} = UA_{ev} / \dot{C}_{e,ev}$	
	$\varepsilon_{ev} = f_{he}(NTU_{ev})$	
	$\dot{Q}_{ev} = \varepsilon_{ev} \dot{C}_{e,ev} (T_{e,mid} - T_{r,e,sat})$	
	$T_{e,o} = T_{e,mid} - \dot{Q}_{ev} / \dot{C}_{e,ev}$	
	$\dot{Q}_{ev,cal} = \dot{m}_{r,e} i_{fg}$	(3-15)
	$\dot{Q}_e = \dot{Q}_{ev} + \dot{Q}_{sh}$	(3-16)

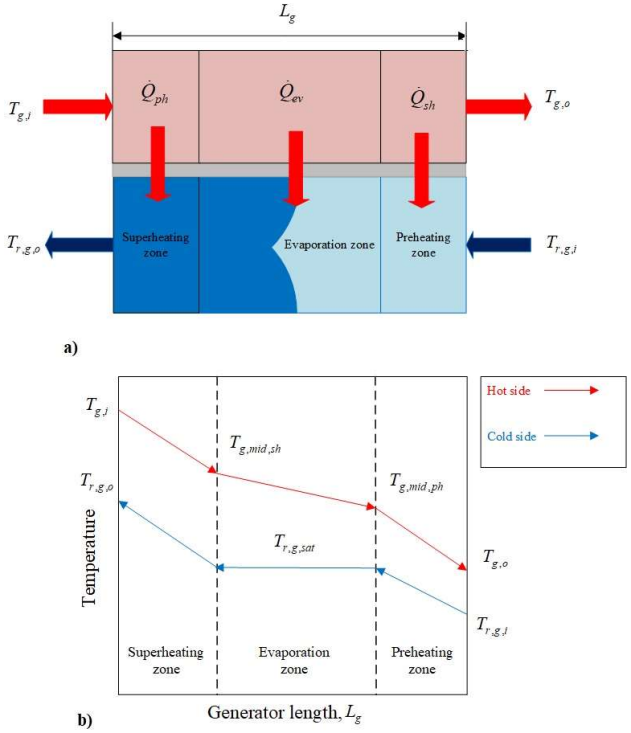

Figure 3-2: (a) Heat transfer along the three zones of the generator (b) thermal plan of both sides

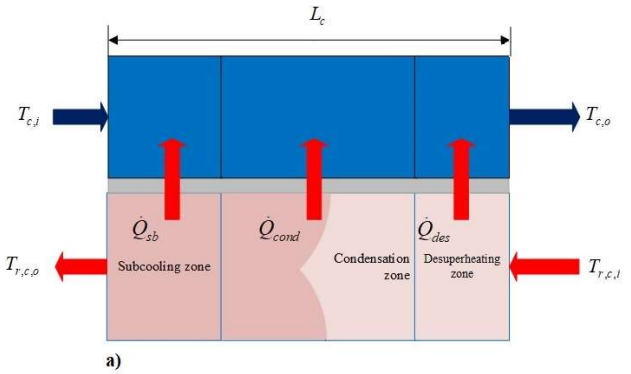

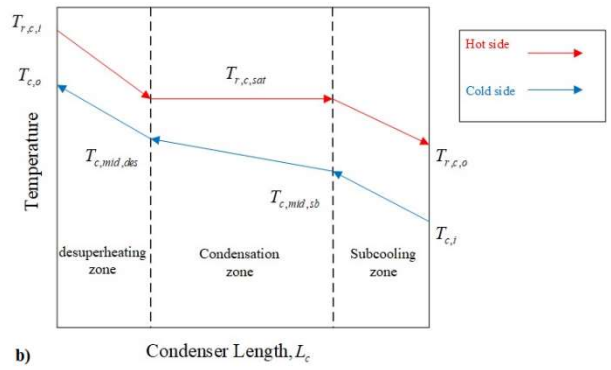

Figure 3-3: (a) Heat transfer diagram along the three zones of condenser (b) thermal plan of both sides

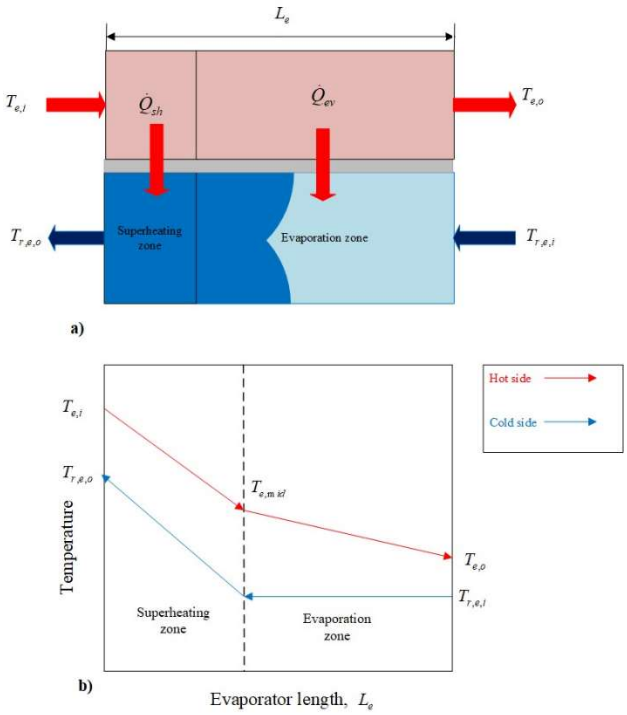

Figure 3-4: (a) Heat transfer diagram along the evaporator's two zones (b) thermal plan of both sides

The parameter U expresses the global heat transfer coefficient (kW m^2 $°C^{-1}$) between the refrigerant and the thermal fluid in each zone of the heat exchangers and is defined using the following equation for a plate heat exchanger:

$$\frac{1}{U} = \frac{1}{h_r} + \frac{1}{h_{th}} \qquad (3\text{-}17)$$

Where h_r and h_{th} are the convective heat transfer coefficients of the refrigerant and thermal fluid side, respectively.

Furthermore, the function f_{he} used to evaluate the ε refers to the heat-exchanger-specific curve used within the effectiveness-NTU method [141].

3.4. Results and discussion

In order to validate the model, experimental data obtained by Hamzaoui et al. [30] were used. The primary flow pressure is chosen as a disturbance to validate the developed models. The interval of variation ranges from 484 kPa to 538 kPa.

3.4.1. Effect of the Primary Flow Pressure on Heat Transfer

Figure 3-5 shows the comparison between numerical and experimental ERS performance based on COP, which is defined as:

$$COP = \frac{\dot{Q}_e}{\dot{Q}_g} \tag{3-18}$$

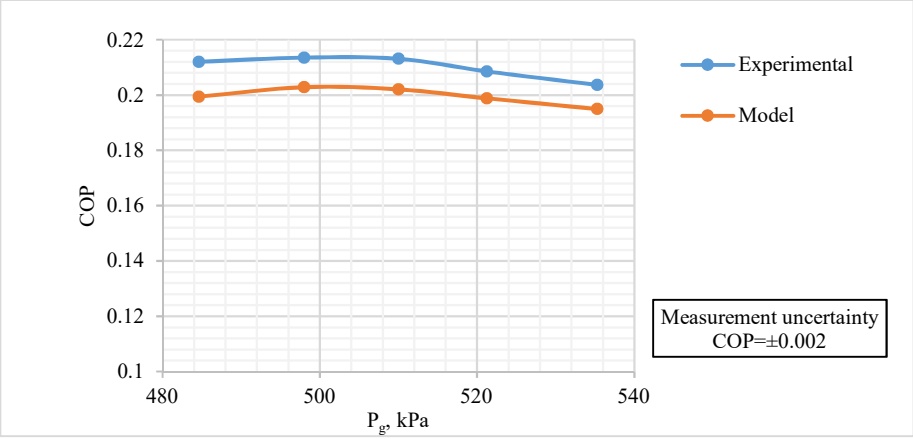

Figure 3-5: Variation of the COP the primary flow pressure

It is observed that generally the COP decreases with an increase in the primary flow pressure. This is because the cooling load in the evaporator is kept constant while the thermal input at the generator increases with a rise in the primary flow pressure as presented in Figure 3-6.

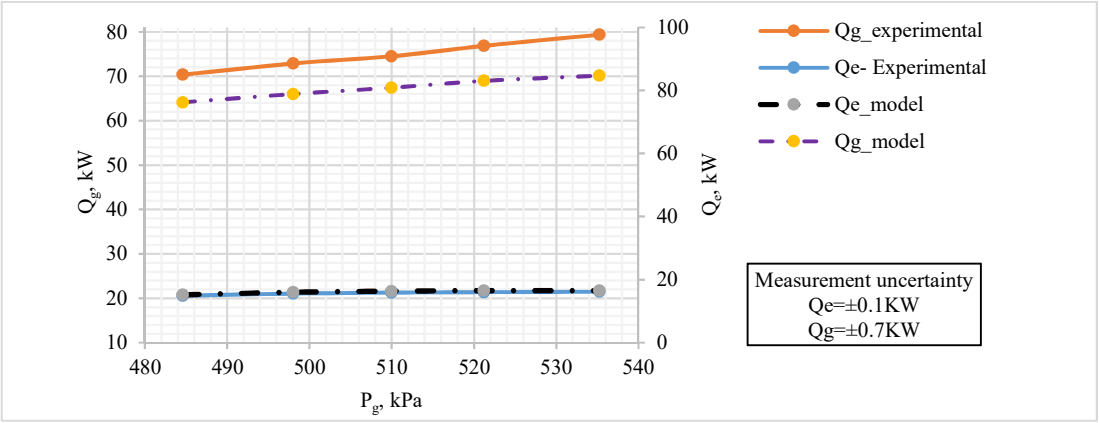

Figure 3-6: Variations of $\dot{Q}_e$ and $\dot{Q}_g$ with the primary flow pressure

Figure 3-7 shows the influences of the primary flow pressure on the predicted thermal conductance (UA) of the evaporator and generator. It can be seen from Figure 3-7 that the UA increases linearly as a function of the primary flow pressure in the generator. However, in the evaporator, there is an optimum primary flow pressure where the minimum UA can be obtained. It can be explained by the fact that in the generator both the primary mass flow rate and the heat transfer rate increase while the temperature difference between two sides decreases with rising the primary flow pressure and consequently, UA increases sharply. On the other hand, in the evaporator, the mass flow rate of the secondary stream remains almost constant and the UA is strongly dependent on the logarithmic temperature difference (ΔT_{lmtd}) between the two sides and the thermal load, which rises to a maximum point then decreases with augmenting the primary flow rate (Figure 3-8).

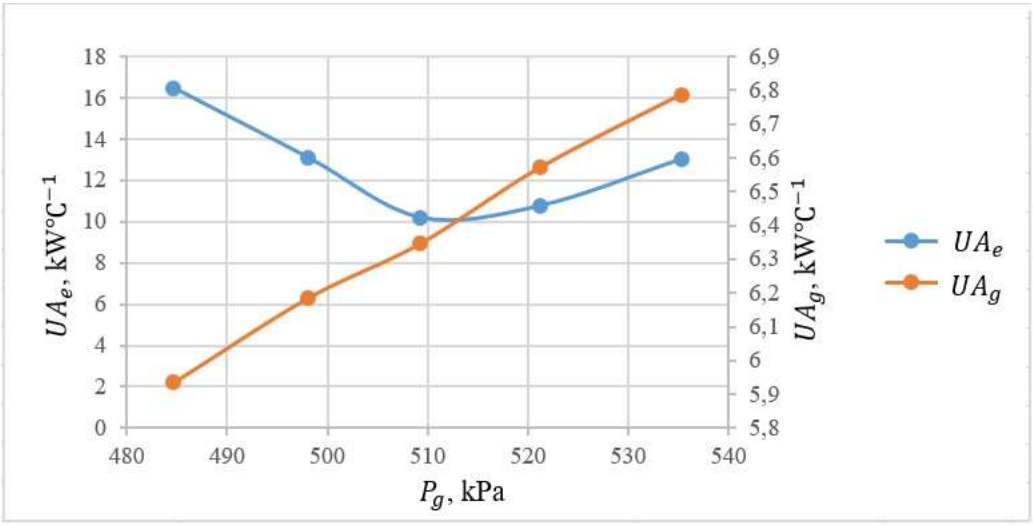

Figure 3-7: Variations of UA in the generator (UA_g) and evaporator (UA_e) with the primary flow pressure

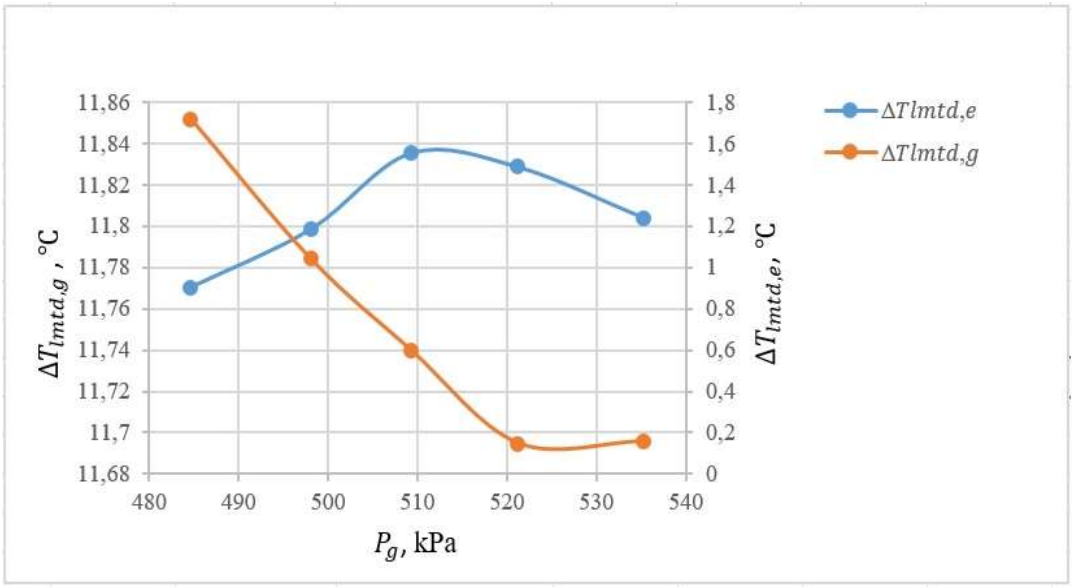

Figure 3-8: Variations of ΔT_{lmtd} in the generator (g) and evaporator(e) with the primary flow pressure

It is believed that the minimum logarithmic temperature difference in the evaporator is related to the minimum evaporation pressure (secondary pressure) at the same point, which is shown in Figure 3-9. The thermal conductance can be crucial from the point of view of the fixed costs and the size of the refrigeration system. The larger the UA, the larger heat exchanger is required.

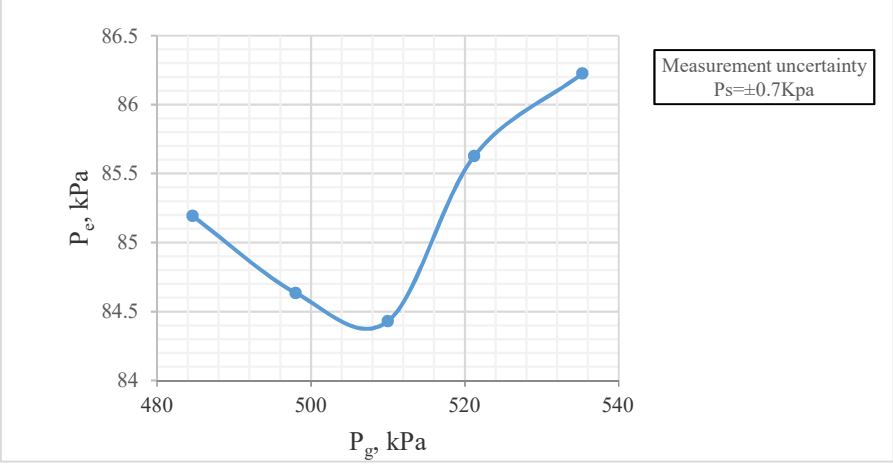

Figure 3-9: Variation of the Secondary Stream Pressure (P_e) with the primary stream pressure (P_g)

3.4.2. Effect of the Primary Flow Rate on the Exergy Efficiency (η_{II}) of the ERS

The exergy analysis of the ERS system can be beneficial to evaluate the irreversibility decrease for the cycle. Here, the exergy efficiency is used as another indicator to demonstrate the efficiency of the ERS defined as follows [142]:

$$\eta_{II} = \frac{E_e}{E_g + W} \tag{3-19}$$

where E_e, E_g and W are exergy of heat rates in the evaporator and generator and pump work, respectively. The pump work is negligible and is not included in the exergy efficiency calculations. To evaluate the exergy of the heat rate the following equations are used:

$$E_e = \dot{Q}_e \left| 1 - \frac{T_r}{T_{sc,e}} \right| \tag{3-20}$$

$$E_g = \dot{Q}_g \left| 1 - \frac{T_r}{T_{sc,g}} \right| \tag{3-21}$$

$$T_{sc,e} = \frac{T_{e,i} + T_{e,o}}{2} \tag{3-22}$$

$$T_{sc,g} = \frac{T_{g,i} + T_{g,o}}{2} \tag{3-23}$$

T_r is the surrounding temperature. The second law or exergy efficiency of the cycle is evaluated using the following formula:

$$\eta_{II} = \frac{\dot{Q}_e \left| 1 - \frac{T_r}{T_{sc,e}} \right|}{\dot{Q}_g \left| 1 - \frac{T_r}{T_{sc,g}} \right|} = COP \frac{\left| 1 - \frac{T_r}{T_{sc,e}} \right|}{\left| 1 - \frac{T_r}{T_{sc,g}} \right|} \tag{3-24}$$

Figure 3-10 depicts the influence of the increase of the primary flow pressure on the exergy efficiency. With the rise in the primary stream pressure, the exergy efficiency increases initially to a maximum value and then decreases. The reason can be explained based on the variation of COP with the primary flow pressure and the second factor of the Eq. (3-24). The COP decreases with augmenting the primary flow pressure, however, the second term of the Eq. (3-24) first increases slightly and then decreases with rising the primary pressure.

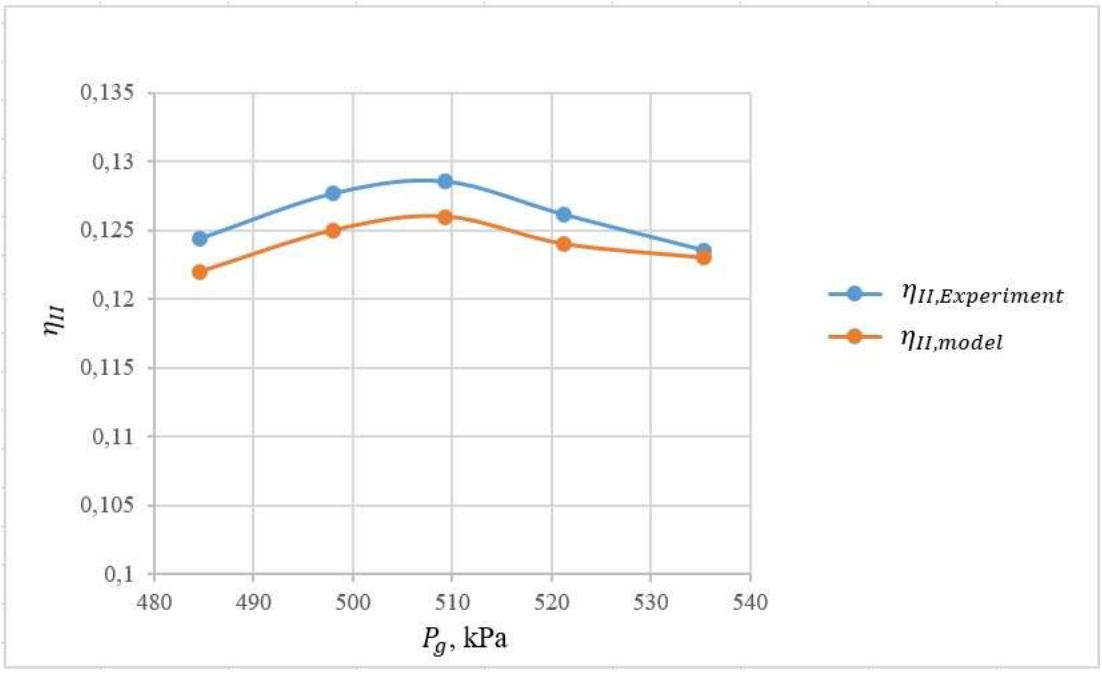

Figure 3-10: Effect of the primary flow pressure on the exergy efficiency

3.5. Conclusions

In the present study, the steady state models of the heat exchangers in an ERS using R245fa refrigerant were developed with EES software. The Moving Boundary method was utilized to study the heat exchangers by calculating the thermal loads, the outlet temperatures of both sides and length factors of various zones at different operation conditions. The proposed model was validated with experimental data, which showed a good agreement. The developed model was used to predict the impact of the primary flow pressure on the COP and η_{II} and it was revealed that increasing the primary flow pressure results in COP drop while η_{II} rises to a maximum point before decreasing.

3.6. Acknowledgment

This project is a part of the Collaborative Research and Development (CRD) Grants Program at 'Université de Sherbrooke'. The authors acknowledge the support of the Natural Sciences and Engineering Research Council of Canada, Hydro-Québec, Rio Tinto, Alcan and Canmet ENERGY Research Center of Natural Resources Canada.

3.7. Nomenclature

Table 3-2: Nomenclature

Symbols	Definition
A	Total heat transfer surface area of a heat exchanger, [m^2]
P	Pressure, [kPa]
$\dot{m}$	Mass flow rate, [kg s^{-1}]
T	Temperature, [°C]
h	Convective heat transfer coefficient, [kWm^{-2}°C^{-1}]
C	Capacity ratio, [-]
$\dot{C}$	Capacitance rate, [kJ. s^{-1}.°C^{-1}]
Cp	Specific heat, [kJ kg^{-1}. °C^{-1}]
U	Overall heat transfer coefficient, [kWm^{-2}. °C^{-1}]
i_{fg}	latent heat of vaporization (condensation) at the heat exchanger pressure, [kJ kg^{-1}]
W	Pump work, [kW]
ΔT_{lmtd}	Logarithmic temperature difference, [°C]
subscripts	
c	Condenser
e	Evaporator
g	Generator
s	Secondary
p	Primary
i	Inlet
o	Outlet
Greek characters	
ε	Effectiveness factor
ρ	Density, kg m^{-3}
η_{II}	Exergy efficiency, [%]
η_{sh}	Length factor for superheating area
η_{ev}	Length factor for evaporation area
η_{ph}	Length factor for preheating area
η_{des}	Length factor for desuperheating area
η_{cond}	Length factor for condensation area
η_{sb}	Length factor for subcooling area
Abbreviation	
COP	Coefficient of performance

CHAPTER 4 Numerical and experimental investigation of the influence of generating pressure on the performance of a one-phase ejector installed within an R245fa refrigeration cycle

Avant-propos

Auteurs et affiliation:

Elhameh Narimani: étudiant au doctorat, faculté de génie, département de génie mécanique, Université de Sherbrooke

Mikhail Sorin: professeur, faculté de génie, département de génie mécanique, Université de Sherbrooke.

Philippe Micheau: professeur, faculté de génie, département de génie mécanique, Université de Sherbrooke.

Hakim Nesreddine: PhD, Chercheur-Chargé de projet, Laboratoire des technologies de l'énergie, Shawinigan (Québec), Canada

Date d'acceptation : 17 April 2019

État de l'acceptation : acceptée

Revue: Applied Thermal Engineering Journal

Titre français: Étude numérique et expérimentale de l'influence de la génération de pression sur les performances d'un éjecteur monophasé installé dans un cycle de réfrigération R245fa

Contribution au document:

Le chapitre suivant de cette thèse étudie l'impact de la pression générée sur la performance du système SRE à l'aide d'études numériques et expérimentales. Le nouveau modèle 1D de l'éjecteur installé dans un système SRE a été utilisé pour expliquer les raisons des phénomènes observés.

Résumé en français:

Le taux de compression le plus élevé (*Cr*) d'un système de réfrigération à éjecteur peut garantir le rendement élevé de ces systèmes. Le présent article étudie l'impact de la génération de pression sur le *Cr* pour l'éjecteur installé dans un SRE. Des techniques de traitement du signal ont été appliquées pour analyser les signaux acquis d'un système de réfrigération à éjecteur R245fa et ont révélé l'existence d'un bruit périodique dans les données expérimentales. La méthode de filtrage à moyenne mobile a atténué le bruit périodique des signaux et ainsi amélioré la précision de la mesure expérimentale. Ensuite, l'influence de la pression générée sur les performances de l'éjecteur a été étudiée à l'aide des données expérimentales filtrées, pour différentes températures de condenseur de 20 à 24°C. Il a été observé qu'il existe une valeur optimale de la pression génératrice qui maximise simultanément l'éjecteur *Cr* et minimise la pression d'aspiration. Le modèle thermodynamique 1-D développé de l'éjecteur a montré que l'éjecteur fonctionne en mode sous-critique lorsque la pression générée est inférieure au point optimal de *Cr*, tout en fonctionnant en mode critique à une valeur égale ou supérieure à cette pression de production optimale.

4.1. Abstract

The highest compression ratio (*Cr*) of an ejector refrigeration system could guarantee the high efficiency for such systems. The present paper studied the impact of generating pressure on *Cr* for the ejector installed in an ERS. Signal processing techniques were applied to analyse the acquired signals of an R245fa ejector refrigeration system and revealed the existence of periodic noise in the experimental data. The moving average filtering method eliminated the periodic noise from the signals and improved the experimental precision. Then, the influence of the generating pressure on the ejector's performance was studied using the filtered experimental data, for different condenser temperatures ranging from 20 to 24°C. It was observed that there is an optimum value of the generating pressure that simultaneously maximizes the ejector *Cr* and minimizes the suction pressure. The developed 1-D thermodynamic model of the ejector showed that the ejector operates in the subcritical mode when the generating pressure is below the Cr optimum point, while operates in critical mode at or above this optimum generating pressure.

Keywords: Ejector refrigeration system (ERS), compression ratio (*Cr*), signal processing, moving average filtering, periodic noise

4.2. Introduction

Ejector refrigeration system (ERS) is known as an appropriate alternative for the conventional vapor compression refrigeration due to its environmental and economic benefits as well as its capability in using the low-grade thermal energy available from the industrial waste heat, solar collector and so forth. However, because of its low coefficient of performance (COP) compared with that of the mechanical refrigeration cycles, it was not utilized in the large industrial scales. Recently, with a significant increase in the cost of the energy and a decrease in the energy resources, the ejector refrigeration systems are concentrated.

Improving the performance of ERS is a crucial objective, which can be quantified in terms of COP, entrainment ratio (ω) and *Cr*. It has been suggested by several experimental and theoretical studies that the performance of an ejector refrigeration system is strongly dependent on the pressure and temperature of the evaporator, generator, and condenser [23][143][20].

The effective parameters to increase COP and entrainment ratio have been investigated in preceding studies. The most recent results in this field can be found in the studies conducted by Chunnanond and Aphornratana [129], Huang et al. [29] Eames et al. [130], Thongtip and Aphornratana (a) [22], Chen et al. [131]. Based on these work, it was observed that increasing the temperature of the generator at a fixed temperature of the condenser (at the ejector backpressure) would lead to a rise in COP to an optimum point. Afterwards, the further increase in the temperature of generator will reduce the COP [21]. On the other hand, at a given boiler temperature, increasing the saturation temperature of the secondary flow (evaporator), increases the COP in a critical mode and subcritical modes [131].

Thongtip and Aphornratana [27] conducted an experimental study using different ejector throat diameters (2.8, 3.2 and 3.8 mm), with identical area ratios (4.6), and with nozzle exit Mach number of 2.5. They observed that for a particular ejector geometry there is an optimal range of the primary fluid mass flow rate that produces the lowest suction pressure at a specified condenser pressure. They mentioned that the advantage of increasing of the

primary fluid mass flow rate to the optimum value is that the ejector would operate at a higher critical condenser pressure.

Jia and Wenjian [144] investigated an air-cooled ejector refrigeration cycle with R134a refrigerant in six various area ratios varying from 2.74 to 5 .They observed that the primary flow pressure strongly influences the performance of the ejector in which there is an optimum primary flow pressure that maximizes entrainment ratio in the fixed back pressure and secondary stream pressure.

Hamzaoui et al. [30] demonstrated the design characteristics and the operation performances of a constant geometry ERS using R245fa with an ejector area ratio of 2.84. They found out that an increase in the generating pressure raises *Cr* to a maximum value. However, the reason for the existence of the maximum *Cr* with increasing generating pressure is not clearly discussed in the preceding studies, and there is still a gap in the literature that investigates the influence of the generating pressure on ERS operating parameters, especially *Cr*.

Furthermore, there are always some unwanted disturbances in the signals of the experimental set-ups that reduce the precision of the experimental study and it was not investigated in the preceding studies in this this field. Signal processing deals with noisy signals in order to remove or reduce the unwanted disturbance using the transformation of signals to forms that could be more informative [145][146]. To process the measurement signals of a system, usually Fourier Transform (FT) is used, which converts the signals from the time domain to the frequency domain.

In the present work the impact of generating pressure on the performance parameters of the ERS, from the points of view of the suction pressure and *Cr*, will be studied using both experimental and numerical methods. The main purpose of this study is to explain the reasons for the existence of maximum *Cr* that occurs when generating pressure is augmented by means of a new 1-D thermodynamic model.

First, the spectral analysis of the ERS signals was conducted. It revealed that there was a periodic disturbance in the experimental data signals. Thus, the Moving average filtering

[147] method was applied to eliminate the periodic disturbance from the experimental data. The filtered experimental data showed the existence of an optimum generating pressure that simultaneously maximizes *Cr* and minimizes the suction pressure.

Second, in order to explain the reasons for the observed phenomenon, a new numerical model of the ejector was developed for a fixed geometry ejector (off-design) and was validated using the filtered experimental data. The unique feature of this model is related to the method it uses to recognize choking regime inside the ejector. It is able to show that the ejector operates in either the critical or the sub-critical conditions at the fixed thermal load of the evaporator using the secondary mass flux comparison with its maximum value in the hypothetical throat. Furthermore, it is the first time that the thermodynamic model of the ejector has been used to investigate the impact of the generating pressure on the suction pressure and *Cr* of the ERS.

4.3. Experimental setup

Figure 4-1 indicates the schematic view of the ejector refrigeration cycle. The experimental set-up is located at Laboratoire des technologies de l'énergie of Hydro-Quebec. The dimensions (mm) of the ejector are presented in Figure 4-2. Its area ratio is 3.89.

The selection of the proper working fluid plays a significant role in improving the performance of the refrigeration cycle. The Thermodynamic and physical properties of the working fluid should match the operating conditions of the process and meet the environmental and safety criteria. In order to have the safe and stable ejector operation in such systems, the compression/expansion process of the ejector should to be dry and droplet free. The dry working fluids satisfy this criterion. The working fluids can be categorized as a dry, isotropic, or wet fluid depending on the inverse of the slope of the saturation vapor curve on a T–s diagram ($\xi = \frac{dS}{dT}$). For a dry fluid the value of ξ is supposed to be positive (> 0) [15] [142]. Moreover, from the environmental point of view, the main concerns involve ozone depletion potential (ODP) and global warming potential (GWP).

In addition to all the mentioned selection criteria, R245fa (1, 1, 1, 3, 3-pentafluoropropane) was chosen as a working medium in this system for the following reasons:

- It is a dry refrigerant which avoids liquid droplet formation during the expansion that may deteriorates ejector's efficiency
- It has the high critical point (154 °C) that makes it convenient for heat recovery.
- Its operating pressure levels are low. This characteristic gives more flexibility and freedom in choosing pumps and mechanical devices.
- It is nearly non-toxic and non-flammable (based on ASHRAE 2013) [148].
- It has a Global Warming Potential (GWP) less than 1000, which is among the lowest in HFC family and a zero Ozone Depletion Potential (ODP).
- Its lifetime in the atmosphere is relatively short (7.2 years).

The heat transfer in the system is carried out through the counter-current brazed plate heat exchangers, which are employed as the condenser (300KW), generator (250 KW) and evaporator (35KW). The 250 kW electric boiler that delivers thermal energy to the ERS vapor generator simulates a waste heat source, using Propylene glycol (50/50 mass-based) as the thermal fluid. Furthermore, a 45 kW electric cartridge heater sends the input heat through the thermal fluid of the Ethylene glycol (50/50 mass-based) to the evaporator in order to simulate the cooling load. A cooling tower with capacity of 400 kW connected to the condenser forms the cooling loop. Propylene glycol (20/80) is used as the thermal fluid in this loop. Its temperature at the inlet of the condenser is controlled by means of a 3-way mixing valve with a standard deviation of ± 0.5 °C.

An electronic expansion valve (EEV) with 2500 steps connects to a controller expands the outlet stream of the condenser in an isenthalpic process to the evaporator pressure. The values of the temperature, pressure and mass flow rate at several points of the system are measured using T type thermocouples (accuracy ±0.5 °C) and pressure transducers (accuracy ±0.25% of reading in the operation pressure range) and Coriolis flow meters (accuracy: ±0.05% uncertainty over the respective flow ranges) respectively. The AC watt transducers (accuracies: ±0.2% reading) was used to measure the electric power provided to the boiler, the thermal load heater and the feed pump. The R245fa is supplied to the generator using a feed pump, which works based on a regenerative turbine impeller technology (known also as vortex pump), and is driven by a 3 hp motor [30]. A data acquisition system recorded the data generated at 5 seconds intervals and HP-VEE software was used to monitor, control

and analyze the produced data from the experimental set-up. The measurements locations for the temperature, pressure and mass flow rate are shown in Figure 4-3.

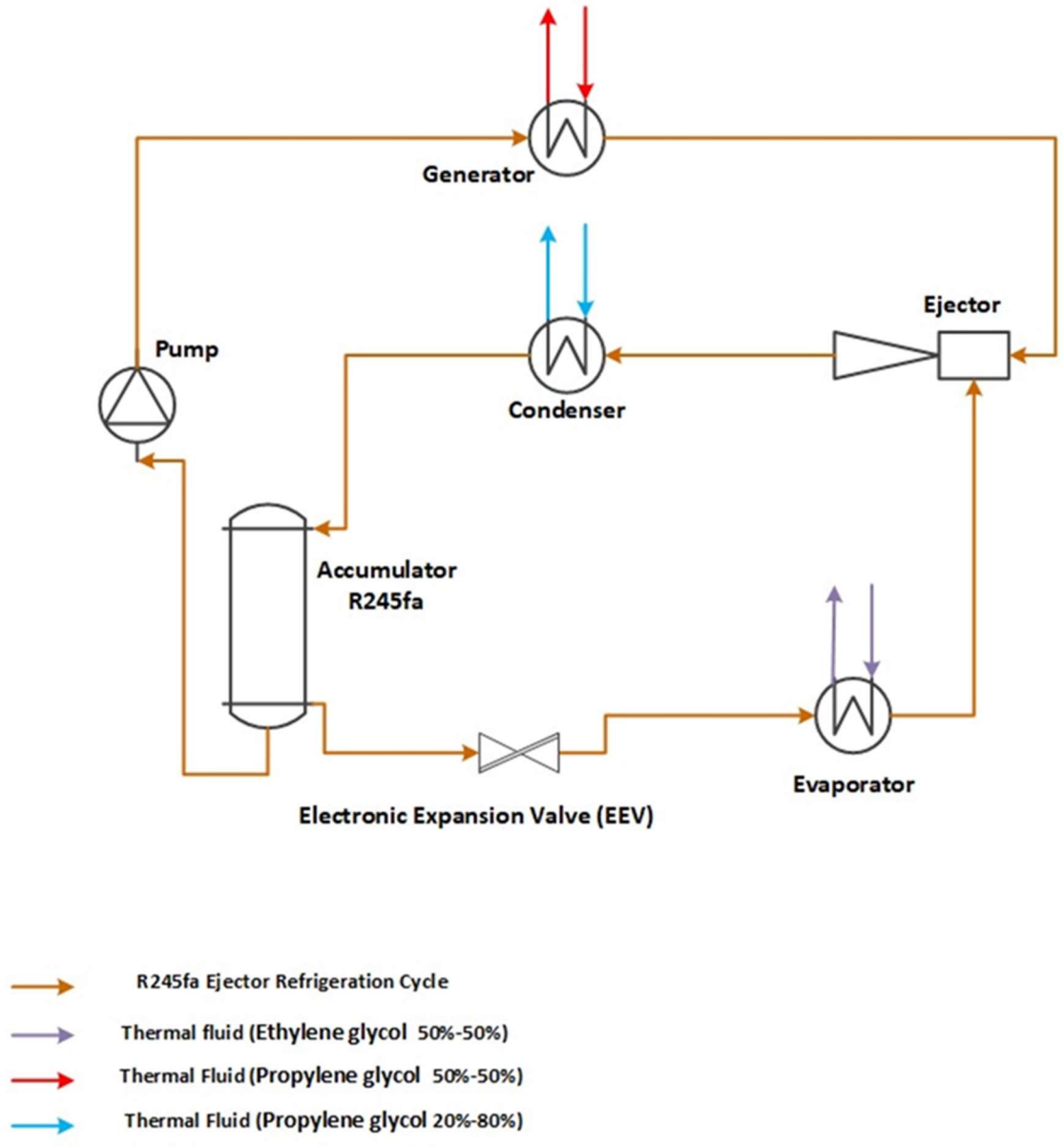

Figure 4-1: Schematic figure of an ejector-based refrigeration circle

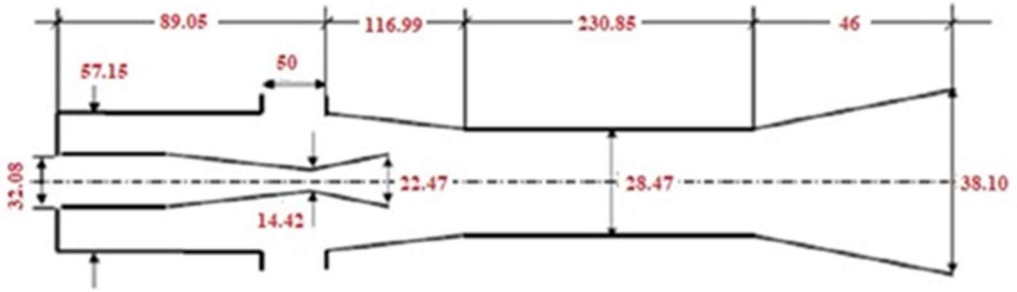

Figure 4-2: The dimensions (mm) of the applied ejector in ERS

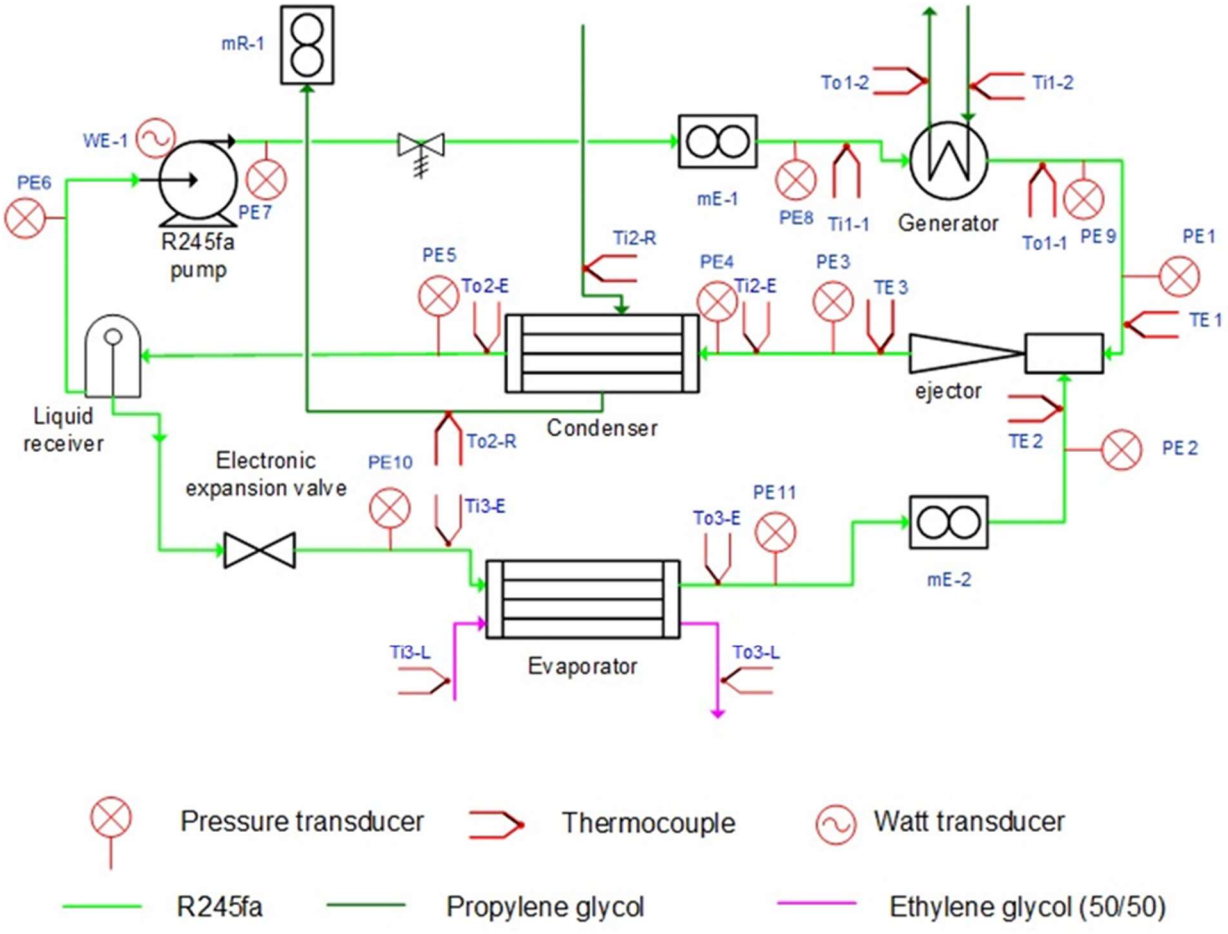

Figure 4-3: Schematic view of the measurements' locations in the experimental setup

4.4. Experimental Analyses

4.4.1. Statistical analyses

At various condenser temperatures (coolant inlet temperature,$T_{c,i}$) ranging from 20 to 24℃, the value of the primary stream mass flow rate ($\dot{m}_P$) was augmented by increasing the frequency of the feed pump, which resulted in an increase in the generating pressure (p_P). The cooling load, simulated with a 45 kW electric cartridge heater, is kept constant at 16 kW in this set of tests. The experimental data of the parameters should be normally distributed to evaluate the values of standard deviation and to estimate the precision of the experiments. The Kolmogorov-Smirnov test (kstest) was conducted and the histograms were plotted for the parameters including p_s and Cr to compare the equality of their probability distributions with the normal distribution. Figure 4-4 shows the histogram plots of the two important parameters and their Kstest results. The Kstest results returns a test decision for the null hypothesis, that the data in vector x comes from a standard normal distribution, against the alternative that it does not come from such a distribution. When the result is 1, it rejects the null hypothesis, thus the examined experimental data are not normally distributed and can not be investigated using standard deviation analysis.

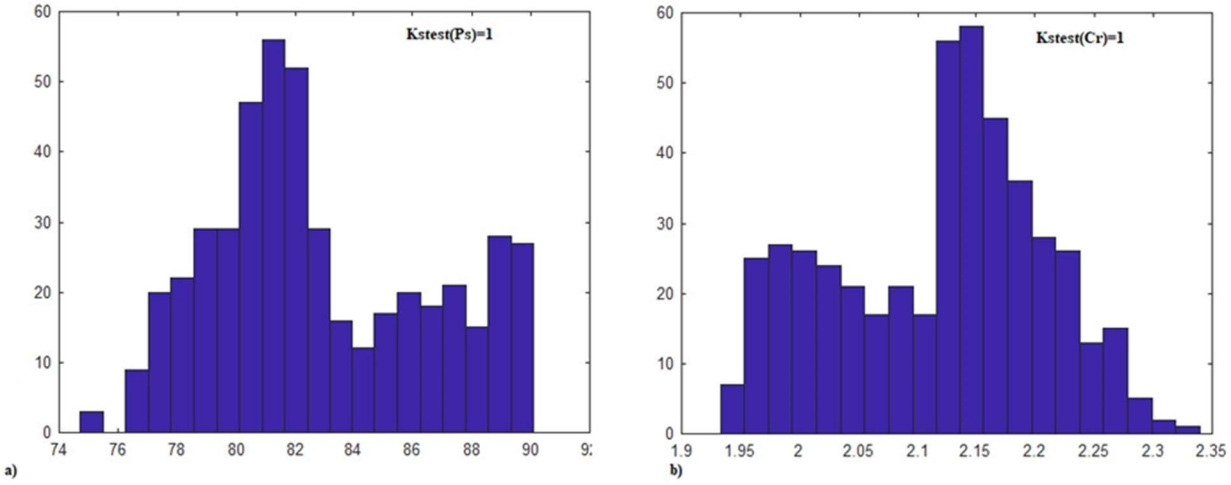

Figure 4-4: Histogram plots and results of Kstest for a) p_s b) *Cr* at p_P=483.71Kpa, $\dot{m}_P$=0.33 Kg/s, $T_{C,i} = 20$℃

4.4.2. Spectral analyses of the signals

For noisy data signals, as was the case during the experimental data collection, it is almost impossible to extract valuable information from the signals in the time domain. Hence, to analyse the periodic noise in the signals, a kind of Fourier transform (FT) called FFT (Fast Fourier transform) used which transforms the signals from the time domain to the frequency domain. The sampling time (T_e) of the experiments is about 5 seconds and the frequency of sampling is evaluated as the inverse of the sampling time.

Figure 4-5 presents the time evolution of four important signals and their frequency transformations in the frequency domain as well as their measured uncertainties. The disturbance time, T_{dist} or the period of the wave is the time it takes for one wavelength of the wave to pass a point in space or the time for one cycle to occur.

Figure 4-5(a) expresses that there is a strong peak at 0.00405 Hz in $\dot{Q}_e$ and some other weak harmonics at higher frequencies. The strongest peak is considered as the fundamental frequency of $\dot{Q}_e$. Having looked at the frequency spectra of the other signals, one can observe that there are the peaks at the same frequency as $\dot{Q}_e$. The reason of this phenomenon can be explained by the fact that the control valve of the electronic expansion valve was set on a set point of superheating degree in the evaporator (T_{she}). The fluctuation in $\dot{Q}_e$. alters the T_{she} and consequently $\dot{m}_s$ and p_s. As it was seen, the harmonic disturbance in $\dot{Q}_e$ caused the disturbance in other signals. It is believed that the fluctuation in the power of the electric cartridge heater used to simulate the thermal load of the evaporator is the source of the disturbance in $\dot{Q}_e$ and other signals.

In order to investigate the impact of generating pressure on the performance of ERS it is required to remove the periodic disturbance from the signals using the signal filtering techniques. The most common filter in digital signal processing is Moving average filtering due to its simplicity. The moving average filter is based on averaging a number of points from the input signal to produce each point in the output signal defined as follows [149]:

$$Y[i] = \frac{1}{N}\sum_{i=0}^{N-1} X[i-j] \tag{4-1}$$

To evaluate the value of N for each set of experiments (in various values of p_P), the following equations were applied:

$$N_c = \frac{T_{dist}}{T_e} = \frac{T_{dist}}{5} \tag{4-2}$$

$$N = round(N_c) \tag{4-3}$$

Where X [] and Y [] are the input and output signals, respectively. To evaluate the filtered signals the Filter function in Matlab was used. Then, the mean values and standard deviation values of the parameters were evaluated using the filtered data. The filtered vector of Cr was evaluated based on the Eq. (4-4):

$$Cr_{fr} = p_{cfr} / p_{efr} \tag{4-4}$$

The time evolution of the parameters and their filtered values using the moving average filter are shown in Figure 4-6. The moving average filter is a simple low pass filter and the most common filter in DSP, mainly because it is the easiest digital filter to understand and use. In spite of its simplicity, the moving average filter is optimal for a common task: reducing random noise while retaining a sharp step response. This makes it the premier filter for time domain encoded signals. Therefore, this filtering method was used in this study to remove the random noise from the experimental data. The red lines present the filtered values of the parameters. Based on Figure 4-6, the moving average filter could effectively remove the periodic disturbance from the experimental data. The uncertainties of filtered parameters are also indicated in Figure 4-6.

Figure 4-7 presents the impact of the generating pressure on *Cr* and suction pressure at various condenser conditions using the filtered experimental data. Based on Figure 4-7 (a) there is an optimum value of the generating pressure that maximizes *Cr*. At the same time, this optimum value of the generating pressure minimizes the secondary pressure (Figure 4-

7 (b). Thus, there is an optimum generating pressure that simultaneously maximizes the ejector *Cr* and minimizes the suction pressure, p_s.

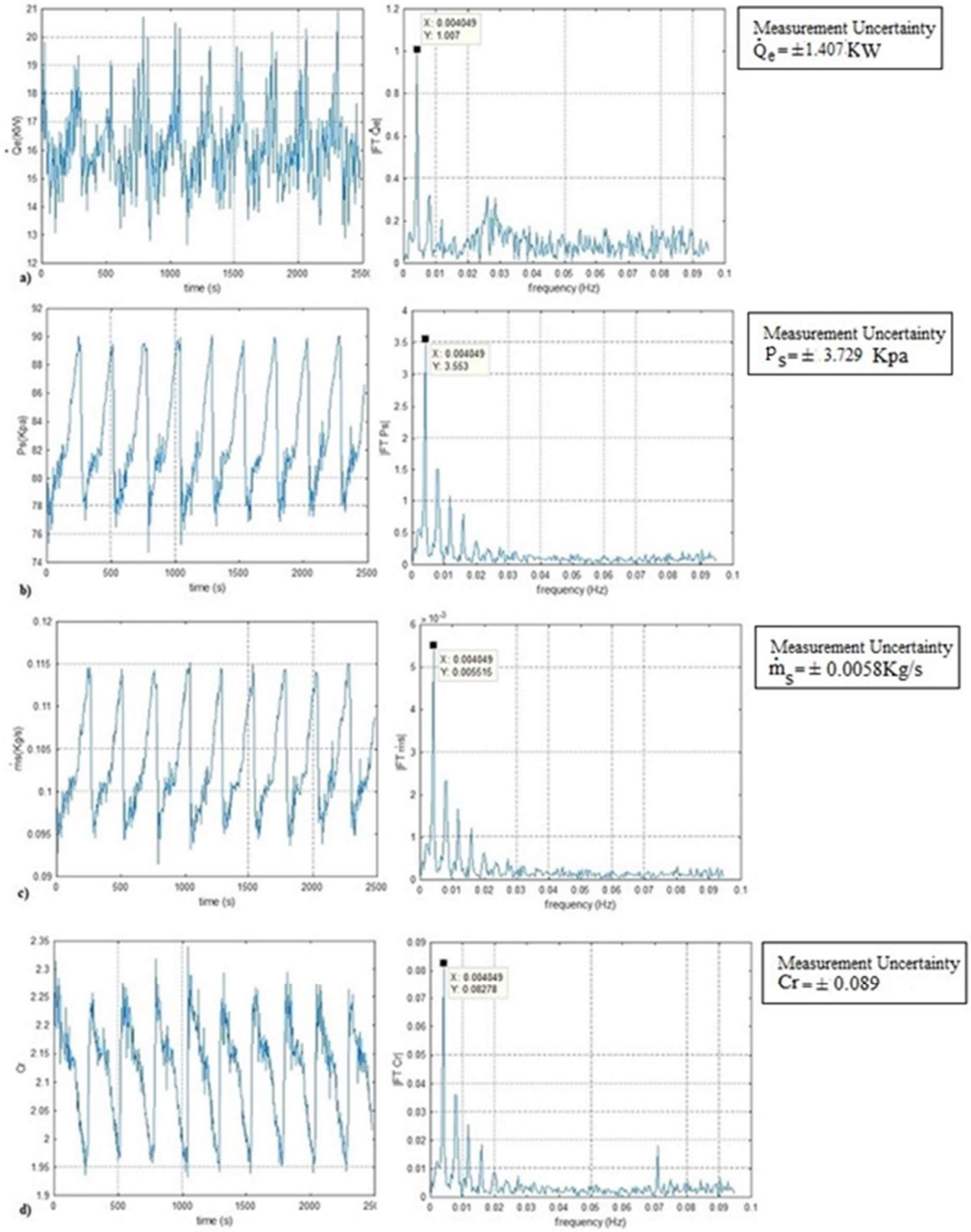

Figure 4-5: The time evolution and spectral analyses of a) $\dot{Q}_e$ b) p_s c) $\dot{m}_s$ d) Cr at T_{dist}=257s, p_P=483.71 Kpa, $T_{C,i} = 20$℃

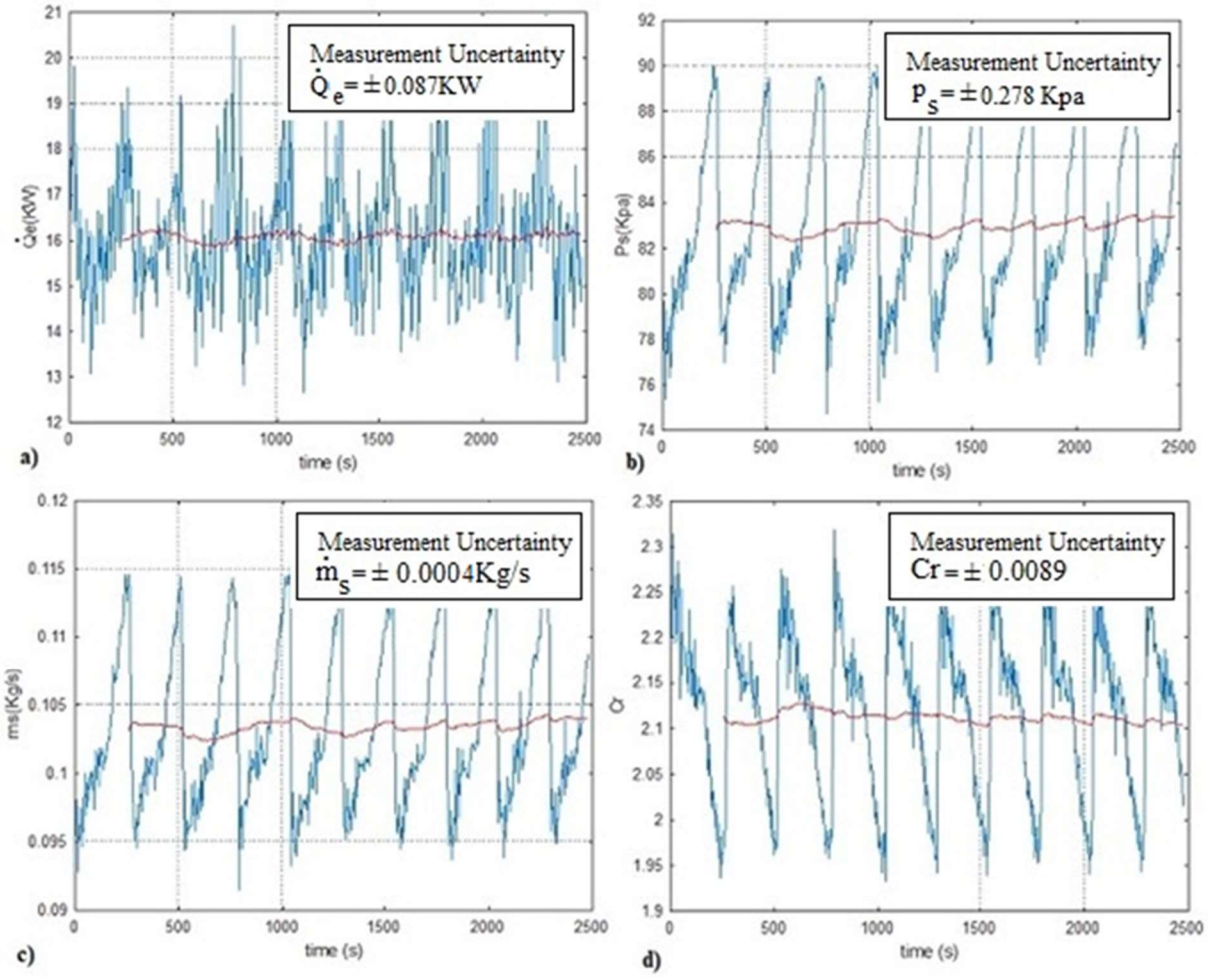

Figure 4-6: The variation of filtered parameters with time at p_P = 483.71 kPa, $\dot{m}_P$ = 0.33 kg/s, $T_{C,i} = 20$℃

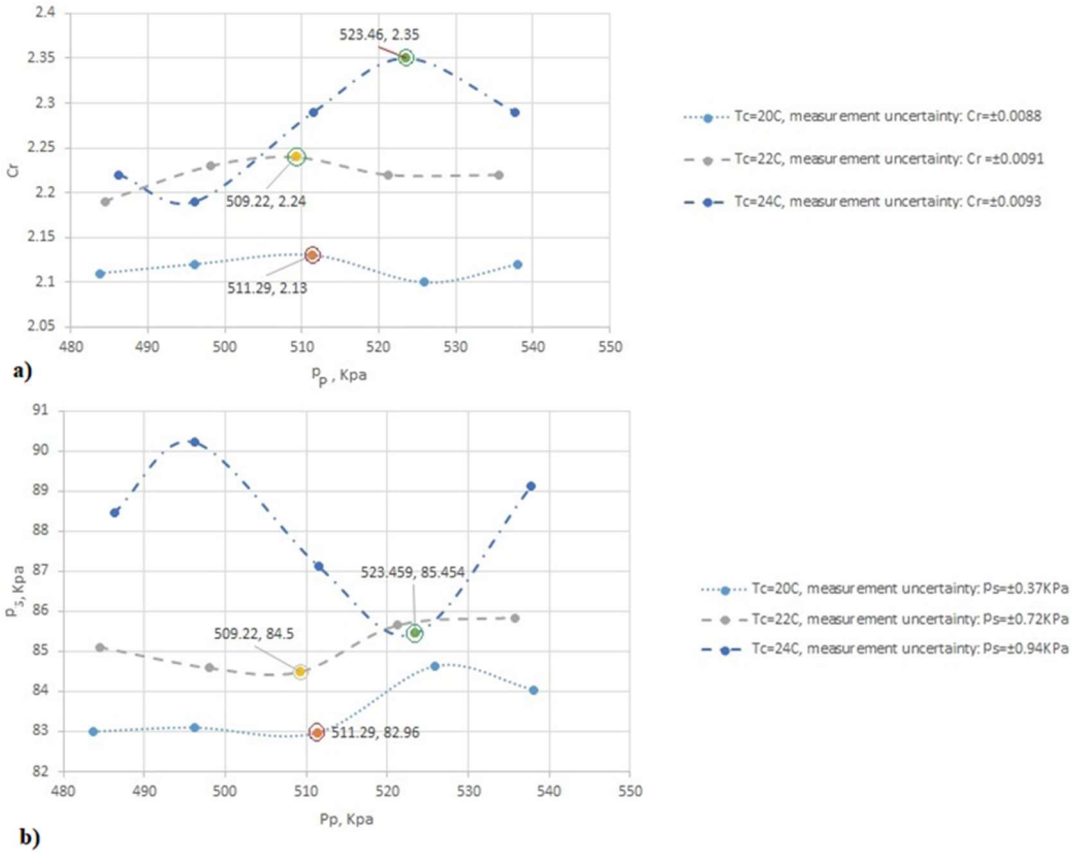

Figure 4-7: Experimental variation of a) Cr b) p_s with p_P

4.5. Modeling of the ejector

There are various models of the ejector in the literature [150] [151]. Due to the complexity of the mathematical description of the flow inside the ejector, most of the available ejector models are 1D thermodynamic models that only use the steady state explicit equations to find the state and operation parameters along the ejector. To study the flow phenomena along the ejector as well as in the radial direction, 2D and 3D models have been applied in the previous studies, which employed non-uniform velocity distribution in the cross-sectional area of the ejector. Keenan et al. [6] considered the mixing of primary and secondary streams could occur at the constant pressure inside the suction (mixing) chamber or in the constant area section. Huang et al. [151] assumed that constant-pressure mixing occurs inside the constant-area section of the ejector. Recently, Taslimi Taleghani et al. [150] developed a

model for two-phase ejector flow in which the surface area occupied by the secondary flow was used to distinguish between the single-choking and double-choking conditions.

In this study, the thermodynamic model was used to solve the equations in one dimension and the variations in the radial flow was ignored since the goal of this work is evaluation of the operation parameters along the ejector. The ejector model developed in this work uses the non-constant mixing pressure assumptions for the both single-choking and double-choking conditions. However, unlike the work of Taslimi Taleghani et al. [150], the mixing efficiency was included in the momentum balance to consider the momentum losses during mixing.

Previously, some studies have also included the friction losses in the mixing process using the mixing efficiency in the constant pressure mixing assumption. [130] [142] [151] [11]. The proposed model in the present study applies the secondary mass flux comparison with the maximum secondary mass flux in the hypothetical throat to define the type of choking regime in the ejector, which is considered as the unique feature of this model.

Refer to Figure 4-8 for the following description of developed model.

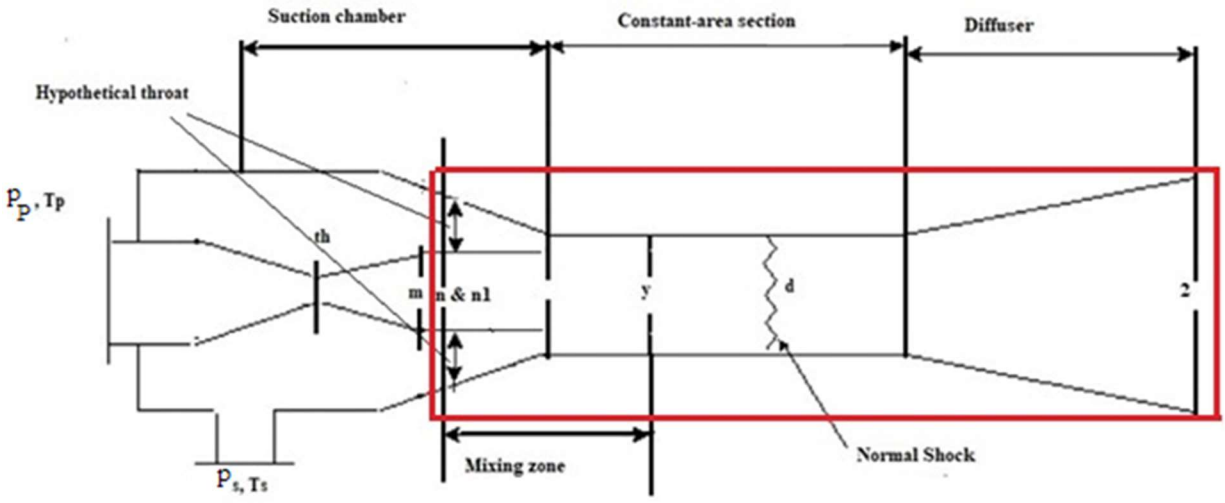

Figure 4-8: Schematic of the modeled ejector

To develop the ejector model, some of the assumptions made by the previous studies are applied [11][12] [142] [150]:

1) It is assumed that the flow inside the ejector is one-dimensional, steady state and adiabatic.

2) The primary (point P) and secondary (point s) flows are supplied to the ejector with zero velocity. Furthermore, the velocity of compressed flow at the outlet of diffuser is negligible (stagnation condition).

3) The primary stream expands until the exiting of the primary nozzle and creates the hypothetical throat for the secondary stream.

4) The back pressure of the ejector (p_2) equals to the condenser pressure (p_C).

5) Mass flux maximization criterion is used for both nozzles as applied by several studies [150][142] [11][12].

6) The friction losses of the mixing are included in the momentum balance using the constant mixing efficiency.

7) The normal shock occurs somewhere in the constant- area section where the mixing is complete.

8) The working fluid is a real gas.

This model assumed that based on the gas dynamics, the primary flow at the throat and the secondary flow at the hypothetical throat could not be sonic due to the friction losses in both streams included in the equations as the isentropic efficiencies. The same assumption was used by Eldakamawy et al. [142]. The reason of the frictional losses in the mixing process can be explained based on the Fanno flow rule in which the supersonic primary stream exiting the primary nozzle mixes with the sonic (in the critical mode) secondary flow. As a result, there is a pressure rise in the mixed flow which causes the mixed flow deceleration [152].

Based on these assumptions, the governing equations for the ejector including conservation equations of the mass, momentum and energy are solved to evaluate the pressure and properties of the refrigerant stream at the exit point of the diffuser (point 3) as well as the pressure of the secondary flow (point 2).

The values of the primary stream flow rate and consequently its pressure increase incrementally in a constant generator inlet condition ($T_{g,i}$). This model was validated using the filtered experimental data at three values of the condenser temperature ranged $20-24$ ℃ ($T_{C,i}$) .

The ejector model flowchart is shown in Figure 4-9 based on which the input parameters to this model are as follows:

- Temperature and pressure of the primary stream
- The mass flow rates of the primary and secondary streams
- The pressure of the condenser
- The primary, suction and diffuser nozzles isentropic efficiencies, as well as the mixing efficiency ($\eta_n, \eta_s, \eta_d, \varphi_{mi}$)
- The geometry of the ejector including the primary throat diameter (D_{th}), constant-area section diameter (D_1), the diameter of the divergent part of the primary nozzle (D_{m}) and the diffuser exit diameter (D_2)

The solution begins with an estimated value for the suction pressure and, following the steps presented in the flowchart in Figure 4-9, the value of the pressure at the ejector outlet is evaluated (p_2). The detailed model is explained as follows:

1) Primary and secondary streams (cross sections “th”, “n”)

The pressure of the primary flow in the cross section (th) is evaluated in an iterative solution using the assumption of the maximum mass flux in the throat. The iterative solution starts with an assumed value of the generating pressure in the throat and in each iteration; the pressure is reduced until obtaining the maximum mass flux.

$$p_{th} = p_p - \Delta p \tag{4-5}$$

$$S_{th} = S_p = Entropy(T_P, p_p) \tag{4-6}$$

$$h_{th,s} = Enthalpy(p_{th}, S_{th}) \tag{4-7}$$

$$h_{th} = \eta_P (h_{th,s} - h_P) + h_P \tag{4-8}$$

$$U_{th} = \sqrt{2(h_P - h_{th})} \tag{4-9}$$

$$\rho_{th} = Density(p_{th}, h_{th}) \tag{4-10}$$

$$G_{th} = \rho_{th} U_{th} \tag{4-11}$$

The iterative solution evaluates the acceleration of the secondary stream in its hypothetical throat "n" based on the maximum mass flux assumption at this cross section. The estimated value of the secondary pressure at cross section "n" is reduced to a value in which the mass flux reaches its maximum value, (G_n). Then, the surface area of the hypothetical throat is calculated using the secondary stream mass flux ($A_{s,m}$).

$$p_n = p_s - \Delta p \tag{4-12}$$

$$S_n = S_s = Entropy(T_s, p_s) \tag{4-13}$$

$$h_{n,s} = Enthalpy(p_n, S_n) \tag{4-14}$$

$$h_n = \eta_s (h_{n,s} - h_s) + h_s \tag{4-15}$$

$$U_n = \sqrt{2(h_s - h_n)} \tag{4-16}$$

$$\rho_n = Density(p_n, h_n) \tag{4-17}$$

$$G_n = \rho_n U_n \tag{4-18}$$

$$A_{s,m} = \frac{\dot{m}_s}{G_n} \tag{4-19}$$

However, it should be taken into account that the secondary stream cannot always chock inside the suction chamber. Thus, the real expansion of the secondary stream is evaluated in an iterative calculation at the hypothetical throat using the evaluated surface area ($A_{s,m}$) of the hypothetical throat. The iteration starts with an assumption of the secondary stream pressure in the hypothetical throat and the conservations of the mass, energy and momentum are solved using isentropic efficiency of the suction chamber. Then, the pressure is corrected until satisfying the secondary stream mass conservation at this cross section and the mass flux is calculated ($G_{n,1}$).

$$p_{n,1} = p_s - \Delta p \tag{4-20}$$

$$S_{n,1} = S_s \tag{4-21}$$

$$h_{n,1s} = Enthalpy(p_{n,1}, S_{n,1}) \tag{4-22}$$

$$h_{n,1} = \eta_s (h_{n,1s} - h_s) + h_s \tag{4-23}$$

$$U_{n,1} = \sqrt{2(h_s - h_{n,1})} \tag{4-24}$$

$$\rho_{n,1} = Density(p_{n,1}, h_{n,1}) \tag{4-25}$$

$$\dot{m}_{s,1} = \rho_{n,1} U_{n,1} A_{s,m} \tag{4-26}$$

$$G_{n,1} = \rho_{n,1} U_{n,1} \tag{4-27}$$

1) Mixing

The value of the secondary mass flux in the hypothetical throat ($G_{n,1}$) is compared with the maximum mass flux G_n. If $G_{n,1} \approx G_n$, then the secondary stream chokes inside the suction chamber and the ejector operates in the double-choking (critical mode). However, for $G_{n,1} \neq G_n$, the ejector operates at sub-critical mode and the secondary stream does not choke inside the suction chamber. Furthermore, in the divergent part of

the primary stream, the pressure of the primary stream is assumed to reach the same pressure as the secondary stream at its hypothetical throat. Then, the conservations of the momentum and energy using the isentropic efficiency of the primary nozzle are solved to obtain the properties of the primary stream at this cross-section ("m").

In both cases, the secondary and primary streams immediately start to mix at cross section "n" based on the non-uniform pressure assumption and the mixing ends inside the constant-area section at cross section "y". The pressure of the mixed flow (p_y) is calculated in an iterative solution, which begins with an estimated value for p_y and the calculation continues to reach the area ratio convergence.

$$p_m = p_n \tag{4-28}$$

$$p_m = p_{n,1} \tag{4-29}$$

$$S_m = S_{th} \tag{4-30}$$

$$h_{m,s} = Enthalpy(p_m, S_m) \tag{4-31}$$

$$h_m = \eta_p (h_{m,s} - h_{th}) + h_{th} \tag{4-32}$$

$$U_m = \sqrt{(2(h_{th} - h_m) + U_{th}^2)} \tag{4-33}$$

$$p_y = p_n + \Delta p \tag{4-34}$$

$$U_y(\dot{m}_s + \dot{m}_P) = (\dot{m}_s U_n + \dot{m}_P U_m)\varphi_{Mix} + p_m A_1 + p_n A_{s,m} - p_y A_y \tag{4-35}$$

$$h_y = (h_m + U_m^2/2 + \omega(h_n + U_n^2/2))/(1+\omega) - U_y^2/2 \tag{4-36}$$

$$p_y = p_{n,1} + \Delta p \tag{4-37}$$

$$U_y(\dot{m}_s + \dot{m}_P) = (\dot{m}_s U_{n,1} + \dot{m}_P U_m)\varphi_{Mix} + p_m A_1 + p_{n,1} A_{s,m} - p_y A_y \quad (4\text{-}38)$$

$$h_y = (h_m + U_m^2/2 + \omega(h_{n,1} + U_{n,1}^2/2))/(1+\omega) - U_y^2/2 \quad (4\text{-}39)$$

$$\rho_y = Density(\rho_y, h_y) \quad (4\text{-}40)$$

$$AR_c = \frac{\dot{m}_s + \dot{m}_p}{U_y \rho_y A_{th}} \quad (4\text{-}41)$$

2) Normal shock wave at constant area section

The normal shock occurs somewhere inside the constant-area section at the cross section "d". To evaluate the properties of the flow at this point, it is assumed that the shock wave decreases the flow velocity to the subsonic velocity and increases its pressure. Due to this phenomenon, the specific volume of the stream after the normal shock would dramatically decrease. The same assumption is used by Eldakamawy et al [142]. The iteration starts with an assumption of the specific volume of the shocked stream at the cross section "d" which is made by dividing the specific volume of the mixed flow in cross section "y" by a large number (Eqs. (4-42) -(4-44)).

The specific enthalpy and pressure of the shocked stream are evaluated based on the energy and momentum balances around points "y" and "d" (Eqs. (4-45) & (4-46)) and the new value of the shocked stream specific volume is evaluated with Eq. (4-47). The calculation will converge to the right value of the shocked stream specific volume after many iterations. Then, the pressure and velocity of the shocked stream are evaluated.

$$v_y = 1/\rho_y \quad (4\text{-}42)$$

$$v_d = \frac{v_y}{200} \quad (4\text{-}43)$$

$$U_d = v_d U_y / v_y \tag{4-44}$$

$$h_d = h_y + U_y^2/2 - U_d^2/2 \tag{4-45}$$

$$p_d = p_y - U_d^2/v_d + U_y^2/v_y \tag{4-46}$$

$$v_{d,new} = 1/Density(p_d, h_d) \tag{4-47}$$

$$S_d = Entropy(p_d, h_d) \tag{4-48}$$

3) Diffuser

To evaluate the properties of the flow at the outlet of the diffuser the iterative solution is required, which begins with an estimation of the flow pressure at the cross section "2" (Eq. (4-49)) and the calculation continues by inclemently increasing this pressure until obtaining the entertainment ratio convergence at the cross section "2". The relation of entrainment ratio is developed based on the energy balance for the control volume around the beginning point of mixing and the outlet point of the ejector shown by a red rectangle in Figure 4-8. Dividing both sides of Eq. (4-52) by $\dot{m}_p$ and rearranging that results in Eq. (4-53). Eq. (4-53) defines the entrainment ratio in the double-choking condition, in which the properties of the secondary stream is shown by "n". Eq. (4-54) is obtained by substituting "n1" for "n" referring to the single-choking condition. In each iteration, the conservation of mass, energy and momentum are solved for an assumed control volume shown by a red rectangle in Fig.8. Next, p_2 is compared with p_C and the new value of p_s is guessed and all the steps explained above are repeated until obtaining the back pressure convergence at cross section "2".

$$\omega_{calc} = (h_m + U_m^2/2 - h_2)/(h_2 - h_n - U_n^2/2)$$

$$p_2 = p_d + \Delta p \tag{4-49}$$

$$h_{2,s} = Enthalpy(p_2, S_d) \tag{4-50}$$

$$h_2 = (h_{2,s} - h_d) / \eta_d + h_d \tag{4-51}$$

$$(\dot{m}_s + \dot{m}_p) h_2 = (U_m^2 / 2 + h_m) \dot{m}_p + (U_n^2 / 2 + h_n) \dot{m}_s \tag{4-52}$$

$$\omega_{calc} = (h_m + U_m^2 / 2 - h_2) / (h_2 - h_n - U_n^2 / 2) \tag{4-53}$$

$$\omega_{calc} = (h_m + U_m^2 / 2 - h_2) / (h_2 - h_{n,1} - U_{n,1}^2 / 2) \tag{4-54}$$

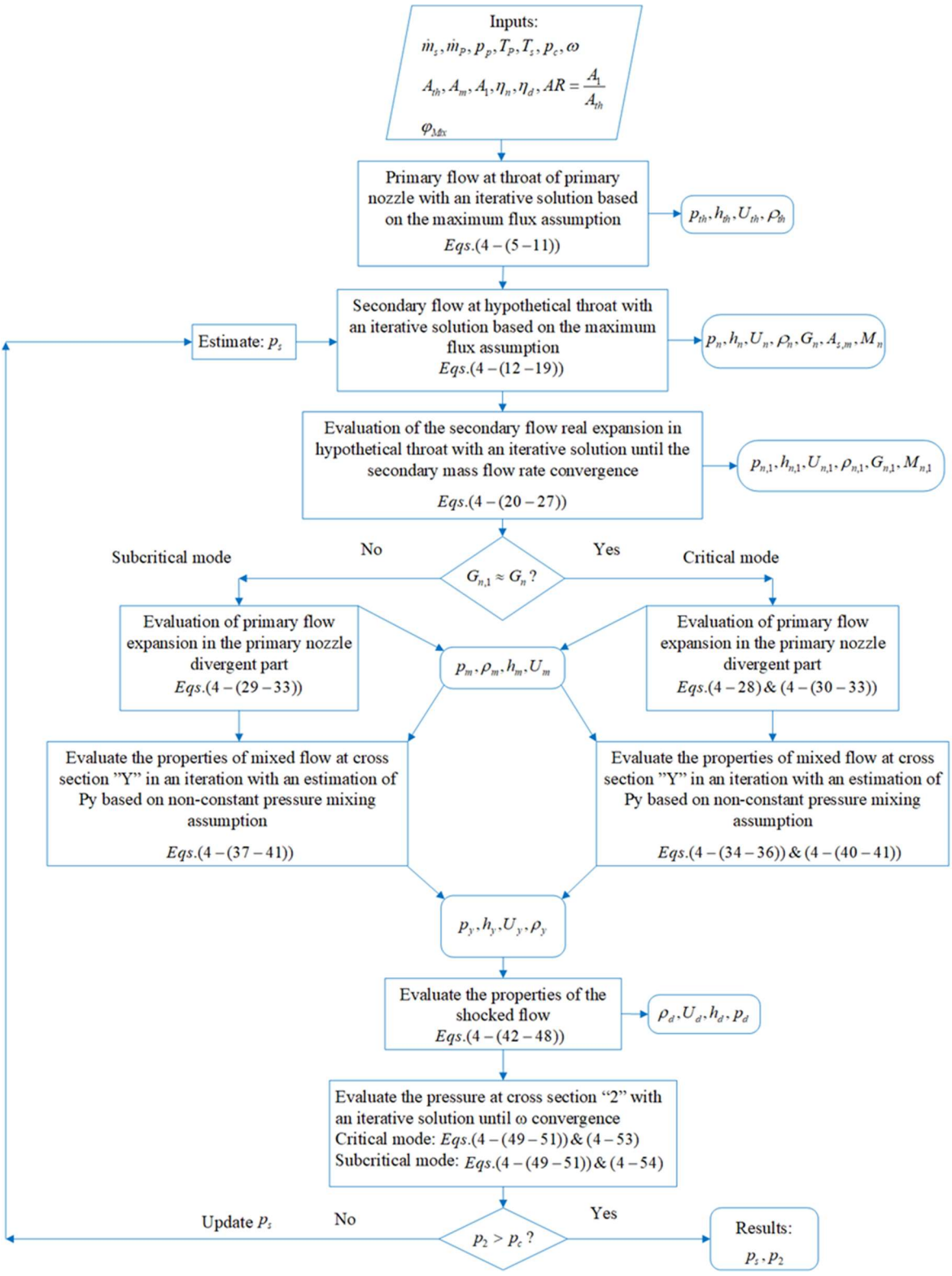

Figure 4-9: The ejector model flowchart

4.6. Results and discussion

4.6.1. Validation

The equations of the proposed model were solved using EES[1] software. In order to validate the model, the filtered experiments were applied. The generating pressure was altered from 484.63 kPa to 535.28 kPa at three values of the condenser temperature ranged from 20 to 24 ºC. The constant parameters used in the numerical model were reported in Table 4-1. The values of constant isentropic and mixing efficiencies are defined based on preceding studies [142][150].

Table 4-1: Constant parameters used in the ejector model

Parameter	Value
η_n	0.98
η_s	0.98
η_d	0.98
φ_{mix}	0.90

The estimated values of the secondary flow pressure by the proposed model at the various values of the generating pressure and condenser inlet conditions were compared with experimental data (shown in Figure 4-7) in Table 4-2.

[1] Engineering Equation Solver

Table 4-2: Validation of the thermodynamic model of the ejector with experimental data

	p_P (kPa)	T_e (°C)	T_P (°C)	$\dot{m}_s$ (kg/s)	$\dot{m}_P$ (kg/s)	$p_2(p_c)$ (kPa)			p_S (kPa)			$T_{C,i}$ (°C)
						Experiment	Model	Error (%)	Experiment	Model	Error (%)	
1	483.71	10.39	78.83	0.103	0.33	175.17	176.014	0.48	82.96	84.09	1.36	20
2	496.14	10.43	78.81	0.103	0.34	176.02	179.537	1.99	83.09	83.09	0.01	
3	511.29	10.41	78.83	0.101	0.35	176.66	183.182	3.69	82.99	81.09	2.28	
4	525.88	10.87	78.81	0.101	0.36	177.79	186.073	4.65	84.62	85.95	1.78	
5	538.04	10.70	78.84	0.102	0.37	178.75	189.903	6.23	84.04	87.97	4.67	
6	484.44	11.02	78.83	0.098	0.33	186.69	185.460	0.65	85.11	86.99	2.21	22
7	498.09	10.87	78.81	0.102	0.34	188.41	189.573	0.62	84.59	85.89	1.54	
8	509.22	10.84	78.82	0.103	0.35	189.23	192.53	1.75	84.50	83.89	0.72	
9	521.24	11.17	78.80	0.105	0.36	190.26	193.22	1.56	85.65	86.99	1.56	
10	535.67	11.22	78.84	0.105	0.37	190.70	196.64	3.11	85.84	87.99	2.51	
11	486.29	11.95	78.85	0.079	0.33	196.73	187.26	4.81	88.46	90.97	2.84	24
12	496.17	11.94	78.84	0.086	0.34	198.06	190.99	3.57	90.21	91.97	1.95	
13	511.50	11.94	78.85	0.089	0.35	199.63	195.79	1.92	87.13	91.07	4.52	
14	523.46	10.97	78.84	0.094	0.36	200.90	197.21	1.83	85.45	85.56	0.13	
15	537.74	11.67	78.84	0.104	0.37	203.54	200.81	1.34	89.13	89.97	0.94	

The proposed thermodynamic model of the ejector predicted with high accuracy the ejector exit pressure p_2, exit and the ejector secondary stream pressure p_S for the various experimental conditions. The highest discrepancies between the predicted values of p_2 and p_S and their experimental values are reported to be 6.23 %, and 4.67%, respectively.

Figure 4-10 presents the ejector thermodynamic model prediction of the secondary stream pressure p_S and compression ratio *Cr* at three various condenser inlet conditions. Based on Figure 4-10(b) as well as the experimental data presented in Figure 4-7, increasing the generating pressure at a constant generator inlet condition ($T_{g,i}$) (by increasing the primary flow mass flow rate) results in a decrease in the secondary stream pressure to a minimum point. However, further increasing the generating pressure increases the secondary pressure. As a result, *Cr* first rises to a maximum point with increasing generating pressure. Then, *Cr* falls as the generating pressure continues to increase, as presented in Figure 4-10(a). Regarding the experimental data and model outputs, the optimum values of the generating pressure for the condenser inlet conditions of 20, 22 and 24ºC are 511.28kPa, 509.22kPa and 523.459 kPa, respectively.

The reason of this phenomenon is related to the operation regime of the ejector. At the lower generating pressure, the pressure difference between the primary and back stream is relatively small; therefore, the secondary flow could be proportionally entrained and as a result, the ejector works at the sub-critical mode. This means, based on the ejector model, at lower generating pressures, the mass flux of the secondary flow in hypothetical throat $G_{n,1}$ is less than the maximum mass flux, G_n at this point. In this operation area of the ejector, any increase in the generating pressure reduces the suction pressure and consequently increases *Cr* until a maximum point. The optimum point is also located in double-choking operation regime.

A further increase in the generating pressure beyond the optimum point leads to an increase in the suction pressure and a decrease in *Cr*. The mass flux of the secondary stream in the hypothetical throat rises to around the maximum mass flux, G_n and the ejector operates in the double-choking mode. In Table 4-3, the values of the secondary mass flux and Mach number in the hypothetical throat are compared with those of the choked secondary stream, which can support the mentioned phenomenon.

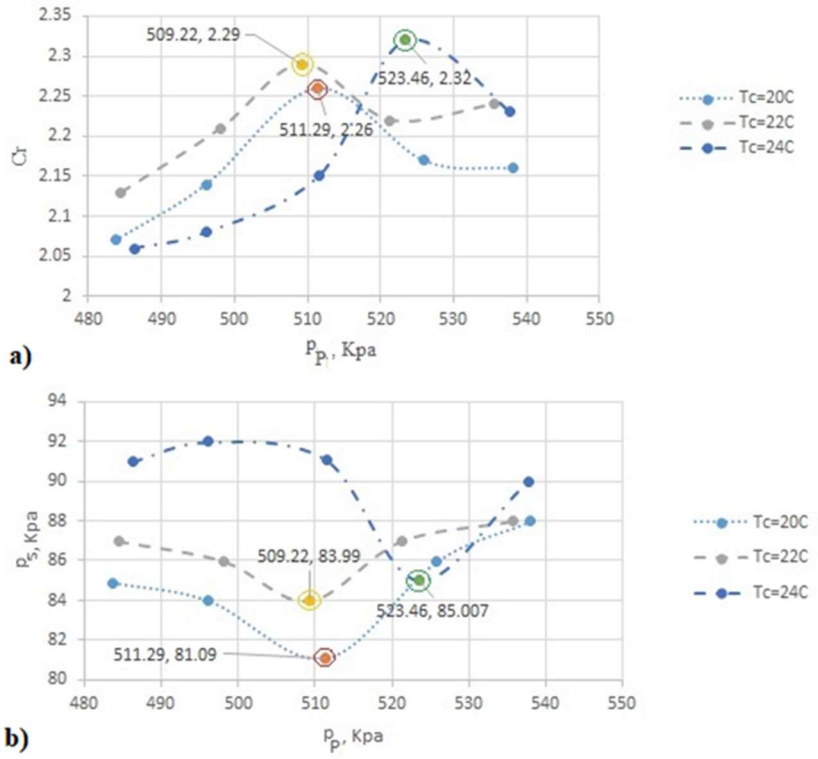

Figure 4-10: Variation of Cr b) p_s versus the generating pressure using the developed model

Table 4-3: The secondary stream choking test based on mass flux and Mach number comparison

p_P (Kpa)	E (%)	E_M(%)	$T_{C,i}$ (ºC)
483.71	9.82	30.05	20
496.13	9.71	29.95	
511.29	0.96	9.79	
525.88	0.98	9.82	
538.04	0.96	9.72	
484.44	10.22	30.99	22
498.09	9.78	30.55	
509.22	0.96	10.16	
521.25	0.94	9.62	
535.67	0.95	9.69	
486.29	12.55	34.24	24
496.17	11.51	32.86	
511.50	11.14	32.38	
523.46	1.06	10.23	
537.74	0.95	9.72	

$E = (G_n - G_{n,1})/G_n \times 100$; $E_M = (M_n - M_{n,1})/M_n \times 100$

4.7. Conclusions

In this work, for an ejector refrigeration system at constant condensing temperature, the influence of the generating pressure on the compression ratio and the suction pressure were investigated numerically and experimentally. Signal processing techniques, specifically the moving average filtering method, was used to remove the periodic noise from the experimental data. The filtered experimental data revealed that there is an optimum generating pressure that maximizes *Cr* while simultaneously minimizes the suction pressure. To explain this phenomenon, a new 1-D thermodynamic model of the ejector was developed. The newly developed model predicted the choking regime inside the ejector at different operating conditions and confirmed the occurrence of the optimum generating pressure. Based on the experimental and numerical results, we concluded that the ejector operates in the single-choking mode when the generating pressure is lower than the optimum pressure, while it operates in the double-choking mode at generating pressures equal to or greater than the optimum pressure.

4.8. Acknowledgments

This project is a part of the Collaborative Research and Development (CRD) Grants Program at “Université de Sherbrooke”. The authors acknowledge the support of the Natural Sciences and Engineering Research Council of Canada, Hydro-Québec, Rio Tinto, Alcan and Canmet ENERGY Research Center of Natural Resources Canada (RDCPJ451917-13).

4.9. Nomenclature

Table 4-4: Nomenclature

Symbol	Definition
p	Pressure, kPa
$\dot{m}$	Mass flow rate, kg s^{-1}
T	Temperature, °C
S	Entropy, kJ kg^{-1} $°C^{-1}$
$\dot{Q}$	Thermal load, kW
U	Flow velocity, m s^{-1}
M	Mach number
A	Surface area, m^2
G	Mass flux, kg m^{-2} s-1
h	Enthalpy, kJ kg^{-1}
v	Specific volume, m^3 kg^{-1}
ρ	Density, kg m^{-3}
ω	Entrainment ratio
Subscripts	
c	Condenser
e	Evaporator
g	Generator
s	Secondary
p	Primary
i	Inlet
o	Outlet
Sh	Superheating
c,i	Inlet coolant to condenser
g,i	Inlet hot fluid to generator
th	Throat of the ejector
s	Isentropic property
y	Mixing process of the ejector
d	Shock wave
Greek characters	
η_{th}	Isentropic expansion efficiency of the primary flow in throat
η_s	Isentropic expansion efficiency of secondary flow in throat
η_d	Isentropic compression efficiency of the diffuser
φ_{Mix}	The mixing efficiency of the ejector
Abbreviation	
Cr	Compression ratio
COP	Coefficient of performance
ERS	Ejector refrigeration system

CHAPTER 5 Dynamic modeling of an R245fa ejector-based refrigeration system

Avant-propos

Auteurs et affiliation:

Elhameh Narimani: étudiant au doctorat, faculté de génie, département de génie mécanique, Université de Sherbrooke

Mikhail Sorin: professeur, faculté de génie, département de génie mécanique, Université de Sherbrooke.

Philippe Micheau: professeur, faculté de génie, département de génie mécanique, Université de Sherbrooke.

Hakim Nesreddine: PhD, Chercheur-Chargé de projet, Laboratoire des technologies de l'énergie, Shawinigan (Québec), Canada

Date d'acceptation : 10 August 2019

État de l'acceptation : acceptée

Revue: International Journal of Refrigeration

Titre français: Modélisation dynamique d'un système de réfrigération à éjecteur R245fa

Contribution au document:
Ce chapitre de ma thèse traite le développement d'un modèle dynamique pour un système de réfrigération à éjecteur R245fa. Le modèle dynamique développé de le SRE sera utilisé pour prédire le comportement transitoire du cycle.

Résumé en français:

Le comportement dynamique du système de réfrigération à éjecteurs (SRE) joue un rôle important dans la prévision de ses performances et la conception de son système de contrôle. Cet article étudie numériquement et expérimentalement le comportement dynamique du système SRE en connectant les modèles dynamiques de générateur, de condenseur et d'évaporateur à un seul modèle dynamique SRE, tant que les échangeurs de chaleur dominant la dynamique thermique du système SRE. Les modèles dynamiques des échangeurs de chaleur développés ont été basés sur l'approche des limites variables. Un modèle thermodynamique 1-D de l'éjecteur a également été développé pour évaluer le comportement du fluide à travers l'éjecteur. La pompe et le détendeur ont été modélisés à l'aide d'équations algébriques, car ils étaient considérés comme des composants d'état stable dans le système. Le modèle dynamique SRE développé a été validé expérimentalement en mesurant la réponse transitoire au changement de vitesse de la pompe. Les études de validation ont révélé que le modèle est capable de capturer la dynamique du système de réfrigération en termes de pressions et d'enthalpies de sortie spécifiques des échangeurs de chaleur, avec des erreurs relatives inférieures à 3,78 et 0,5%, respectivement.

5.1. Abstract

The dynamic behavior of the ejector refrigeration system (ERS) plays an important role in its performance prediction and control system design. This paper numerically and experimentally investigated ERS dynamic behavior by connecting generator, condenser and evaporator dynamic models into a single ERS dynamic model, as the heat exchangers dominate ERS thermal dynamics. The developed dynamic models of the heat exchangers were based on the moving boundary approach. A 1-D thermodynamic model of the ejector was also developed to evaluate the fluid behavior through the ejector. The pump and expansion valve were modeled using algebraic equations, as they were considered as steady state components in the system. The developed ERS dynamic model was validated experimentally by measuring the transient response to the step change of the pump speed. The validation studies revealed that the model is able to capture the refrigeration system's

dynamics in terms of the pressures and outlet specific enthalpies of the heat exchangers, with relative errors of less than 3.78 and 0.5 %, respectively.

Keywords: Ejector refrigeration system (ERS), dynamic modeling, moving boundary approach, heat exchange, ejector, pump, expansion valve

5.2. Introduction

The ejector refrigeration system (ERS) is known as an appropriate alternative to the conventional vapor compression refrigeration due to its environmental and economic advantages. However, its low efficiency compared with that of mechanical refrigeration cycles has limited its industrial application. A high compression ratio (*Cr*) of an ejector refrigeration system could guarantee its high efficiency in terms of ejector operation criteria [27] [30] [153]. It has been suggested in preceding studies that an increase in the generating pressure or primary stream mass flow rate could maximize *Cr* in the ERS [27] [30] [153][144]. Hence, this paper focuses on investigating ERS dynamic behavior when a change in the generating pressure (primary flow mass flow rate) occurs while the other parameters are kept constant.

A dynamic simulation of vapor compression systems is an efficient tool to analyse the transient performance of such systems and optimize the operation conditions. Furthermore, to develop a control strategy, it is required to understand the main features of ERS dynamic behavior. The dynamics of the vapor compression systems strongly depends on the dynamics of the heat exchangers since the thermal inertia of other components are much smaller than those of the heat exchangers [154].

As mentioned by Bendapudi and Braun [46], two different principles have been used to model heat exchangers: finite-volume distributed parameter and moving boundary lumped parameter approaches. Although the latter is much faster than the former [155] [156] [157], it is not as accurate as the finite volume approach to fully predict the system transients [47]. However, it should be taken into account that it is usually required to run the code in real-time for many control applications; therefore, the moving boundary approach is more

practical to develop control-oriented dynamic models for complicated systems, such as vapor compression systems.

The moving boundary approach splits the heat exchanger into a minimum number of control zones (maximum 3) representing zones where refrigerant is in the superheated vapor, saturated mixture, or sub-cooled liquid phases. The model parameters are lumped in each zone. In contrast, in the finite volume method, the heat exchanger is divided into a number of stationary elements with fine mesh resolution, which causes the slow solution speed.

There are various implementations of the moving boundary model in the literature, which have been developed to address the shortcomings of the original one. Many early versions of the moving boundary model assumed a fixed number of zones, which severely restricted the operating range, especially within the start-up and shut-down periods. To address this issue, "switching models" were developed by Zhang and Zhang [54] that employed multiple modeling frameworks in one simulation. They used a time-dependent mean void fraction in investigating the evaporator transient behavior under large disturbances. McKinley and Alleyne [31] introduced pseudo-state variables into their implementation of the switched model and used a switching criteria based on void fraction. Li and Alleyne[158] improved the previous study by applying novel switching schemes between different modeling frameworks.

Horst et al. [159] developed a dynamic model of the exhaust gas heat exchanger in the Rankine Cycle by employing a moving boundary, with a novel approach to evaluating the wall temperature distribution, and applying the zone switching criteria. The vast majority of dynamic models developed for heat exchangers are only able to explain their transient behavior as an individual component, whereas in complicated systems, the transient behaviors of the components are interconnected. Chen and Yu [160] modified the evaporator model by introducing a new input variable i.e. time derivative of the evaporator inlet specific enthalpy in the dynamic modeling of a heat pump.

ERS dynamic modeling is more complicated than that of conventional vapor compression cycle due to the existence three heat exchangers as well as the ejector, which add programing complexity and slow down the solver. Furthermore, ERS system performance is strongly

influenced by the flow behavior through an ejector. Therefore, a considerable effort has been made in the literature to develop ejector models and investigate the impact of various operational parameters on its efficiency. The most recent ejector model results can be found in work carried out by Narimani et al. [153], Chunnanond and Aphornratana [129], Huang et al. [29], Eames et al. [130], Thongtip and Aphornratana [22] and Chen et al. [131].

This paper mainly focuses on the development of the first ERS dynamic model. A 1-D thermodynamic ejector model will be developed based on real gas properties. This model was introduced by the authors in their previous study and used to predict the impact of an increase in the primary stream mass flow rate on ejector performance with respect to Cr [153]. The expansion valve and pump will be modeled with algebraic equations. To capture the transient behavior of the heat exchangers the moving boundary approach introduced by Rasmussen et. al. [161] and Rasmussen and Alleyne[62] is used, yet unlike their work, in the present study the time derivatives of inlet specific enthalpies of the generator and evaporator are included in the dynamic model. According to the ERS thermodynamic configuration, the inlet specific enthalpies of the evaporator and generator are roughly equal to the outlet specific enthalpy of the condenser. Using the developed dynamic model, the transient responses of the pressures and outlet specific enthalpies of the generator, condenser, evaporator, and the primary stream mass flow rate will be simulated for step changes of the pump speed. The results will be verified with experimental data.

5.3. Model development

The dynamic model of the R245fa ERS consists of models of the generator, condenser, evaporator, ejector, pump and expansion valve. Figure 5-1 illustrates the schematic view of the typical ERS and its P-h diagram. The individual components model was first developed and then interconnected to create a single ERS dynamic model.

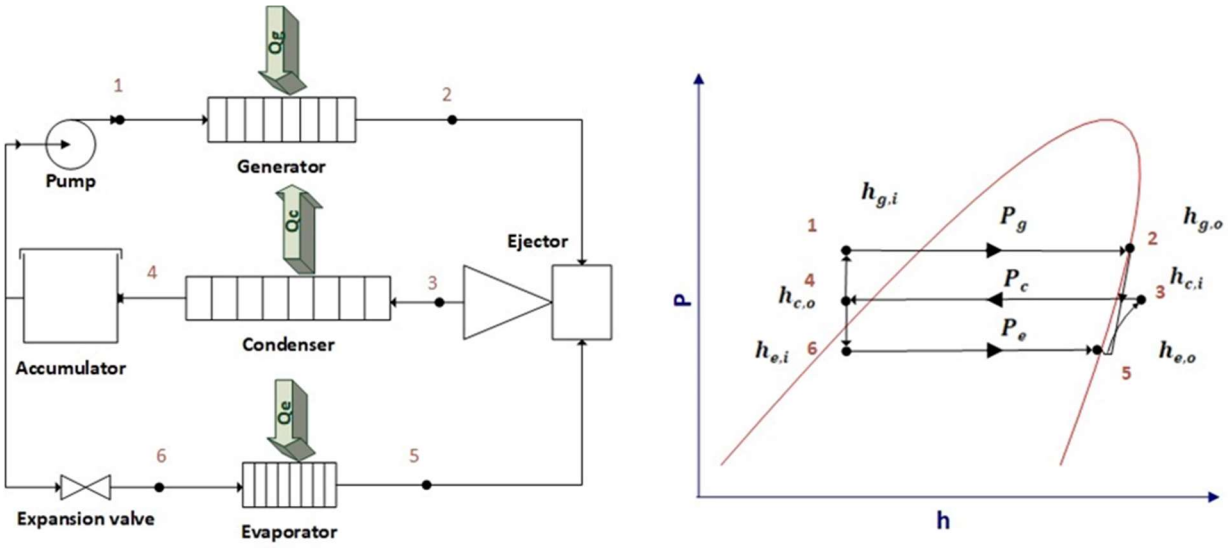

Figure 5-1: Schematic representation of the ERS setup and its P-h diagram

5.3.1. Pump

The R245fa is fed to the generator using a vortex pump. The relation among the mass flow rate and pump speed is expressed using the pump Affinity law, which can be found in references [162][163].

$$\frac{\dot{m}_{g,r,i,1}}{\dot{m}_{g,r,i,2}} = \frac{N_{p,1}}{N_{p,2}} \tag{5-1}$$

Where $\dot{m}_{g,r,i}$ and N_p are the mass flow rate of the pump in kg/s and the pump speed in rpm, respectively. For a given pump efficiency σ_p, and mean specific volume $\bar{v}_p$, the enthalpy is evaluated as follows [164]:

$$h_{g,i} = h_{c,o} + \frac{\bar{\upsilon}_p (P_g - P_c)}{\sigma_p} \tag{5-2}$$

The second term of the right side of Eq. (5-2) is negligible, which means that the inlet and outlet enthalpies of the pump are roughly equal:

$$h_{g,i} \approx h_{c,o} \tag{5-3}$$

$$\dot{h}_{g,i} \approx \dot{h}_{c,o} \tag{5-4}$$

The dynamic response of the pump evolves much faster than that of the heat exchanger, therefore, the pump operation is considered as steady state process.

5.3.2. Expansion valve

Two algebraic relationships are used to model the electronic expansion valve (EEV). Eq.(5-5) evaluates the mass flow rate passing through the valve ($\dot{m}_{eev}$) assuming the standard orifice flow [68]. Furthermore, the expansion process is an isenthalpic process (Eq. (5-6)).

$$\dot{m}_{e,r,i} = C_{eev} A_{eev} \sqrt{2\rho_i (P_c - P_e)} \tag{5-5}$$

$$h_{c,o} = h_{e,i} \tag{5-6}$$

$$\dot{h}_{c,o} = \dot{h}_{e,i} \tag{5-7}$$

Where C_{eev}, ρ_i, P_c and P_e are the discharge coefficient, the refrigerant density at the valve inlet, and the expansion valve inlet and outlet pressures, respectively. A_{eev} is known as the effective passage flow area and is defined as follows:

$$A_{eev} = \frac{A_v A_0}{100} \tag{5-8}$$

A_v and A_0 are the valve opening (%) and nominal orifice cross-sectional area (1.79 cm^2), respectively. The expansion process operation is assumed to occur under the steady state conditions.

5.3.3. Liquid accumulator

It is assumed that the liquid accumulator is large enough to maintain the sub-cooled state of the refrigerant even if its inlet condition is changed. Thus, the liquid accumulator can be considered as a steady state component. The inlet specific enthalpy to the accumulator equals its outlet specific enthalpy and the pressure drop is negligible, hence there is no need to model the accumulator and its model was not included in the overall dynamic model.

5.3.4. Ejector

In this study, the model developed by Narimani et al. [153] is used to evaluate the parameters of the ejector in the ERS dynamic model. The 1-D thermodynamic model of the ejector developed by Narimani et al. operates in subcritical mode when the generating pressure is below the Cr optimum point, while it operates in the critical mode at or above the optimum generating pressure. Figure 5-2 shows a schematic of the ejector applied in the current work.

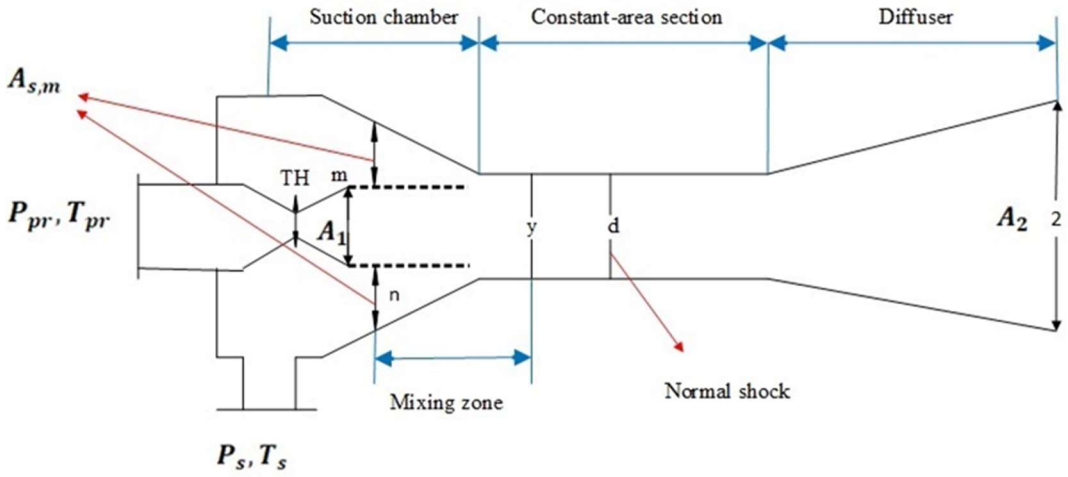

Figure 5-2: Schematic of the modeled ejector

The ejector model developed in this work uses the non-constant mixing pressure assumption for the both single-choking and double-choking conditions. The mixing efficiency was also included in the momentum balance to consider the momentum losses during mixing. To define choking regime in the ejector, the secondary mass flux is compared to the maximum secondary mass flux at the hypothetical throat[153]. The assumptions are made to develop the model include:

1) one-dimensional, steady state and adiabatic flow inside the ejector[153]
2) stagnation conditions at the inlet points of primary and secondary, and diffuser exit
3) mass flux maximization criterion is used for both nozzles [11][12] [142] [150] [153]
4) occurrence of the normal shock in the constant- area section [153]

Based on these assumptions, the governing equations of the ejector, including the conservation of mass, momentum and energy, are solved to evaluate the primary and

secondary stream mass flow rates in the ejector. Figure 5-3 outlines the flowchart of the ejector model.

The key element of this model is related to its ability to recognize the chocking regime inside the suction chamber based on which it was assumed that the secondary stream cannot always chock inside the suction chamber. To define the chocking regime, the value of the secondary mass flux in the hypothetical throat ($G_{n,1}$) is compared with the maximum mass flux G_n. If $G_{n,1} \approx G_n$, then the secondary stream chokes inside the suction chamber and the ejector operates in the double-choking regime (critical mode). However, for $G_{n,1} \neq G_n$, the ejector operates at sub-critical mode and the secondary stream does not choke inside the suction chamber. More information about the ejector modeling approach and relevant assumptions was discussed in [153].

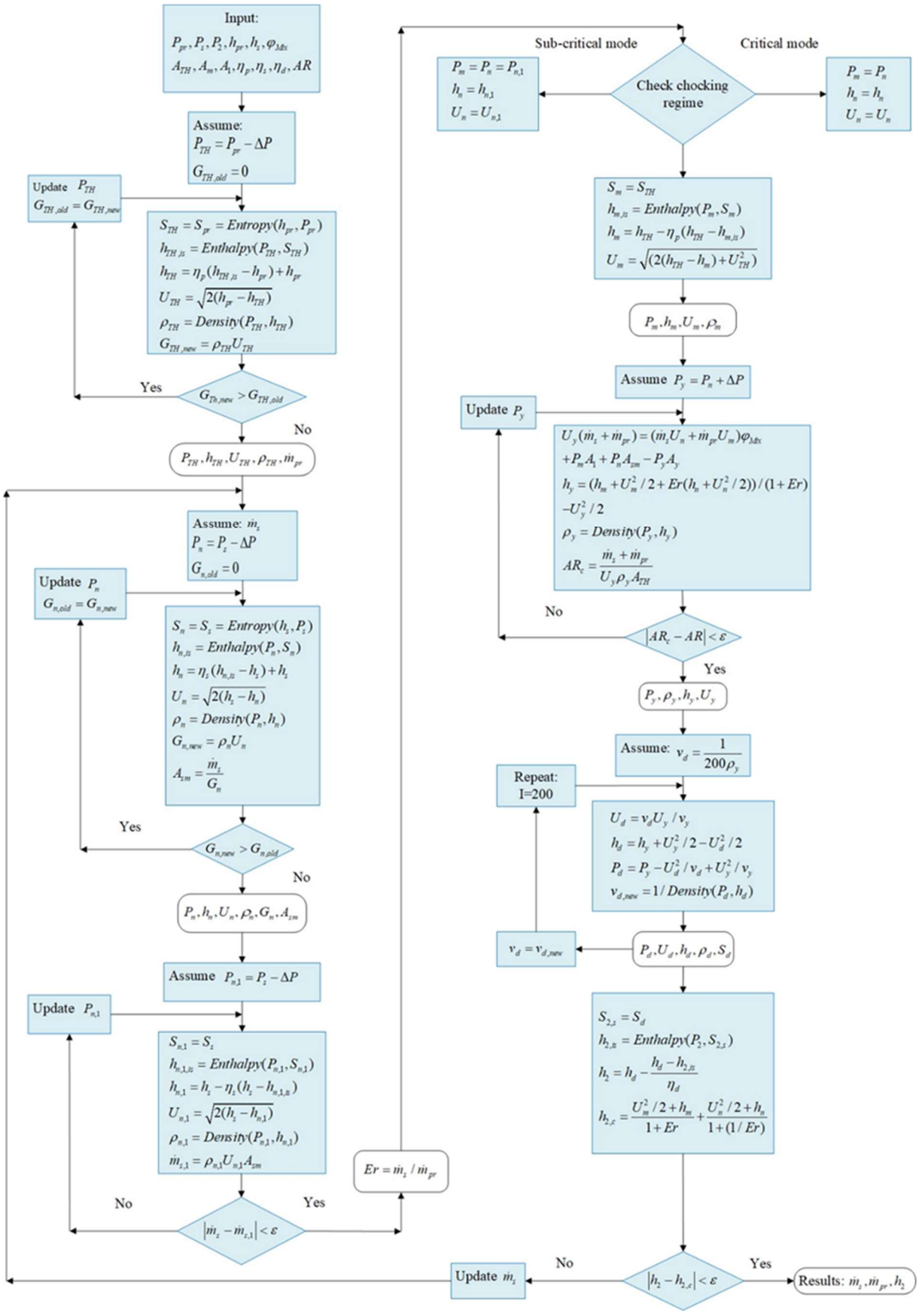
Input:
$P_{pr}, P_s, P_2, h_{pr}, h_s, \varphi_{Mix}$
$A_{TH}, A_m, A_1, \eta_p, \eta_s, \eta_d, AR$
Assume:
$P_{TH} = P_{pr} - \Delta P$
$G_{TH,old} = 0$
Update P_{TH}
$G_{TH,old} = G_{TH,new}$
$S_{TH} = S_{pr} = Entropy(h_{pr}, P_{pr})$
$h_{TH,is} = Enthalpy(P_{TH}, S_{TH})$
$h_{TH} = \eta_p(h_{TH,is} - h_{pr}) + h_{pr}$
$U_{TH} = \sqrt{2(h_{pr} - h_{TH})}$
$\rho_{TH} = Density(P_{TH}, h_{TH})$
$G_{TH,new} = \rho_{TH} U_{TH}$
Yes
$G_{TH,new} > G_{TH,old}$
No
$P_{TH}, h_{TH}, U_{TH}, \rho_{TH}, \dot{m}_{pr}$
Assume: $\dot{m}_s$
$P_n = P_s - \Delta P$
$G_{n,old} = 0$
Update P_n
$G_{n,old} = G_{n,new}$
$S_n = S_s = Entropy(h_s, P_s)$
$h_{n,is} = Enthalpy(P_n, S_n)$
$h_n = \eta_s(h_{n,is} - h_s) + h_s$
$U_n = \sqrt{2(h_s - h_n)}$
$\rho_n = Density(P_n, h_n)$
$G_{n,new} = \rho_n U_n$
$A_{1m} = \frac{\dot{m}_s}{G_n}$
Yes
$G_{n,new} > G_{n,old}$
No
$P_n, h_n, U_n, \rho_n, G_n, A_{1m}$
Assume $P_{n,1} = P_s - \Delta P$
Update $P_{n,1}$
$S_{n,1} = S_s$
$h_{n,1,is} = Enthalpy(P_{n,1}, S_{n,1})$
$h_{n,1} = h_s - \eta_s(h_s - h_{n,1,is})$
$U_{n,1} = \sqrt{2(h_s - h_{n,1})}$
$\rho_{n,1} = Density(P_{n,1}, h_{n,1})$
$\dot{m}_{s,1} = \rho_{n,1} U_{n,1} A_{1m}$
No
$|\dot{m}_s - \dot{m}_{s,1}| < \varepsilon$
Yes
$Er = \dot{m}_s / \dot{m}_{pr}$
Sub-critical mode
Critical mode
Check chocking regime
$P_m = P_n = P_{n,1}$
$h_n = h_{n,1}$
$U_n = U_{n,1}$
$P_m = P_n$
$h_n = h_n$
$U_n = U_n$
$S_m = S_{TH}$
$h_{m,is} = Enthalpy(P_m, S_m)$
$h_m = h_{TH} - \eta_p(h_{TH} - h_{m,is})$
$U_m = \sqrt{(2(h_{TH} - h_m) + U_{TH}^2)}$
P_m, h_m, U_m, ρ_m
Assume $P_y = P_n + \Delta P$
Update P_y
$U_y(\dot{m}_s + \dot{m}_{pr}) = (\dot{m}_s U_n + \dot{m}_{pr} U_m)\varphi_{Mix}$
$+P_m A_1 + P_n A_{1m} - P_y A_y$
$h_y = (h_m + U_m^2/2 + Er(h_n + U_n^2/2))/(1+Er)$
$-U_y^2/2$
$\rho_y = Density(P_y, h_y)$
$AR_c = \frac{\dot{m}_s + \dot{m}_{pr}}{U_y \rho_y A_{TH}}$
No
$|AR_c - AR| < \varepsilon$
Yes
P_y, ρ_y, h_y, U_y
Assume: $v_d = \frac{1}{200\rho_y}$
Repeat: I=200
$U_d = v_d U_y / v_y$
$h_d = h_y + U_y^2/2 - U_d^2/2$
$P_d = P_y - U_d^2 / v_d + U_y^2 / v_y$
$v_{d,new} = 1/Density(P_d, h_d)$
$v_d = v_{d,new}$
$P_d, U_d, h_d, \rho_d, S_d$
$S_{2,s} = S_d$
$h_{2,is} = Enthalpy(P_2, S_{2,s})$
$h_2 = h_d - \frac{h_d - h_{2,is}}{\eta_d}$
$h_{2,c} = \frac{U_m^2/2 + h_m}{1+Er} + \frac{U_n^2/2 + h_n}{1+(1/Er)}$
No
$|h_2 - h_{2,c}| < \varepsilon$
Yes
Update $\dot{m}_s$
Results: $\dot{m}_s, \dot{m}_{pr}, h_2$

Figure 5-3: The ejector model flowchart

5.3.5. Heat exchangers

The heat exchangers used in this study are counter-current brazed plate heat exchangers with multiple fluid channels. To simplify the mathematical model, it is assumed that the heat exchangers are made up of two channels and only one separating wall, which is shown in Figure 5-4. The dynamic models of heat exchangers are developed based on the moving boundary approach applied by [161] and [62]. To derive the equations of dynamic models, the heat exchangers are split into control volumes or zones. The numbers of zones are defined depending on the outlet and inlet refrigerant states. The subcooled stream is fed to the generator and the superheated stream leaves it (vice versa for the condenser). Therefore, it is assumed that the generator and condenser are made up of three zones. While, the input stream to the evaporator is either the saturated liquid or a two-phase stream and it exits as a superheated vapor. Hence, the evaporator is divided into two zones in the dynamic model.

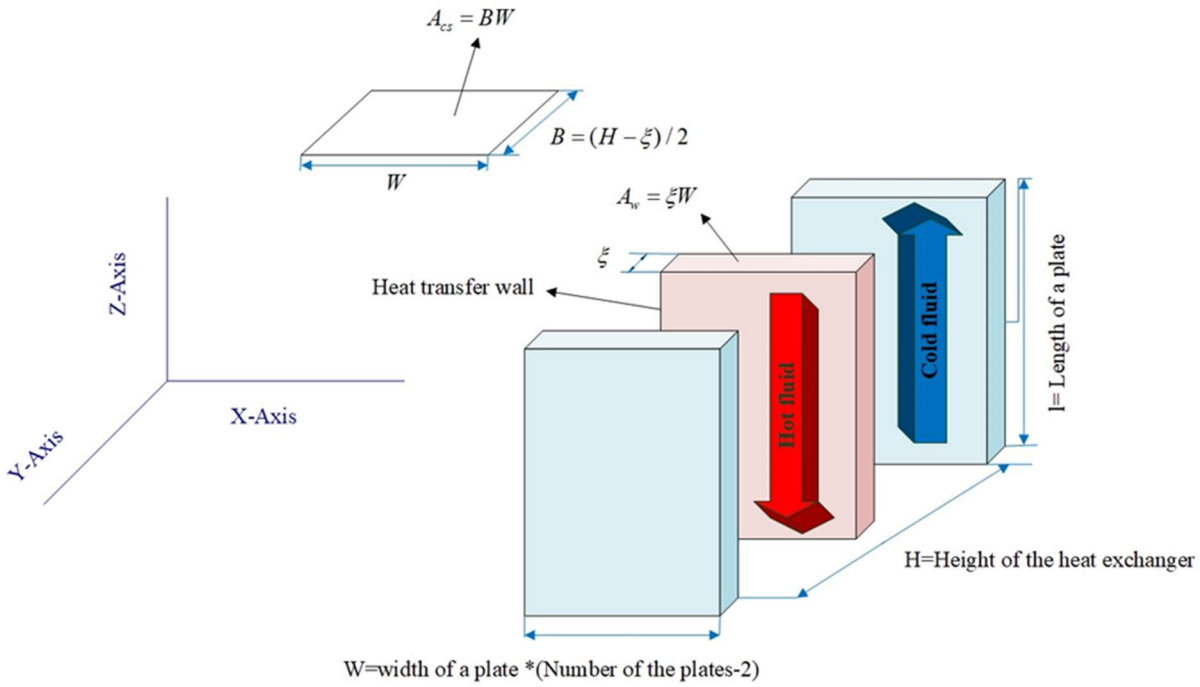

Figure 5-4: The simplified plate heat exchanger

The following assumptions are made to reduce the complexity of the heat exchangers' dynamic modeling:

- The axial conduction of refrigerant is negligible due to the refrigerant large Péclet number (Pe) which diminishes the influence of thermal conductivity to a minimum value [54][31][161][62].
- The refrigerant flow is one-dimensional, compressible, and unsteady.
- The pressure drop of the refrigerant flow is negligible (i.e. no need for the conservation of momentum).
- The dynamic behavior of the refrigerant is adequate to capture the dynamics of the heat exchanger.
- The heat loss from the exchanger wall to the environment is negligible.
- The fluid exiting a component immediately enters the next component, and the transport delays, pipelines dynamics, etc. are negligible.

The pipelines dynamics are negligible due to the efficient tubing design connecting components which involves the adequately short pipes and their efficient thermal isolation which prevents or significantly reduces the pressure drop and heat transfer losses in the pipelines.

However, despite the efficient tubing design, the dynamics are always present in the pipe connections between the components. To detect the dynamics caused by pipelines, the more accurate measuring system including more temperature and pressure measurements are required.

Figure 5-5 indicates the features of the dynamic models of the generator, condenser and evaporator.

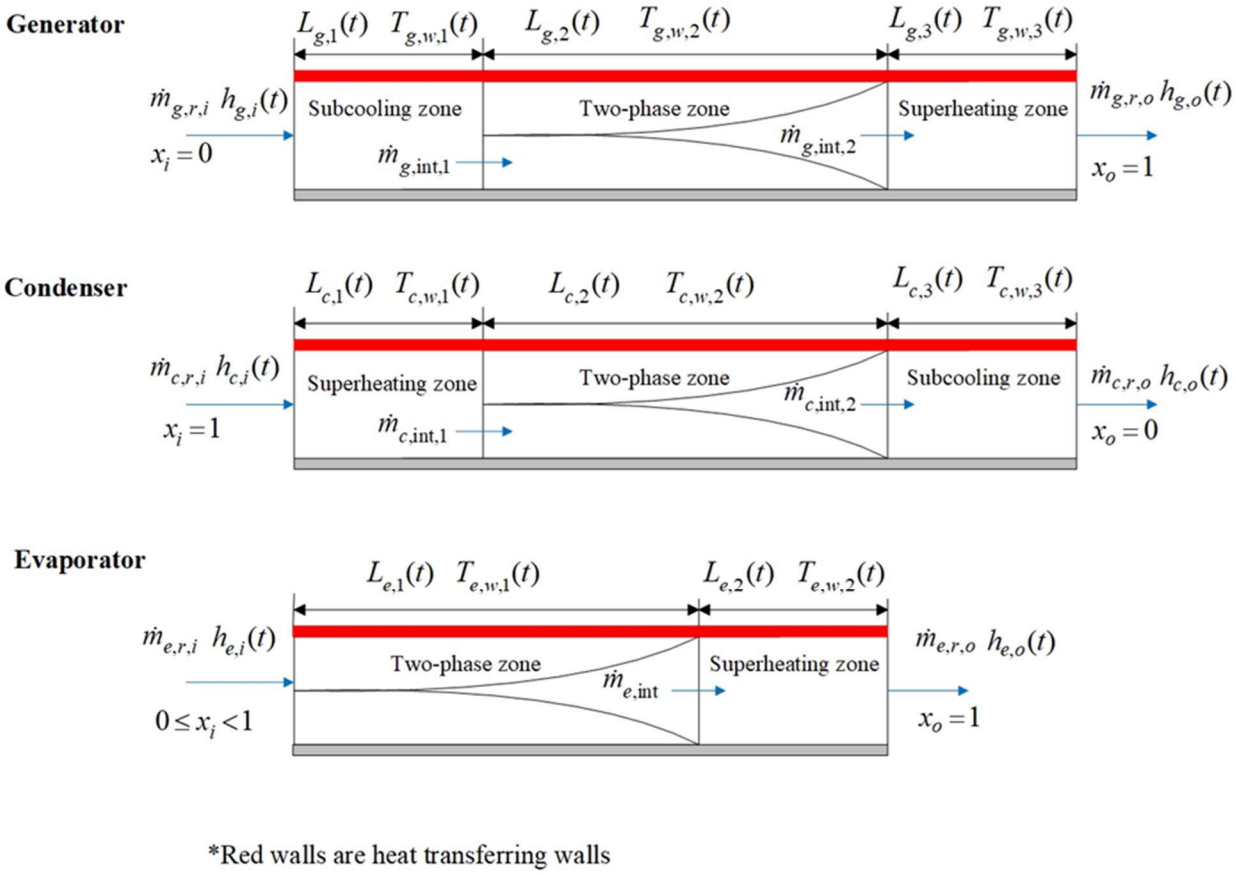

Figure 5-5: Schematic representation of heat exchangers model

To develop the ordinary differential equations using the moving boundary approach, the governing partial differential equations, including the conservation of the refrigerant mass, energy and wall energy, are integrated along the length of the heat exchanger channel, which results in the spatial dependence removal. The governing equations of refrigerant flow are in each zone:

$$\frac{\partial(\rho A_{cs})}{\partial t} + \frac{\partial \dot{m}}{\partial z} = 0 \tag{5-9}$$

$$\frac{\partial(\rho A_{cs} h - A_{cs} P)}{\partial t} + \frac{\partial(mh)}{\partial z} = p_r \alpha_r (T_w - T_r) \tag{5-10}$$

Furthermore, the energy balance for the plate heat exchanger wall reads:

$$\rho_w Cp_w A_w \frac{\partial T_w}{\partial t} = \alpha_r p_r (T_r - T_w) - \alpha_{th} p_{th} (T_w - T) \tag{5-11}$$

T_w, T, T_r , p, α, A_{cs} and A_w refer to wall, thermal fluid and the mean refrigerant temperatures, heat transfer perimeter, heat transfer coefficient, the heat exchanger channel cross-sectional area and wall area, respectively. The concept of the lumped parameters in subcooling and superheating zones are applied as explained in previous works.

In the current work, it is assumed that the mean void fraction in the generator and condenser is among the time-invariant variables as the outlet and inlet streams of those heat exchangers are superheated and subcooled streams with constant qualities. However, the time derivative of the mean void fraction is included in the dynamic model of the evaporator.

Generator model

Eqs. (5-9) and (5-10) are integrated along the length of the three zones of the generator. The detailed information about the derivation of the equations can be accessed in studies carried out by Rasmussen et al. [161] and Rasmussen and Alleyne [62]. However, they did not include the time derivative of inlet enthalpy ($\dot{h}_{g,i}$) in the model. In this study, $\dot{h}_{g,i}$ is included in the equations. Therefore, the mass and energy conservation equations in subcooling, two-phase and superheating zones of the generator are obtained as follows:

$$\begin{aligned}&[((\frac{\partial \rho_{g,1}}{\partial P_g}\Big|_{h_{g,1}})+\frac{1}{2}(\frac{\partial \rho_{g,1}}{\partial h_{g,1}}\Big|_{P_g})(\frac{dh_{g,f}}{dP_g}))(h_{g,1}-h_{g,f})+\frac{1}{2}(\frac{dh_{g,f}}{dP_g})\rho_{g,1}-1]L_{g,1}A_{g,cs}\dot{P}_g\\&+\frac{1}{2}[(\frac{\partial \rho_{g,1}}{\partial h_{g,1}}\Big|_{P_g})(h_{g,1}-h_{g,f})+\rho_{g,1}]L_{g,1}A_{g,cs}\dot{h}_{g,i}+\rho_{g,1}(h_{g,1}-h_{g,f})A_{g,cs}\dot{L}_{g,1}=\\&\dot{m}_{g,r,i}(h_{g,i}-h_{g,f})+A_{g,1}\alpha_{g,r,1}(T_{g,w,1}-T_{g,r,1})\end{aligned} \tag{5-12}$$

$$
\begin{aligned}
&[((\frac{\partial \rho_{g,1}}{\partial P_g}\Big|_{h_{g,1}})+\frac{1}{2}(\frac{\partial \rho_{g,1}}{\partial h_{g,1}}\Big|_{P_g})(\frac{dh_{g,f}}{dP_g}))h_{g,f}L_{g,1}+(\frac{d\rho_{g,f}h_{g,f}}{dP_g}(1-\overline{\gamma}_g)+\frac{d\rho_{g,g}h_{g,g}}{dP_g}\overline{\gamma}_g-1)L_{g,2}\\
&+((\frac{\partial \rho_{g,3}}{\partial P_g}\Big|_{h_{g,3}})+\frac{1}{2}(\frac{\partial \rho_{g,3}}{\partial h_{g,3}}\Big|_{P_g})(\frac{dh_{g,g}}{dP_g}))h_{g,g}L_{g,3})]A_{g,cs}\dot{P}_g+\frac{1}{2}[(\frac{\partial \rho_{g,3}}{\partial h_{g,3}}\Big|_{P_g})h_{g,g}L_{g,3}]A_{g,cs}\dot{h}_{g,o}+\\
&\frac{1}{2}[(\frac{\partial \rho_{g,1}}{\partial h_{g,1}}\Big|_{P_g})h_{g,f}L_{g,1}]A_{g,cs}\dot{h}_{g,i}+[(\rho_{g,f}h_{g,f}-\rho_{g,g}h_{g,g})\overline{\gamma}_g+(\rho_{g,g}-\rho_{g,3})h_{g,g}]A_{g,cs}\dot{L}_{g,2}+\\
&[\rho_{g,1}h_{g,f}-\rho_{g,3}h_{g,g}]A_{g,cs}\dot{L}_{g,1}=\dot{m}_{g,r,i}h_{g,f}-\dot{m}_{g,r,o}h_{g,g}+A_{g,2}\alpha_{g,r,2}(T_{g,w,2}-T_{g,r,2})
\end{aligned}
\tag{5-13}
$$

$$
\begin{aligned}
&[((\frac{\partial \rho_{g,3}}{\partial P_g}\Big|_{h_{g,3}})+\frac{1}{2}(\frac{\partial \rho_{g,3}}{\partial h_{g,3}}\Big|_{P_g})(\frac{dh_{g,g}}{dP_g}))(h_{g,3}-h_{g,g})+\frac{1}{2}(\frac{dh_{g,g}}{dP_g})\rho_{g,3}-1]L_{g,3}A_{g,cs}\dot{P}_g\\
&+\frac{1}{2}[(\frac{\partial \rho_{g,3}}{\partial h_{g,3}}\Big|_{P_g})(h_{g,3}-h_{g,g})+\rho_{g,3}]L_{g,3}A_{g,cs}\dot{h}_{g,o}+\rho_{g,3}(h_{g,g}-h_{g,3})A_{g,cs}(\dot{L}_{g,1}+\dot{L}_{g,2})\\
&=\dot{m}_{g,r,o}(h_{g,g}-h_{g,o})+A_{g,3}\alpha_{g,r,3}(T_{g,w,3}-T_{g,r,3})
\end{aligned}
\tag{5-14}
$$

$$
\begin{aligned}
&[((\frac{\partial \rho_{g,1}}{\partial P_g}\Big|_{h_{g,1}})+\frac{1}{2}(\frac{\partial \rho_{g,1}}{\partial h_{g,1}}\Big|_{P_g})(\frac{dh_{g,f}}{dP_g}))L_{g,1}+(\frac{d\rho_{g,f}}{dP_g}(1-\overline{\gamma}_g)+\frac{d\rho_{g,g}}{dP_g}\overline{\gamma}_g)L_{g,2}+((\frac{\partial \rho_{g,3}}{\partial P_g}\Big|_{h_{g,3}}\\
&+\frac{1}{2}(\frac{\partial \rho_{g,3}}{\partial h_{g,3}}\Big|_{P_g})(\frac{dh_{g,g}}{dP_g}))L_{g,3}]A_{g,cs}\dot{P}_g+\frac{1}{2}[(\frac{\partial \rho_{g,3}}{\partial h_{g,3}}\Big|_{P_g})L_{g,3}]A_{g,cs}\dot{h}_{g,o}+\frac{1}{2}[(\frac{\partial \rho_{g,1}}{\partial h_{g,1}}\Big|_{P_g})L_{g,1}]A_{g,cs}\\
&+(\rho_{g,1}-\rho_{g,3})A_{g,cs}\dot{L}_{g,1}+[(\rho_{g,f}-\rho_{g,g})\overline{\gamma}_g+(\rho_{g,g}-\rho_{g,3})]A_{g,cs}\dot{L}_{g,2}=\dot{m}_{g,r,i}-\dot{m}_{g,r,o}
\end{aligned}
\tag{5-15}
$$

The time derivative of a parameter is indicated with a dot above it.

The governing equations of the wall energy in three zones are obtained by integrating Eq. (5-11) over each zone as shown by Willatzen et al. [58]. As a result, the energy equations for the generator wall are derived as:

$$
\rho_w Cp_w A_w[\dot{T}_{g,w,1}L_{g,1}+(T_{g,w,1}-T_{g,w,2})\dot{L}_{g,1}]=\alpha_{g,r,1}A_{g,1}(T_{g,r,1}-T_{g,w,1})+\dot{Q}_{g,th,1} \tag{5-16}
$$

$$
\rho_w Cp_w A_w\dot{T}_{g,w,2}L_{g,2}=\alpha_{g,r,2}A_{g,2}(T_{g,r,2}-T_{g,w,2})+\dot{Q}_{g,th,2} \tag{5-17}
$$

$$\rho_w Cp_w A_w[\dot{T}_{g,w,3}L_3 + (T_{g,w,2} - T_{g,w,3})(\dot{L}_{g,1} + \dot{L}_{g,2})] = \alpha_{g,r,3}A_{g,3}(T_{g,r,3} - T_{g,w,3}) + \dot{Q}_{g,th,3} \quad (5\text{-}18)$$

$A_{g,1}$, $A_{g,2}$ and $A_{g,3}$ represents the heat transfer surface areas of each zone.

Condenser model

The same approach as the generator is used to develop the dynamic model of the condenser. For brevity, the condenser dynamic model equation set is presented in Appendix D. However, it can be accessed in the reference [62].

Evaporator model

In the current study, the time derivative of inlet specific enthalpy ($\dot{h}_{e,i}$) is included in the evaporator dynamic model, which was fixed at zero by Rasmussen et al.[161]. The details concerning the derivations of the evaporator governing equations were shown in a study conducted by Chen and Yu[160]. The difference between the model in this paper and Chen and Yu, 2018 work is related to the evaluation of $\dot{h}_{e,i}$. They considered $\dot{h}_{e,i}$ as an additional input variable in their model while in the present study it is assumed that the evaporator inlet specific enthalpy equals the condenser outlet specific enthalpy since the expansion valve operates in an isenthalpic manner (Figure 5-1). Thus, the time derivatives of these two parameters also equal (Eq. (5-7)). The equations of the evaporator model are shown in appendix E.

The heat transfer coefficients for the refrigerant side and thermal fluid side are evaluated separately in each heat exchanger using the empirical relations suggested in the literature. The heat transfer coefficients in single-phase zones of all heat exchangers are evaluated using the well-known Gnielinski correlation[139]. To evaluate the boiling and condensation heat transfer coefficients of two-phase zones in the generator, evaporator and condenser, the correlations introduced by Yan and Lin and Yan et al. in reference [165] are applied.

5.4. Solution procedure

The overall dynamic model of the system is generated by interconnecting the component models. The coupling among physical parameters is shown in Figure 5-6. To solve the entire

closed cycle, it is required to know the starting point of the simulation. As the dynamic responses of the ejector, pump and expansion valve are faster than those of the heat exchangers, it is assumed that their state parameters do not change at each time step. However, the heat exchangers are simulated with dynamic models and their state parameters vary at each time step. Thus, the simulation starts with solving the models of the pump, expansion valve and ejector to evaluate the mass flow rates, which are fed to the dynamic model of the heat exchangers as inputs at each calculation step.

The solution algorithm of the overall dynamic model is explained in the flowchart in Figure 5-7. The differential equations are solved in MATLAB using the fourth order Runge–Kutta method. The thermodynamic properties are called from REFPROP 9.0 database developed Lemmon et al. [166].

It should be mentioned that the values of the primary and secondary stream pressures and enthalpies (P_{pr}, P_s, P_2, h_{pr} and h_s) used as inputs to the ejector model are equivalent to the generator, evaporator and condenser pressures and their output enthalpies ($P_g, P_e, P_c, h_{g,o}$ and $h_{e,o}$), respectively. The outputs of the ejector model including $\dot{m}_s, \dot{m}_{pr}$ and h_2 are equivalent to $\dot{m}_{e,r,o}, \dot{m}_{g,r,o}\ and\ h_{c,i}$, respectively and are used as inputs to the heat exchangers model.

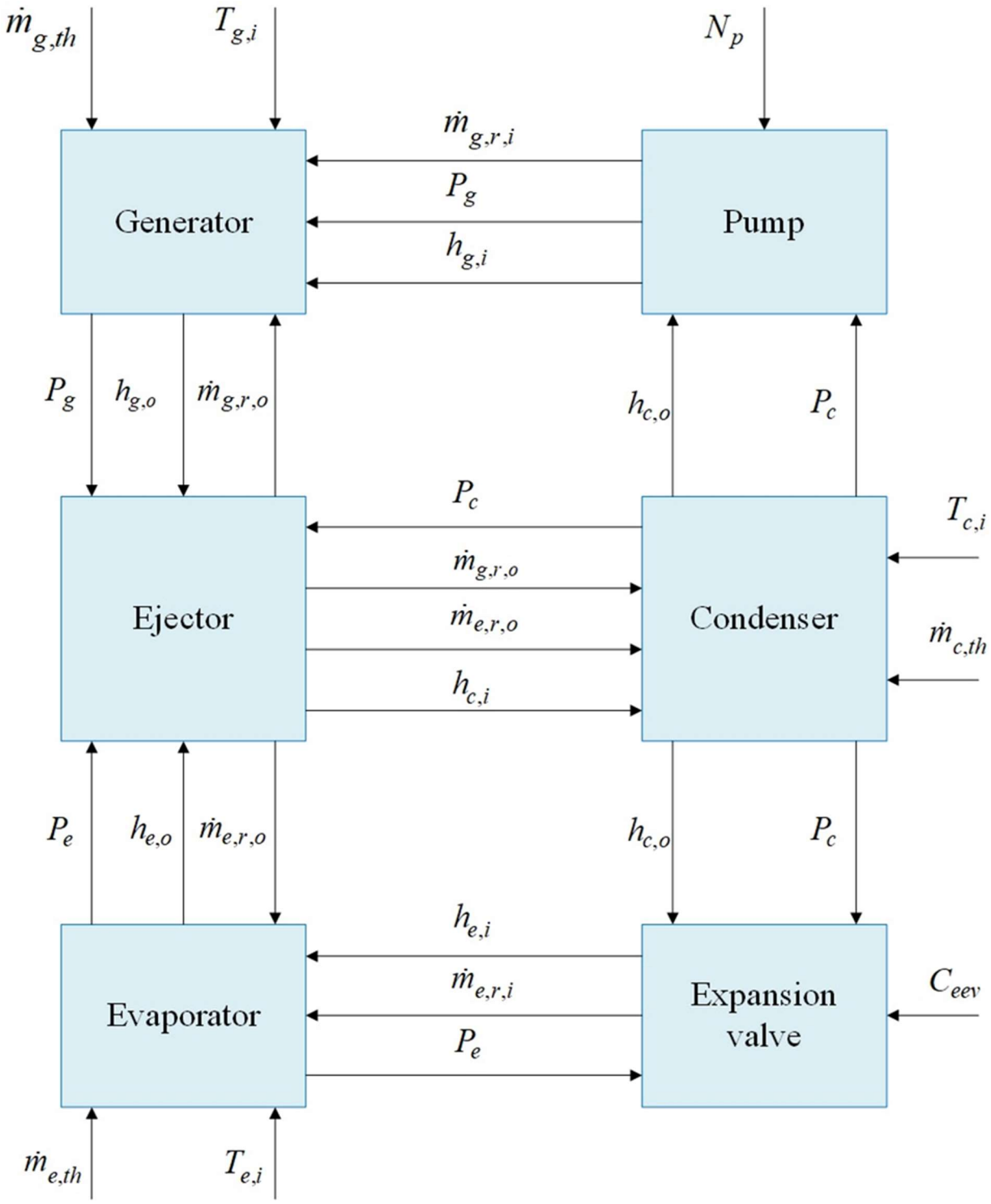

Figure 5-6: Physical parameters coupling of ERS

The control input is N_p

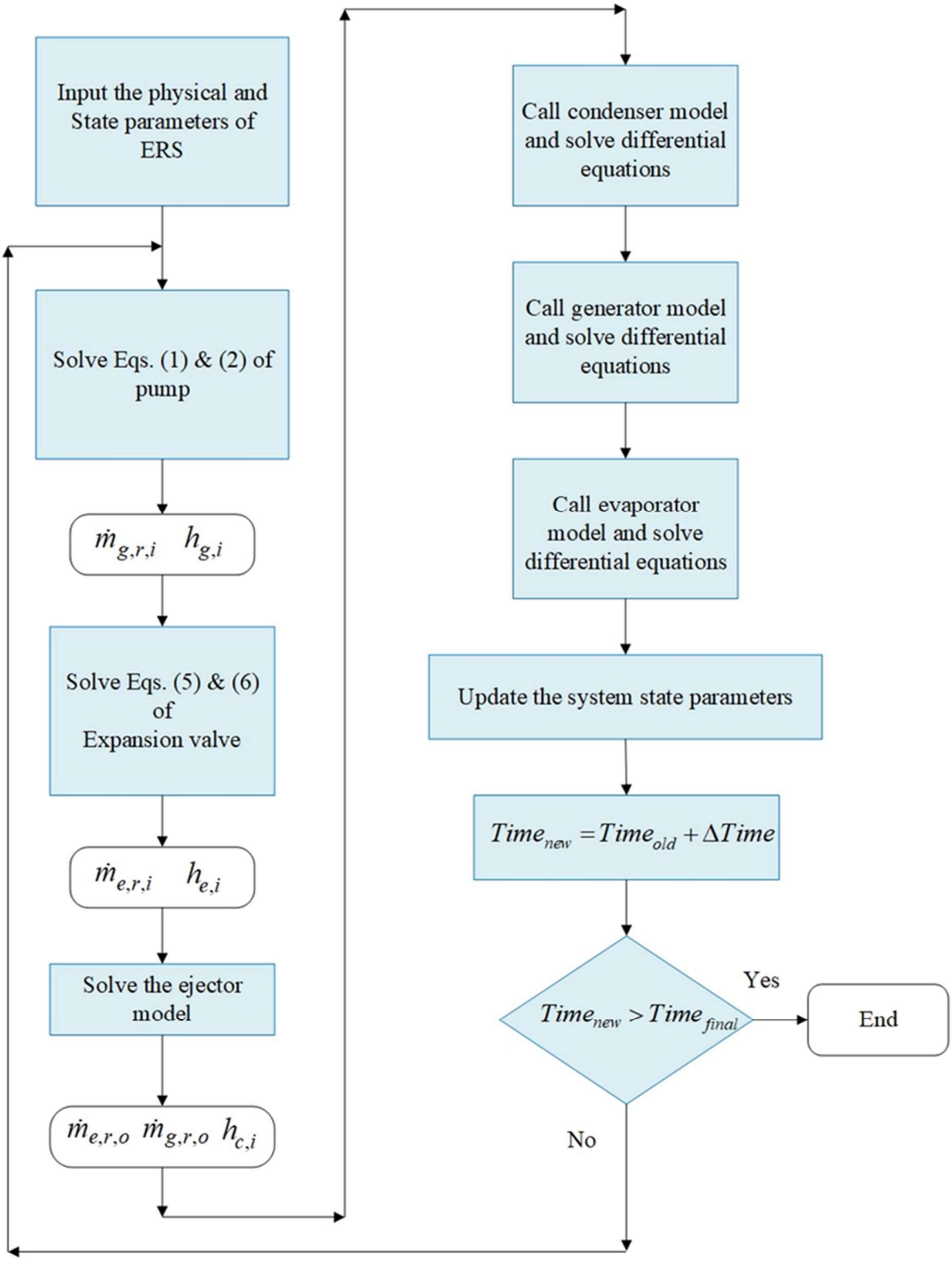

Figure 5-7: ERS dynamic model flowchart

5.5. Results and discussion

5.5.1. Experimental setup

The discussed modeling framework is validated using the data obtained from the experimental setup located at the Laboratoire des technologies de l'énergie of Hydro-Québec. R245fa was used as a refrigerant. Figure 5-8 indicates the measurements locations for the temperature, pressure and mass flow rate in the experimental setup of ERS utilized in this study.

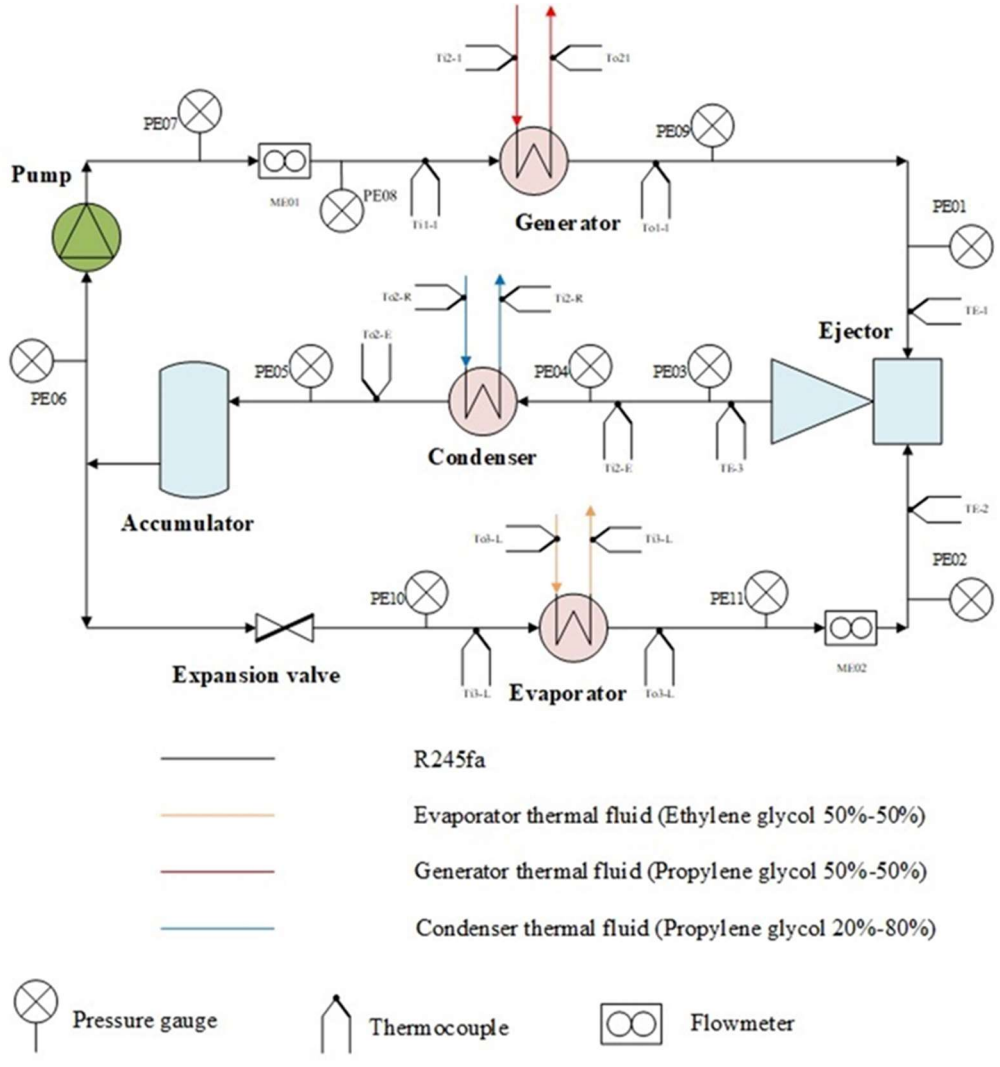

Figure 5-8: Schematic view of the measurements' locations in the experimental setup of ERS

The heat transfer in experimental setup is through counter-current brazed plate heat exchangers, which are employed as the condenser (300 kW), generator (250 kW) and evaporator (35 kW). The 250 kW electric boiler that delivers thermal energy to the ERS vapor generator simulates a waste heat source, using Propylene glycol (50/50 mass-based) as the thermal fluid. To simulate the cooling load, a 45 kW electric cartridge heater is used than sends the input heat through the thermal fluid (Ethylene glycol 50/50 mass-based) of the evaporator. A cooling tower with a capacity of 400 kW connects to the condenser and completes the cooling loop. Propylene glycol (20/80) is used as the thermal fluid in this loop. Its condenser inlet temperature, with a standard deviation of ± 0.5 °C, is controlled by means of a 3-way mixing valve.

A controller operated electronic expansion valve (EEV) with 2500 steps expands the condenser outlet stream in an isenthalpic process to the evaporator pressure. The values of the temperature, pressure and mass flow rate at several points of the system are measured using T type thermocouples (accuracy ±0.5 °C) and pressure transducers (accuracy ±0.25% of reading in the operation pressure range) and Coriolis flow meters (accuracy: ±0.05% uncertainty over the respective flow ranges) respectively. The AC watt transducers (accuracies: ±0.2% reading) was used to measure the electric power provided to the boiler, the thermal load heater and the feed pump. The R245fa is supplied to the generator using a feed pump, which works based on a regenerative turbine impeller technology (known also as vortex pump) and is driven by a 3 hp motor. A data acquisition system recorded the data generated at 5 seconds intervals and HP-VEE software was used to monitor, control and analyze the produced data from the experimental set-up.

5.5.2. Model validation results

In order to study the transient response of the developed ERS dynamic model, the tests and simulations are carried out by incrementally applying step changes to the pump speed. The inlet temperatures and the mass flow rates of the thermal fluids in all heat exchangers are kept constant. The operation conditions of the system are reported in Table 5-1.

Table 5-1: The constant operation conditions

Variable	Value
Generator thermal fluid inlet temperature, ℃	85±0.05
Generator thermal fluid mass flow rate, kg s^{-1}	6.69±0.039
Condenser thermal fluid inlet temperature, ℃	20±0.06
Condenser thermal fluid mass flow rate, kg s^{-1}	4.16±0.027
Evaporator thermal fluid inlet temperature, ℃	19.95±0.05
Evaporator thermal fluid mass flow rate, kg s^{-1}	1.02±0.0029

The dynamic behavior of the heat exchangers is mostly characterized by the pressure and the outlet enthalpy, which can define the other thermodynamic properties of the system. Figure 5-9 and Figure 5-10 illustrate the experimental and simulation results of the transient responses to pump speed step changes, as measured by the heat exchangers' pressures and outlet enthalpies. To have a clear image of the experimental data, the moving average filtering method is used to filter the noisy experimental data [153]. The red line represents the filtered experimental data.

Figure 5-9 and Figure 5-10 indicate that both the response speeds and numerical values of the heat exchangers' pressures and outlet enthalpies are in good agreement with the experimental data. When the pump speed is suddenly augmented, the generator and condenser pressures increase to peaks (overshooting) and then reach a new relatively stable state, which matches with experimental data of the condenser pressure, but it is not well matched with the experimental data of the generator pressure. It should be taken into account that the response speeds of the heat exchangers in terms of the pressures and outlet enthalpies to the pump speed variation cannot be easily quantified using the observed experiments due to the existence of the noise.

Regarding the results of the model, the rise time of the generator and condenser pressures are approximately 110 seconds based on the model, while, the estimated time response of the evaporator pressure is around 90 seconds. These values are beneficial in estimation of the parameters of the reduced dynamic models of the system where the extraction of such data from the noisy experimental data is not straightforward. The evaporator response to the step change of the pump speed is different from that of the two other heat exchangers (Figure 5-9 (c) & Figure 5-10 (c)). The evaporator pressure first decreases with an increase in the pump speed then increases. This phenomenon is discussed by preceding studies and its

reasons are investigated in detail [30] [153]. The ERS dynamic model in the present study is able to predict the steady state values of the evaporator pressure and outlet enthalpy with good accuracy; however, its accuracy in predicting the responses' speed is low. It is believed that the poor agreement with the experimental data in the responses' speed of the evaporator is mostly attributed to the experimental noise, which cannot be predicted by the developed model.

Figure 5-11 illustrates the variations of the primary stream mass flow rate and the entrainment ratio (Er) of the ejector to the step change of the pump speed using the developed model. The mass flow rate of the primary flow increases after the pump speed increases, while the Er decreases since the secondary stream mass flow rate stays roughly constant. The rise time of the primary stream mass flow rate and Er are 112 seconds, which roughly matches with the generator and condenser responses' speed to the pump speed step change.

The maximum relative error (δ) of the model perditions compared to the filtered experimental data are reported in Table 5-2.

$$\delta = \max \left| \frac{(u_{filt} - u_{Mod})}{u_{filt}} 100 \right| \tag{5-19}$$

Table 5-2: The maximum relative error of the dynamic model predictions

Variable, (u)	δ, %
P_g	1.5
$h_{g,o}$	0.5
P_c	0.89
$h_{c,o}$	0.17
P_e	3.78
$h_{e,o}$	0.17

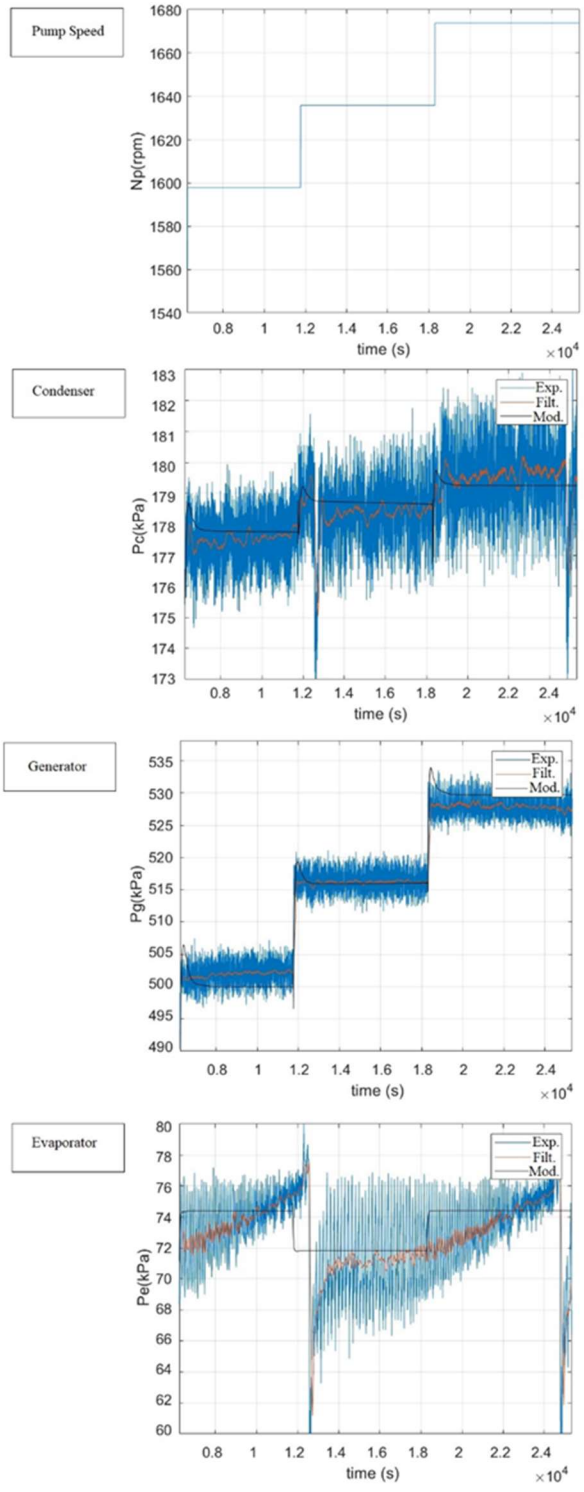

Figure 5-9: Heat exchangers model validation based on pressure for step change of pump speed

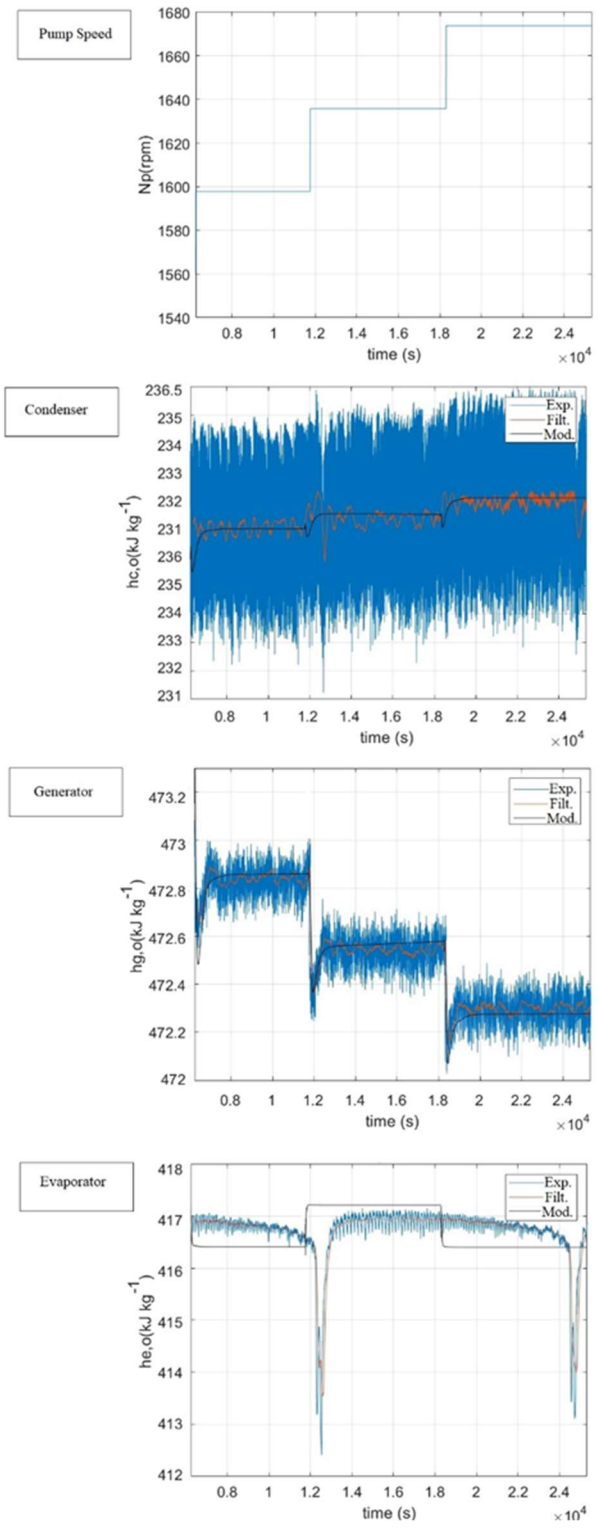

Figure 5-10: Heat exchangers model validation based on outlet enthalpies for step change of pump speed

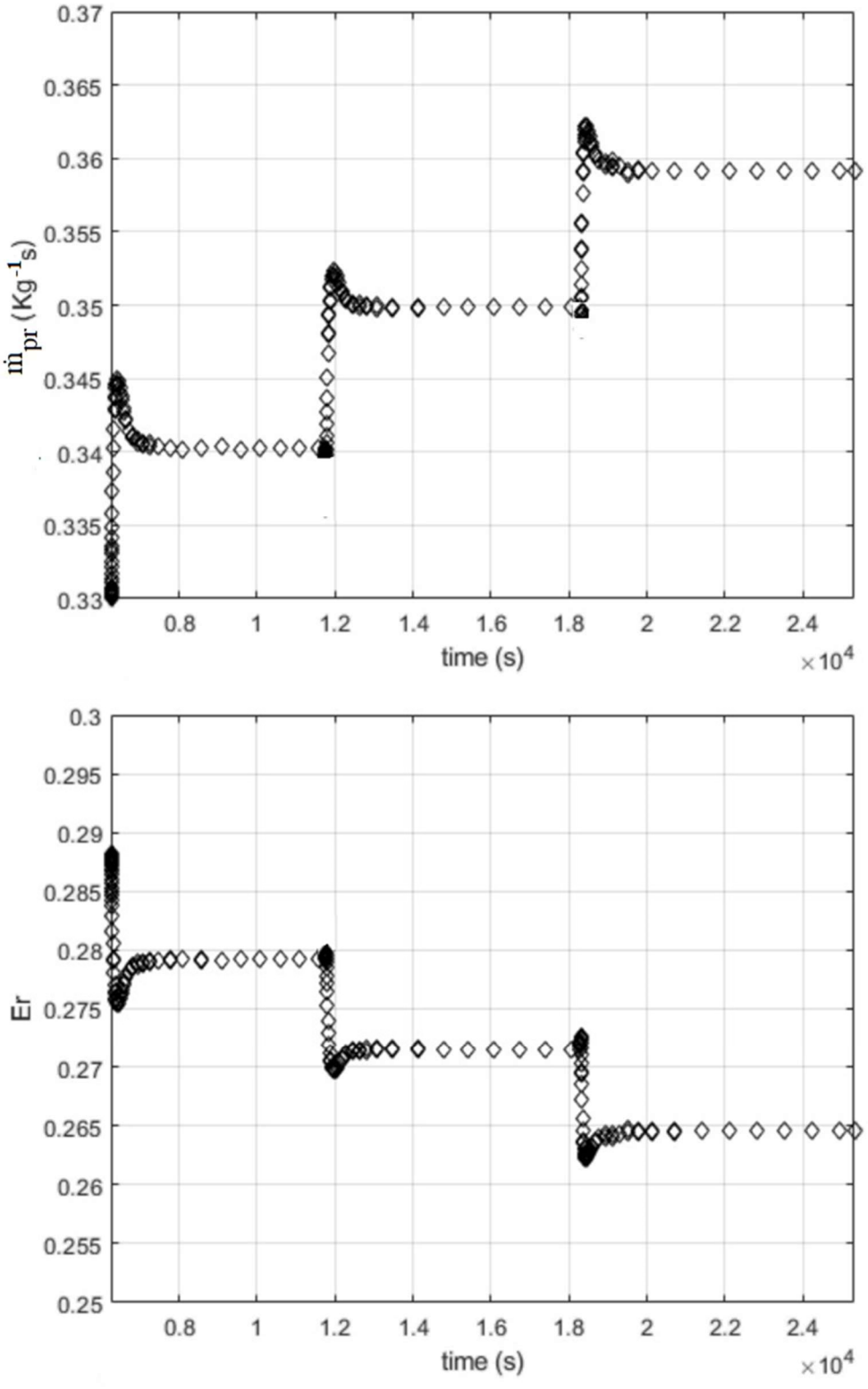

Figure 5-11: Variations of primary stream mass flow rate and Er with the step change of the pump speed using the model

5.6. Conclusions

To the authors' knowledge, this paper presents the first dynamic model of an ejector-based refrigeration system (ERS). Regarding the fact that the heat exchangers have the greatest influence on the ERS dynamic behavior, moving boundary dynamic models were developed for the generator, condenser and evaporator. The pump, ejector and expansion valve were modeled by sets of the algebraic equations. The time derivatives of the inlet specific enthalpies of the generator and evaporator were included in the model using the assumption of the equality between the condenser outlet specific enthalpy and the generator and evaporator inlet specific enthalpies. This assumption was made based on the negligible enthalpy increase in the pump and isenthalpic expansion in the expansion valve. The transient responses of the system on the pressures and outlet enthalpies of the generator, condenser and evaporator were simulated and measured experimentally against different values of the pump speed. The increase in the pump speed augments the generator and condenser pressures, whereas the evaporator pressure first decreases, then increases. The results of the validation study revealed that the developed dynamic model of ERS is able to capture the relevant transient behavior qualitatively and quantitatively with the relative error less than 4 % for both the pressures and outlet enthalpies in the heat exchangers. In the future study, the developed model will be used in designing a control model and predicting the cycle performance.

5.7. Acknowledgements

The authors wish to thank Hydro-Québec laboratory Shawinigan for their valuable contribution during this research study. This project is a part of the Collaborative Research and Development (CRD) Grants Program at 'Université de Sherbrooke'. The authors also acknowledge the support of the Natural Sciences and Engineering Research Council of Canada, Rio Tinto Alcan and CanmetEnergy Research Center of Natural Resources Canada.

5.8. Nomenclature

Table 5-3: Nomenclature

Latin	Definition
A	Cross-section area of the heat exchanger channel, [m2]
A	Heat transfer surface area, [m2]
A_{eev}	Effective passage flow area of expansion valve, [m2]
A_v	Valve opening of expansion valve, [%]
A_0	Nominal orifice cross-sectional area, [m2]
B	Gap between two plates of the heat exchanger area, [m]
Cp	Specific heat capacity $[kJ\ kg^{-1}K^{-1}]$
C_{eev}	Discharge coefficient of expansion valve, [-]
D	Diameter of the ejector components, [m]
ρ	Density, $[kg\ m^{-3}]$
G	Mass flux, $[kgm^{-2}s^{-1}]$
H	Height of the heat exchanger, [m]
h	Specific enthalpy, $[kJ\ kg^{-1}]$
l	length of the heat exchanger, [m]
L	Length of the heat exchanger's zone, [m]
$\dot{m}$	mass flow rate, $[kg\ s^{-1}]$
N_P	Pump speed, [rpm]
P	Pressure, [kPa]
p	Perimeter, [m]
Pe	Péclet number, [-]
Q	Heat load, [kW]
S	Entropy, $[kJ\ kg^{-1}℃^{-1}]$
T	Temperature of a zone, [°C]
U	Flow velocity, $[m\ s^{-1}]$
$\bar{v}_p$	Mean specific volume, $[m^3kg^{-1}]$
v_p	Specific volume, $[m^3kg^{-1}]$
W	Width of heat exchanger, [m]
x	Quality of a stream, [-]
z	Longitudinal coordinate [m]
Greek	
α	Heat transfer coefficient, $[kW\ m^{-2}K^{-1}]$
σ_p	Pump efficiency, [-]
ξ	Width of the heat exchanger wall, [m]
η_s	Isentropic expansion efficiency of secondary flow in hypothetical throat, [-]
η_p	Isentropic expansion efficiency of primary flow in throat, [-]
η_d	Isentropic compression efficiency of flow in diffuser, [-]
φ_{Mix}	Mixing efficiency of the ejector, [-]
$\bar{\gamma}$	Mean void fraction, [-]
δ	Maximum relative error, [%]
subscripts	
c	condenser
$c,1$	Superheating zone of condenser
$c,2$	Two-phase zone of condenser
$c,3$	Subcooling zone of condenser

c, f	Saturated liquid in condenser pressure
c, g	Saturated vapor in condenser pressure
c, i	Inlet stream to condenser
c, o	Outlet stream to condenser
$c, w, 1$	Wall of superheating zone of condenser
$c, w, 2$	Wall of two-phase zone of condenser
$c, w, 3$	Wall of Subcooling zone of condenser
c, cs	Cross-section area of the condenser
e	Evaporator
$e, 1$	Two-phase zone of the evaporator
$e, 2$	Superheating zone of the evaporator
e, f	Saturated liquid in evaporator pressure
e, g	Saturated vapor in evaporator pressure
e, i	Inlet stream to evaporator
e, o	Outlet stream from evaporator
$e, w, 1$	Wall of two-phase zone of evaporator
$e, w, 2$	Wall of superheating zone of evaporator
g	Generator
$g, 1$	Subcooling zone of generator
$g, 2$	Two-phase zone of generator
$g, 3$	Superheating zone of generator
g, g	Saturated vapor in the generator pressure
g, f	Saturated liquid in the generator pressure
g, cs	Cross-section area of the generator
g, i	Inlet stream to generator
g, o	Outlet stream from generator
$g, w, 1$	Wall of Subcooling zone of generator
$g, w, 2$	Wall of two-phase zone of generator
$g, w, 3$	Wall of superheating zone of generator
g, cs	Cross-section area of the generator
int	internal
is	Isentropic process
pr	Primary
r	Refrigerant
s	Secondary
Sat	Saturation
TH	Throat
th	Thermal fluid
w	Wall
Abbreviation	
COP	Coefficient of performance
ERS	Ejector refrigeration system
Exp	Experimental
Filt	Filtered
Mod	Model
Er	Entrainment ratio

CHAPTER 6 Batch phasor Extremum Seeking control of an R245fa ejector-based refrigeration system

Avant-propos

Auteurs et affiliation:

Elhameh Narimani: étudiant au doctorat, faculté de génie, département de génie mécanique, Université de Sherbrooke

Mikhail Sorin: professeur, faculté de génie, département de génie mécanique, Université de Sherbrooke.

Philippe Micheau: professeur, faculté de génie, département de génie mécanique, Université de Sherbrooke.

Hakim Nesreddine: PhD, Chercheur-Chargé de projet, Laboratoire des technologies de l'énergie, Shawinigan (Québec), Canada

Date d'acceptation : 5 Septembre 2019

État de l'acceptation : soumis

Revue: Applied Energy Journal

Titre français: Commande extrêmale par phaseur et trame d'un système de réfrigération à éjecteur R245fa

Contribution au document:

Ce chapitre traite de la conception d'une stratégie de commande extrêmale pour un système de réfrigération à éjecteur R245fa

Résumé en français:

Le système de réfrigération à éjection (SRE) a suscité l'attention considérable des experts en climatisation et en refroidissement à cause de ses avantages environnementaux et économiques. Pour un fonctionnement robuste du système SRE, il est souhaitable de développer une stratégie de contrôle visant à le régler à son efficacité maximale. Les stratégies de commande optimale basées sur un modèle précis du système à commander manquent gravement de robustesse : les performances sont sensibles aux imprécisions sur les modèles et aux incertitudes sur les paramètres. Pour régler au mieux les performances du SRE nous proposons une stratégie d'optimisation en-ligne sur le procédé, connue sous le nom de commande extrêmale (ESC). Les études expérimentales ont révélé que, dans une condition d'entrée fixe du condenseur, il existe une vitesse optimale de la pompe (un débit massique primaire optimal) qui maximise simultanément le taux de compression et l'efficacité exergétique tout en minimisant la pression d'évaporation. Afin de proposer une ESC implémentable en temps discret sur une installation réelle sujette à un bruit de mesure important et contrainte à un traitement hors-ligne par trame, une nouvelle commande extrémale basée sur une approche par phaseur avec une procédure de traitement de signal par trame (BPESC) a été développée et simulée avec le modèle numérique. Ce schéma novateur de commande extrêmale appelé BPESC (Batch Phasor ESC) permet de minimiser la pression P_e du système à une température d'entrée du condensateur de 18°C, lorsque le SRE fonctionne au coefficient de performance le plus élevé. Les résultats de la simulation numérique effectuée pour les températures d'entrée de fluide thermique constantes des échangeurs de chaleur montrent que le BPESC peut trouver la commande optimale de la pompe qui minimiser la pression P_e avec des bonnes performances en termes de précision et de vitesse de convergence.

6.1. Abstract

The ejector refrigeration system (ERS) has received considerable attention among air conditioning and cooling systems due to its environmental and economic benefits. For robust ERS operation, it is desirable to develop a control strategy that aims to maintain the maximum efficiency of such systems. Since the performance of model-based optimization/control strategies is severely deteriorated by inaccurate system models, in this work a self-optimizing model-free control strategy known as Extremum Seeking Control model (ESC) is proposed to optimize ERS performance. The experimental studies revealed that for the fixed condenser thermal fluid's inlet temperature, there exists an optimum pump speed (i.e. primary mass flow rate) that simultaneously maximizes the compression ratio (Cr) and exergy efficiency (η_{II}), while minimizing the evaporating pressure (P_e). A novel scheme of ESC, hereafter named batch phasor ESC (BPESC), was applied to minimize the system P_e for a fixed condenser thermal fluid's inlet temperature of 18 ℃, since at this temperature the ERS operates at the highest coefficient of performance (COP). BPESC evaluated the gradient by estimating the phasor of the output for each batch time. A dynamic compensator was also included in the gradient estimator. The simulation results conducted for fixed heat exchangers thermal fluids' inlet temperature indicated that the BPESC could seek and find the minimum P_e, with good performance in terms of the convergence rate and of predicting the optimal pump speed input value.

Keywords:

Ejector refrigeration system (ERS); compression ratio (CR); exergy efficiency (η_{II}), batch phasor Extremum seeking control strategy (ESC), Dynamic compensator

6.2. Introduction

Nowadays, vapor compression systems including heat pumps, refrigeration, and air-conditioning systems, are widely used in both industrial and domestic sectors. As a result, the performance improvement of such systems has received considerable research interest. In the refrigeration sector, the ejector-based refrigeration system provides a promising

approach for producing cooling effect, by harvesting the waste heat from the industrial processes or using renewable energy, such as solar radiation and geothermal energy, which makes such systems particularly interesting in this energy-conscious era. However, the efficiency of the ejector-based refrigeration system is relatively low, which has limited its industrial applications. A limited number of research works have studied the working characteristics of ejector-based refrigeration systems to improve their performance and promote their use. Hence, optimization and the design of control models for such systems are essential tasks for energy and environmental sustainability.

Numerical and experimental studies so far have indicated that the performance of an ERS can be optimized through COP, entrainment ratio (Er), or Cr. For instance, Yapici et al. indicated that increasing the temperature of the generator at a fixed condenser temperature (at a fixed ejector backpressure) would lead to a rise in COP to a maximum value [21]. Thongtip and Aphornratana observed that for a particular ejector geometry there is an optimal range of the primary fluid mass flow rate that produces the lowest suction pressure at a specified condenser pressure. The advantage of increasing of the primary fluid mass flow rate to the optimum value is that the ejector would be able to operate at a higher critical backpressure [27]. Another study, conducted by Jia and Wenjian, implied that an air-cooled R134a ejector refrigeration cycle could reach the maximum Er with an optimum primary flow pressure, where both the back pressure and secondary stream pressure are fixed [144]. Hamzaoui et al. demonstrated that an increase in the generating pressure raises Cr to a maximum value [30]. Furthermore, Narimani et al.[153] conducted a numerical and experimental study to investigate the effect of the primary stream pressure on the performance of ERS with respect to Cr.

Various control strategies could be employed based on performance objectives with different combinations of control inputs for each. The vast majority of the proposed control approaches in the literature for vapor compression systems are model-based control strategies to optimize the performance with respect to both first and second law efficiency metrics [167], or they minimize power consumption [168]. However, in our judgement, there is still a gap in the literature studying the development of control strategies for the ERS.

Model-based control strategies are typically based on a static or dynamic system model and used to determine the optimal set points that maximize system efficiency. For instance, Salazar and Méndez [169] employed a proportional–integral–derivative (PID) control scheme to find the best scenarios of a transcritical CO_2 refrigeration cycle. Many available dynamic model-based control strategies are developed using linear dynamic models of the system, and therefore they could only operate near some nominal conditions from which the linear model was developed. Moreover, there are always unknown disturbances that cannot be included in the models, such as errors in the temperature or pressure sensors, which reduce the accuracy of the model-based control strategies.

To overcome the obstacles of the model-based control strategies, model-free adaptive controllers have emerged in this context. The extremum seeking control (ESC) strategy is considered a self-optimizing model-free control approach, introduced in 1922 by Leblanc [75] as the first adaptive controller reported in the literature. Although, the original idea of ESC is quite old, the academic and industrial interest was boosted 40 years later when the first proofs of ESC stability were published by Krstić and Wang [89] and Ariyur and Krstić [77]. Since then, ESC has been widely used to maximize power generation in various fields, such as combustion processes (for IC engines, steam generating plants, and gas furnaces), grinding processes, and blade adjustment in water turbines and wind mills.

Unlike many adaptive controllers, which can only adjust the control variable to a known set-point, the classical ESC could search for the unknown extremum of a steady-state input/output map. In this context, the main goal of the classical ESC is to find a set of inputs that minimize or maximize the system's output. The gradient estimation of the system's map is the key element of each ESC method, which is implemented by numerically perturbing the system using an external excitation signal. In the classical algorithms this task is accomplished by using a combination of high- and low-pass filters and perturbation signals.

Recently a wide range of ESC applications in designing the control models of HVAC systems have appeared in the literature. Burns and Laughman [126] modeled an energy optimizing ESC for a vapor compression system (VCS), which could automatically discover sets of inputs minimizing the energy consumption. Burns et al. [125] employed a model-free

extremum seeking algorithm that adjusted the compressor discharge temperature setpoints to optimize the system's energy efficiency. In another study, Koeln and Alleyne [127] used ESC to find the optimal subcooling in an improved vapor compression system with a receiver and an additional electronic expansion valve and found out that there was a significant improvement in the efficiency using the alternative architecture and ESC. Li et. al. [123] applied an ESC based self-optimizing strategy to minimize the energy consumption, with the feedback of the chilled water supply command in a single-duct air-handling unit (AHU). The COP of the air-source transcritical CO_2 heat pump was maximized using an ESC strategy in which the discharge pressure setpoint was considered as the input to the ESC controller, while the system COP was taken as the performance index, in Hu et. al. [128].

Having reviewed the literature, one can realize that development of a control strategy for an ERS has not been investigated yet. In this context, this paper mainly aims to build the theoretical basis for developing a control model for an ERS. In the present study, to define the objective function of the control model, experimental analysis of an ERS was carried out. The experimental study revealed that there is a pump speed that simultaneously maximizes the Cr and η_{II}, while minimizing P_e, for a fixed condenser thermal fluid inlet temperature. At the same time, COP linearly decreases as pump speed increases. Hence, the minimum P_e is chosen as the objective function for the control model development.

Based on the features of the experimental ERS and the chosen objective function, an innovative ESC scheme is proposed to design a control model. This ESC estimates the gradient of the system by evaluating the output phasor in the discrete time scheme using the batch processing of the captured data in batch time, therefore, it was named batch phasor ESC(BPESC). The input and output of the proposed BPESC model are the pump speed and the evaporating pressure, respectively. A dynamic compensator is also included in the gradient estimation to the proposed model efficiency to compensate the influence of the phase shift caused by the system dynamics. Finally, the simulation results are presented to demonstrate the effectiveness of the batch phasor ESC.

6.3. Experimental Setup

The schematic view of the ejector refrigeration cycle and its P-h diagram is indicated in Figure 6-1. The experimental setup is located at Laboratoire des technologies de l'énergie of Hydro-Quebec. Counter-current brazed plate heat exchangers are used in the current setup as the condenser (300 kW), generator (250 kW) and evaporator (35 kW). The 250 kW electric boiler that delivers thermal energy to the ERS vapor generator simulates a waste heat source, using Propylene glycol (50/50 mass-based) as the thermal fluid.

The cooling load is simulated using a 45 kW electric cartridge heater that sends the input heat through the thermal fluid (Ethylene glycol 50/50 mass-based) of the evaporator. A cooling tower with a capacity of 400 kW connected to the condenser forms the cooling loop. Propylene glycol (20/80 mass-based) is used as the thermal fluid in this loop. Its condenser inlet temperature, with a standard deviation of ± 0.5 °C, is regulated by means of a 3-way mixing valve.

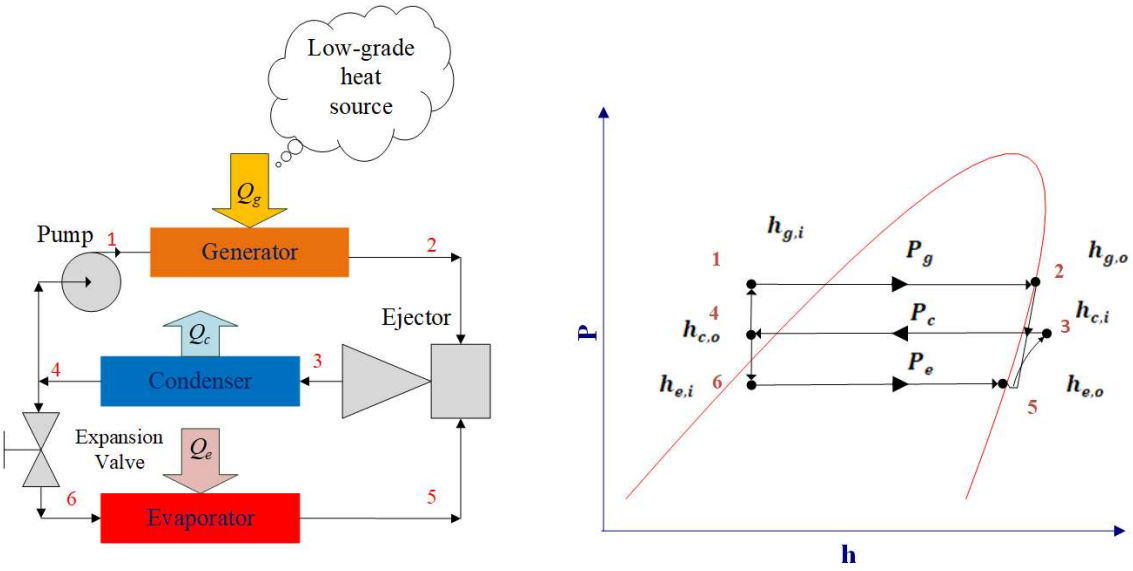

Figure 6-1: a) Schematic representation of the ERS setup b) its P-h diagram

An electronic expansion valve (EEV) with 2500 steps, connected to a controller, expands the outlet stream of the condenser in an isenthalpic process to the evaporator pressure. The values of the temperature, pressure and mass flow rate at several points of the system are

measured using T type thermocouples (accuracy ±0.5 °C) and pressure transducers (accuracy ±0.25 % of reading in the operation pressure range) and Coriolis flow meters (accuracy: ±0.05% uncertainty over the respective flow ranges), respectively. AC watt transducers (accuracies: ±0.2 % reading) are used to measure the electric power provided to the boiler, the thermal load heater and the feed pump. The R245fa is supplied to the generator using a feed pump, which works based on a regenerative turbine impeller technology (known also as vortex pump) and is driven by a 3 hp motor. A data acquisition system records the data generated at 5 seconds intervals and HP-VEE software is used to monitor, control and analyze the produced data from the experimental set-up.

6.4. Experimental analyses

At various condenser temperatures (coolant inlet temperature, $T_{c,i}$) ranging from 18℃ to 26℃, the value of the primary stream mass flow rate ($\dot{m}_P$) was augmented by increasing the pump speed (N), which resulted in an increase in the generating pressure (P_g). The inlet temperatures of the thermal fluids were kept constant in the generator and evaporator. Moreover, the thermal fluids mass flow rates in all heat exchangers remained unchanged. The operation conditions of the system are reported in Table 6-1.

Table 6-1: The constant operation conditions

Variable	Value
Generator thermal fluid inlet temperature, ℃	85±0.05
Generator thermal fluid mass flow rate, kg s^{-1}	6.69±0.039
Condenser thermal fluid mass flow rate, kg s^{-1}	4.16±0.027
Evaporator thermal fluid inlet temperature, ℃	19.95±0.05
Evaporator thermal fluid mass flow rate, kg s^{-1}	1.02±0.0029
Pump work, kW	0.25±0.0009

The impact of increasing the pump speed on the performance indicators of the ERS was investigated using the experimental data. The performance indicators of the system are defined using three important metrics:

- The coefficient of the performance (COP) which is evaluated as the ratio of the evaporator cooling effect over the summation of consumed energy by the system:

$$COP = \frac{\dot{Q}_e}{\dot{Q}_g + W_p} \tag{6-1}$$

The pump work, W_p is negligible.

- The exergy efficiency which is calculated as the ratio of the recovered exergy over the total supplied exergy [170]:

$$\eta_{II} = \frac{E_e}{E_g + W_p} \approx \frac{E_e}{E_g} \tag{6-2}$$

where E_e, E_g and W_p are the recovered exergy rate of the evaporator, the supplied exergy rates to the generator and pump, respectively. The supplied exergy to the pump is negligible and not included in the exergy efficiency calculations. To evaluate the exergy efficiency the following equations are used:

$$E_e = \dot{Q}_e \left| 1 - \frac{T_r}{T_{sc,e}} \right| \tag{6-3}$$

$$E_g = \dot{Q}_g \left| 1 - \frac{T_r}{T_{sc,g}} \right| \tag{6-4}$$

$$T_{sc,e} = \frac{T_{e,i} + T_{e,o}}{2} \tag{6-5}$$

$$T_{sc,g} = \frac{T_{g,i} + T_{g,o}}{2} \tag{6-6}$$

$$\eta_{II} = \frac{\dot{Q}_e \left| 1 - \frac{T_r}{T_{sc,e}} \right|}{\dot{Q}_g \left| 1 - \frac{T_r}{T_{sc,g}} \right|} = COP \frac{\left| 1 - \frac{T_r}{T_{sc,e}} \right|}{\left| 1 - \frac{T_r}{T_{sc,g}} \right|} \tag{6-7}$$

Where, the inlet and outlet temperatures of the thermal fluids (secondary side) in the heat exchangers are shown by $T_{e,i}$, and $T_{e,o}$ in the evaporator, $T_{c,i}$, and $T_{c,o}$ in the condenser and $T_{g,i}$, and $T_{g,o}$ in the generator. Furthermore, T_r is the reference temperature which is assumed to be equal to the environmental temperature of 25℃.

- Compression ratio (*Cr*), which is the ratio of the condensing pressure to the evaporating pressure.

$$Cr = \frac{P_c}{P_e} \tag{6-8}$$

The ejector performance graph is represented in Figure 6-2, which was built using the experimental data and indicates the ejector critical backpressure of 203.545kPa at primary stream mass flow rate of 0.37 kg/s.

Figure 6-1 illustrates the influence of a rise in the pump speed on COP and η_{II}. The COP decreases with increasing pump speed, for all of the evaluated condenser thermal fluid's inlet temperatures except 22 and 24℃ which reach the maximum values before decreasing. While, η_{II} first goes up to a maximum point and then decreases with increasing pump speed, for all condenser thermal fluid's temperatures except 26℃ (which is located in the ejector subcritical operation mode of the ejector (Figure 6-2).

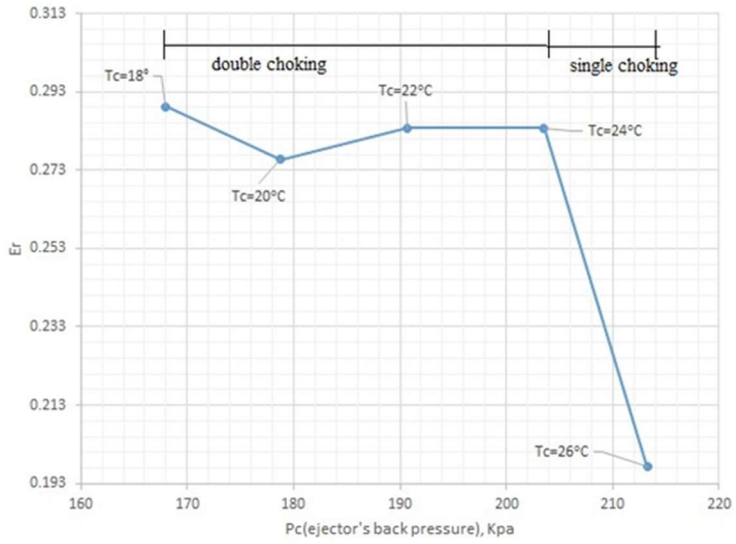

Figure 6-2: Ejector performance curve at $T_{g,i} = 80$℃, $T_{e,i} = 20$℃, $\dot{m}_P = 0.37$kg/s

The variation of *Cr*, P_e and the cooled product temperature at the evaporator outlet ($T_{e,o}$) with pump speed are illustrated in Figure 6-4. According to Figure 6-4, there exists an optimum pump speed which maximizes the *Cr*, meanwhile minimizes the P_e and $T_{e,o}$ at fixed condenser inlet temperatures ($T_{c,i}$). Furthermore, it was observed that the highest COP can

be obtained at the lowest condenser thermal fluid's inlet temperature, 18 ℃. The relation of P_e with N and $T_{c,i}$ can be defined using Eq. (6-9):

$$P_e = g(N, T_{c,i}) \tag{6-9}$$

Therefore, the control strategy will be designed to minimize P_e, since at minimum P_e the ERS operates at both the maximum Cr and η_{II}. Furthermore, as mentioned by Thongtip and Aphornratana [27], increasing the primary stream mass flow rate to an optimum value for a fixed condenser condition enables the ejector to operate at the higher critical backpressure. In the following sections, first the classic Extremum Seeking Control (ESC) approach will be reviewed and then a novel ESC will be introduced to seek the optimal input (N^*) that minimizes the output (P_e) for a fixed condenser thermal fluid's inlet temperature of $T_{c,i}$ =18 ℃. The optimization problem can be symbolically expressed as follows:

$$N^* = \arg \min_{N} P_e(N) \tag{6-10}$$

In fact, the controller will be a SISO controller.

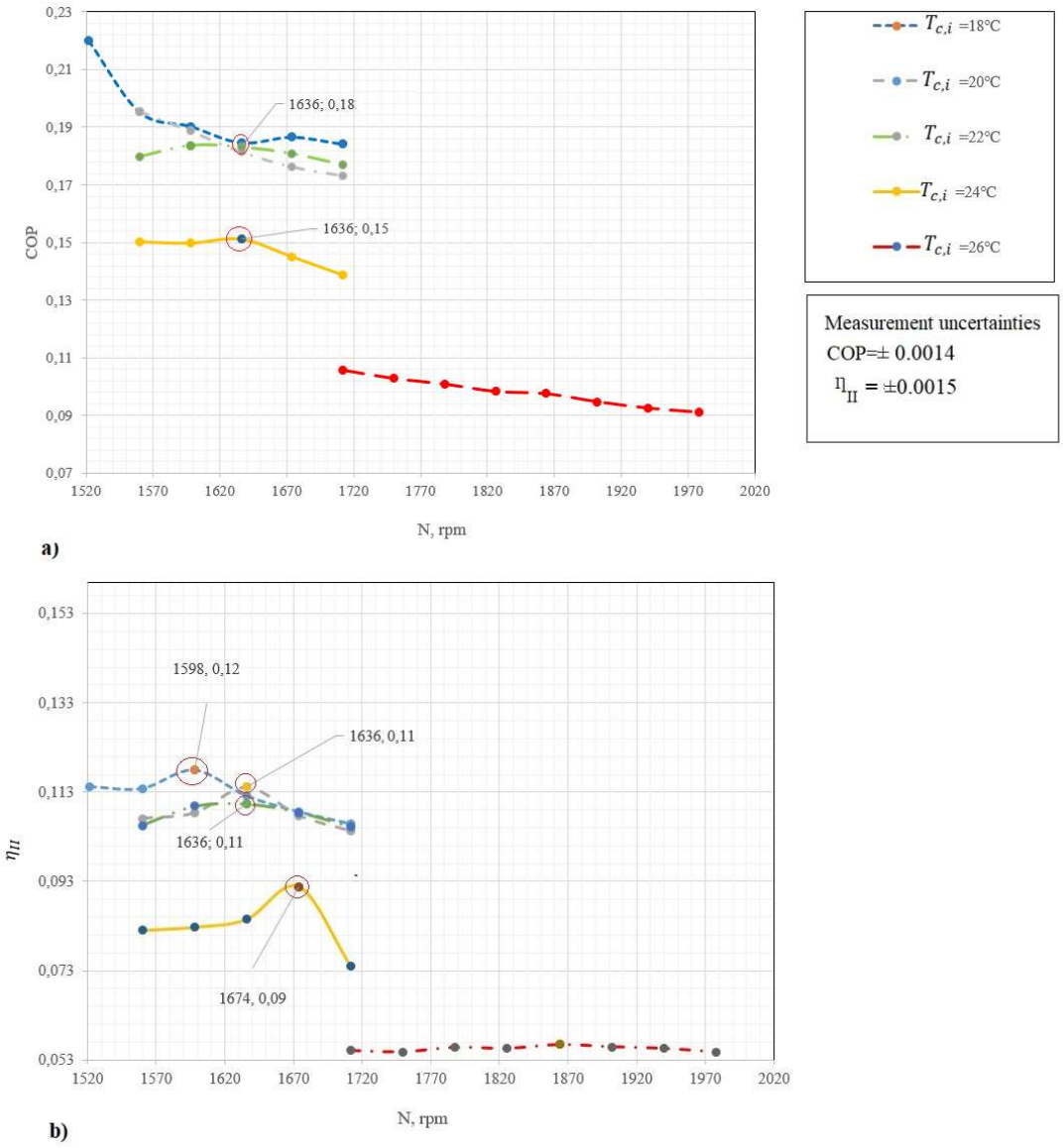

Figure 6-3: a) Variations of COP and b) η_{II} with an increase in N

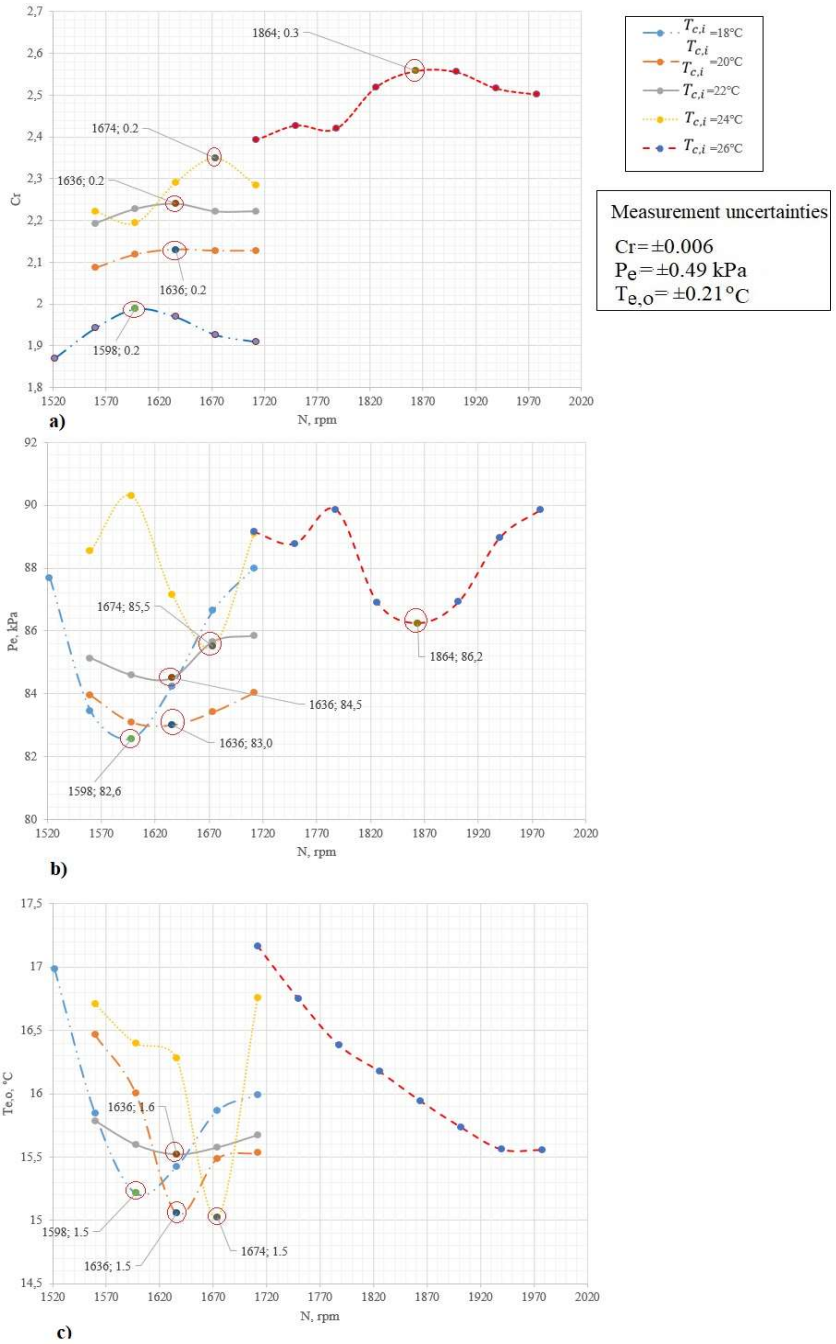

Figure 6-4: Variation of a) Cr b) P_e c) $T_{e,o}$ with increasing N

6.5. Extremum seeking control (ESC)

Figure 6-5 indicates the schematic representation of a typical Extremum seeking control (ESC) used for a single input single output (SISO) system. In earlier studies, like the work

conducted by Krstic and Wang [89], ESC was typically applied to a nonlinear time varying process, called the "plant" in control literature, with a single objective (sometimes also called index). A single objective system can be described using the following state space representation [171]:

$$\frac{dx}{dt} = f(x,u) \tag{6-11}$$

$$y = h(x) \tag{6-12}$$

where $x \in \mathbb{R}^n$ and $u \in \mathbb{R}^m$ are the state and manipulated (input) vectors, respectively. The $y \in \mathbb{R}$ denotes the output, which is a scalar representing the criterion (also called the output objective) for minimization (or maximization). The $f: \mathbb{R}^n \times \mathbb{R} \to \mathbb{R}^n$ and $h: \mathbb{R}^n \to \mathbb{R}$ are static maps and assumed to be sufficiently smooth. It is also assumed that the process (plant) is stable, which implies that the steady state output, y_{ss}, is a function of a constant input (u_0). In fact, u_0 is the output of the integrator and is almost constant during the cycle.

$$y_{ss} = g(u_0) \tag{6-13}$$

To apply ESC, the function g must have a unique minimum (a concave map) or maximum (a convex map), and be sufficiently smooth, for u_0, where $u_0 \in [u_{min}, u_{max}] \in \mathbb{R}$.

In order to include the system's dynamics in ESC, it is assumed by many studies [172] [173] [100] [174] that the non-linear plant (Eqs. (6-11) and (6-12)) can be approximated by a Wiener-Hammerstein model consisting of three parts: the stable input dynamics (F_i) , the stable output dynamics (F_O) and the nonlinear static map (g) between the input and output dynamics (shown in Figure 6-5). In fact, ESC is a model-free, self-optimizing control strategy, which minimizes (or maximizes) the steady state output (y_{ss}) by driving the constant input (u_0) towards its optimum value (u_0^*). In other words, it is designed to solve the following optimization problem in the on-line mode:

$$u_0^* = \arg \min_{u_0} g(u_0) \tag{6-14}$$

According to the ESC algorithm presented in Figure 6-5, the input is perturbed by a dither signal, which is usually a small-amplitude sinusoidal signal (with amplitude "α" and angular frequency "ω") [89] or by a random signal in the stochastic ESC [94]. The dither signal is

employed to estimate the gradient of the smooth static map for a given constant input (u_0) as follows:

$$G(u_0) = \left.\frac{\partial g}{\partial u}\right|_{u_0} \tag{6-15}$$

In fact, the gradient estimator evaluates the local slope of g by observing the small perturbation in the static output y_{ss} with respect to the small perturbation (*e.g.* the dither signal) in the input u. In Figure 6-5, this computation is represented by the gradient estimator block. The gradient estimation is shown by $\hat{G}$.

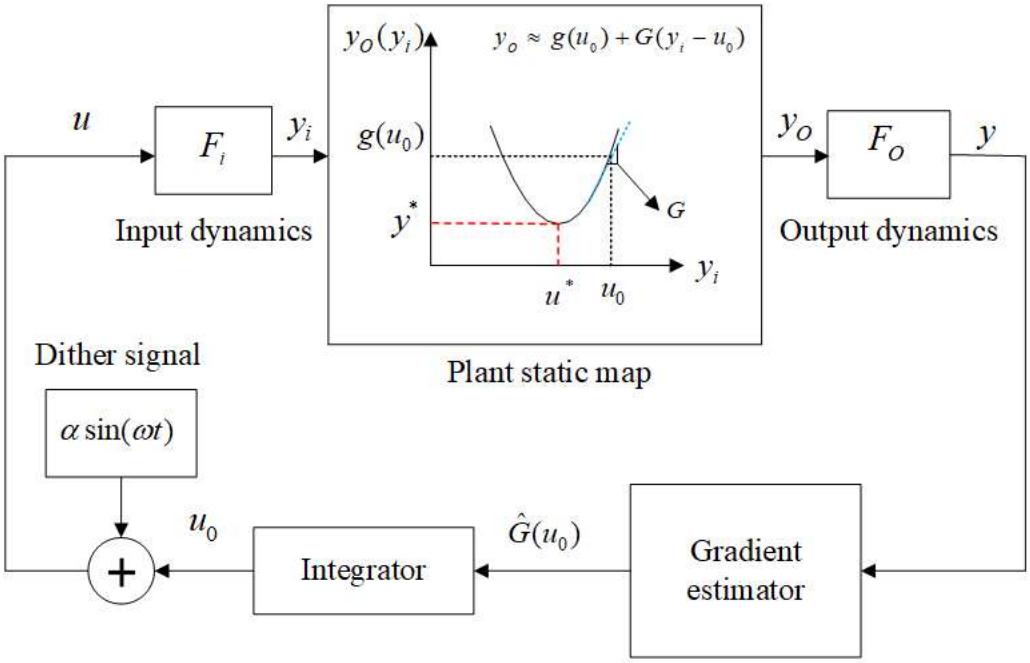

Figure 6-5: Principles of the classic ESC

The gradient estimation $\hat{G}(u_0)$ is conducted by adding the dither signal ($\alpha \sin(\omega t)$) to a SISO system's input u_0. According to Figure 6-6, the sinusoidal dither is added to the input and the same periodic component is observed in the output with different amplitude and phase. The output signal is a combination of two components: a constant component and a periodic component. It can be seen from Figure 6-6 that the sinusoidal output is in-phase (in the same phase) when u_0 is above the minimum point ($u_0 > u_0^*$), while it is out-of-phase (in the opposite phase) (e.g. its real part is negative) when u_0 is below the minimum point,

($u_0 < u_0^*$), and the amplitude of the output signal is almost zero at the optimum point ($u_0 \approx u_0^*$).

The gradient must be driven to zero in a stable system when the command u_0 reaches its optimal value u_0^* [127]. Three different conditions can happen in the evaluation of the gradient shown in Figure 6-6.

i) If $G < 0$, the algorithm needs to increase u_0 , then u_0 converges to u_0^*

ii) If $G \approx 0$, the algorithm needs to freeze u_0, $u_0 \approx u_0^*$

iii) If $G > 0$, the algorithm needs to decrease u_0 , then u_0 converges to u_0^*

To apply these rules, the plant input u is updated according to the steepest descent method explained as follows [175]:

$$\frac{du_0}{dt} = -\zeta G(u_0) \tag{6-16}$$

In Figure 6-5, equation (6-16) is applied in the integrator unit by integrating the gradient estimation $\hat{G}(u_0)$ in order to update the input u_0.

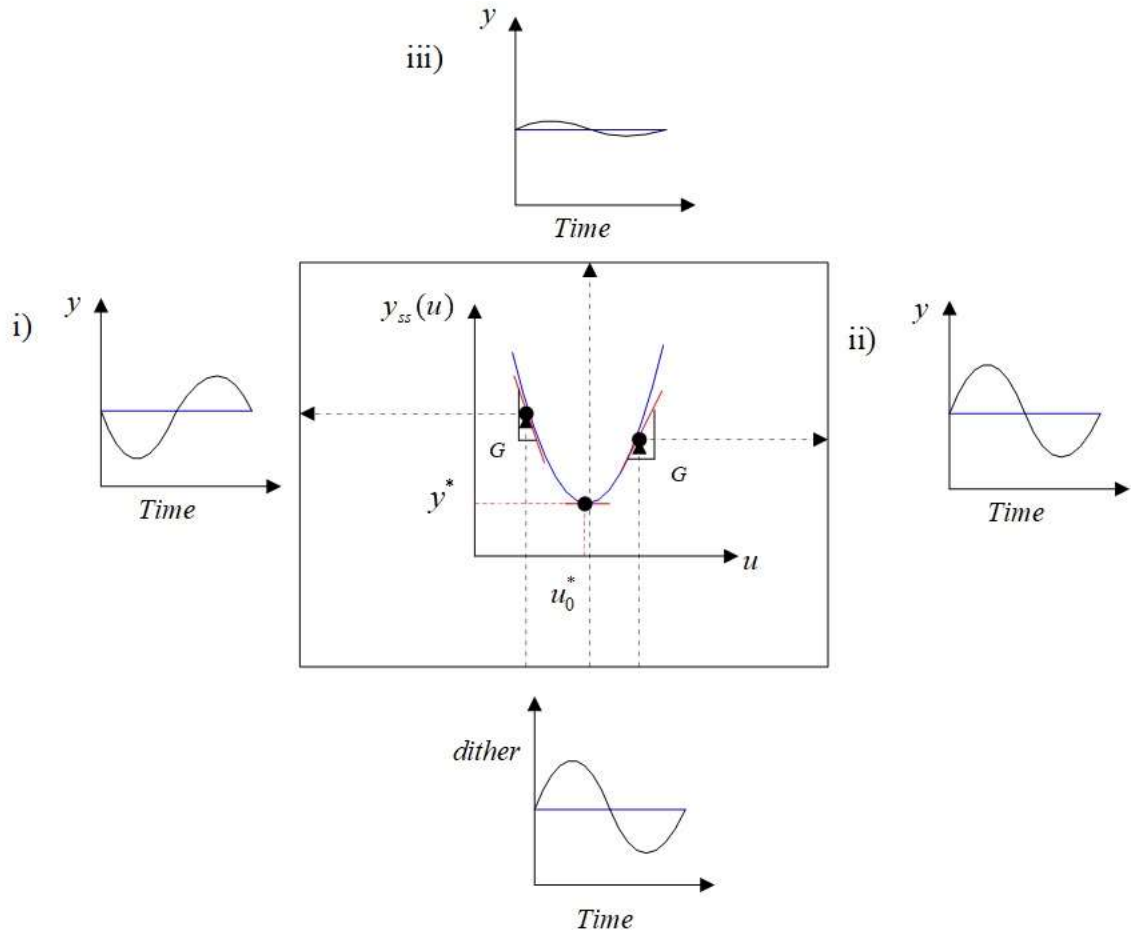

Figure 6-6: Effect of the dither on the static map

For a dynamic system, the gradient estimation problem has been recently solved using the continuous time Kalman filter[172], the discrete time Kalman filter [176] or periodogram [177]. Moreover, Atta et al. [172] and some other researchers like Skogestad and Postlethwaite [29] used an estimation of the phasor to evaluate both the gradient and the phase shift of the plant, whereas the conventional ESC only could estimate the gradient of the static map.

The gradient estimation which is the basis of the perturbation-based ESC is typically evaluated using a unit consisting of a high pass filter, a multiplier (demodulation signal, which is often a signal with the same frequency and amplitude as the dither but with some phase shift) and a low pass filter [89]. Tan et al. [90] proved that the gradient can also be estimated by only a multiplier, or a multiplier with low pass filter. Henning et al. [108] and

Gelbert et al. [178] employed an Extended Kalman Filter to estimate the gradient designed for static systems or very fast dynamic systems, and assumed that the dither signal has the slower frequency than the slowest time constant of the system.

However, the pulsation of the dither (ω) usually cannot be small enough to offset the effect of the phase shift resulting from the system's dynamics. Therefore, some recent studies used dynamic compensators in their proposed ESC models [173][179]. Unlike many studies in this field, which used a very slow perturbation for the static maps, Trollberg et al. [180] indicated that increasing the frequency of perturbation will allow increasing the integrator gain, leading to a faster but sub-optimal response. They solved this problem by adding a phase compensator, however, it may cause instability in the overall system especially in the presence of the time varying phase lag. It should be taken into consideration that in dynamic systems there exits an additional phase shift resulting from the output dynamics. If this phase shift in the output signal is more than $\pi/4$, then it must be compensated to ensure the convergence of ESC.

The vast majority of aforementioned ESC models have been developed in continuous time. However, in a real system to analyze and visualize data, digital signal processing (DSP) is required, where the analog input signals (like temperature, pressure, light intensity), which are continuous in time and amplitude, are converted to the digital signals via several steps, which are also discrete both in time and amplitude. Then, after digital signal processing according to DSP rules such as lowpass, highpass, or any other algorithm, the reconstruction filter converts the processed digital signals to an analog output signal [181]. Therefore, in the current study, instead of the classic ESC designed in the continuous time, we presented a novel scheme of ESC designed to seek the optimal pump speed (N_0^*) to minimize P_e in discrete time. Since, the proposed ESC method updates the command of the system using the batch estimation of the gradient, we named this approach the batch phasor ESC (BPESC). The batch processing was used to estimate gradient using a set of captured data since it is an efficient way for processing the high-volume data. A group of data is collected over the time then processed to evaluate the requested variable. The dynamics of the system are accounted for in the proposed method and compensated in the evaluation of the gradient by multiplying it by a dynamic compensator [179]. The rest of this paper will explain the development of

BPESC to minimize P_e in an ERS for a fixed condenser thermal fluid's inlet condition ($T_{c,i} =$ 18℃).

6.6. The simulation of BPESC

6.6.1. The batch processing

Figure 6-7 represents the block diagram of the developed BPESC model. Without loss of generality, it is assumed that the purpose of BPESC in the ERS is to adjust the input variable (N_0) to obtain the minimum output (P_e^*).

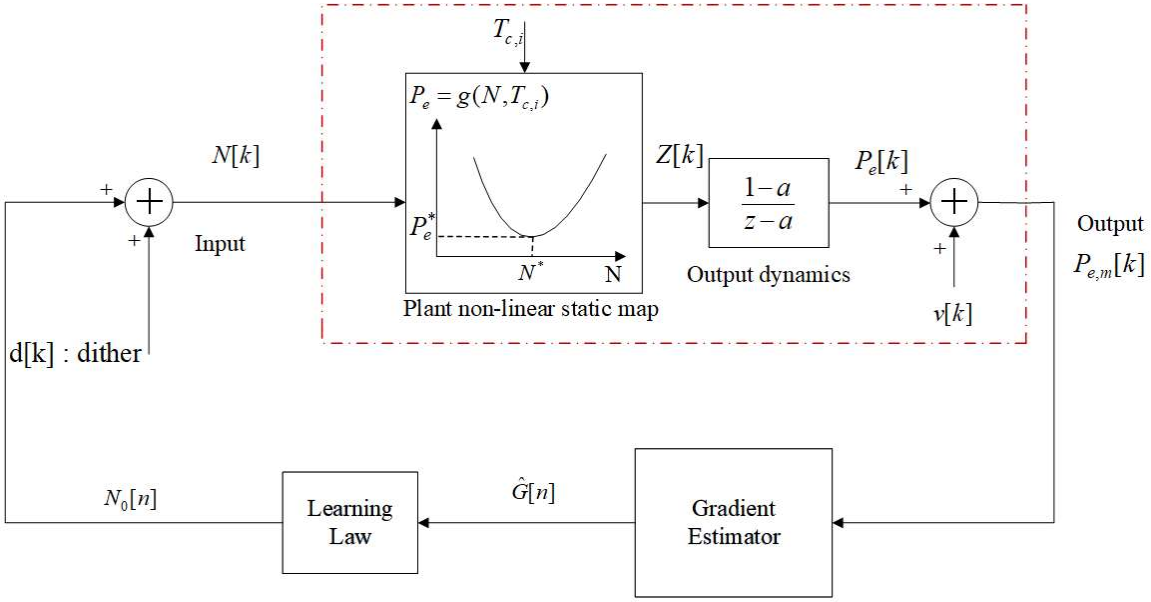

Figure 6-7: Block diagram of discrete time phasor Extremum seeking control

The input to the discrete time non-linear plant shown inside the red dashed rectangle in Figure 6-7 is the pump speed ($N[k]$) actualized at the sampling frequency ($1/t_s$). The output from the plant is the measured evaporating pressure $P_{e,m}[k]$.

Regarding the BPESC block diagram presented in Figure 6-7, the plant input signal in discrete time is generated by adding dither $d[k]$ to the constant pump speed (N_0), as follows:

$$N[k] = N_0[n] + d[k] \tag{6-17}$$

The dither is a sinusoidal signal defined by following relation:

$$d[k] = \mathrm{Re}[A_d e^{i\omega k t_s}] \quad \omega = 2\pi f \tag{6-18}$$

The terms t_s, A_d and f refer to the sampling time, phasor and frequency of the dither, respectively. In addition, the real part of a complex number is shown by "Re". The frequency of dither is evaluated as $f = N_{cycle}/t_b$ where N_{cycle} refers to the number of cycles of the sinusoidal dither per one batch time, t_b. It should be pointed out that the imaginary part of A_d is almost zero which means A_d approximately equals to the amplitude of the dither.

Generally, there exist two different time scales in the BPESC, which are the sampling time (t_s), and batch time (t_b) scales. Based on these two time scales, there are also two different data processing schemes in the proposed BPESC algorithm. These include the discrete time data acquisition done in the sampling time, and the batch processing conducted in batch time. Figure 6-8 depicts the discrete time data acquisition steps based on the batch time index.

Regarding Figure 6-8, the data acquisition is implemented by capturing K samples (one sample per t_s) of $P_e[k]$, from $k = nK$ to $k = nK + K - 1$. The batch processing starts using the K captured data to estimate the gradient when the last data ($(nK + K - 1)th$ sample) is captured, and then the pump speed command N_0 is updated. The t_b batch time is defined by $Kt_s = t_b$, where K represents the number of the samples captured during the batch time.

The K data captured in the discrete time are used in the batch processing (at the batch processing index n) to estimate the gradient using the output phasor A_p defined as follows:

$$A_p[n] = \frac{2}{K}\sum_{m=0}^{K-1} h[m](P_{e,m}[m] - \bar{P}_{e,m}[n])e^{i\omega m t_s} \tag{6-19}$$

The term "m" refers to the summation index and $h[m]$ and $\bar{P}_{e,m}[n]$ are Hanning window of length K and mean value of $P_{e,m}$ calculated at the batch processing index n. The $\bar{P}_{e,m}[n]$ is calculated as follows:

$$\bar{P}_{e,m}[n] = \frac{1}{K}\sum_{m=0}^{K-1} P_{e,m}[m] \tag{6-20}$$

The removal of the mean value from the $P_{e,m}$ in Eq. (6-19) is equivalent to the application of a high pass filter in the classical ESC [127]. Then, the gradient of the static map is

estimated by dividing the output phasor $(A_p[n])$ by the product of the input phasor (A_d) and an estimation of the system's output dynamics at the dither frequency ($\hat{H} = F_O(e^{i\omega k t_s})$) as follows:

$$\hat{G}[n] = \mathrm{Re}\left(\frac{A_p[n]}{\hat{H}A_d}\right) \tag{6-21}$$

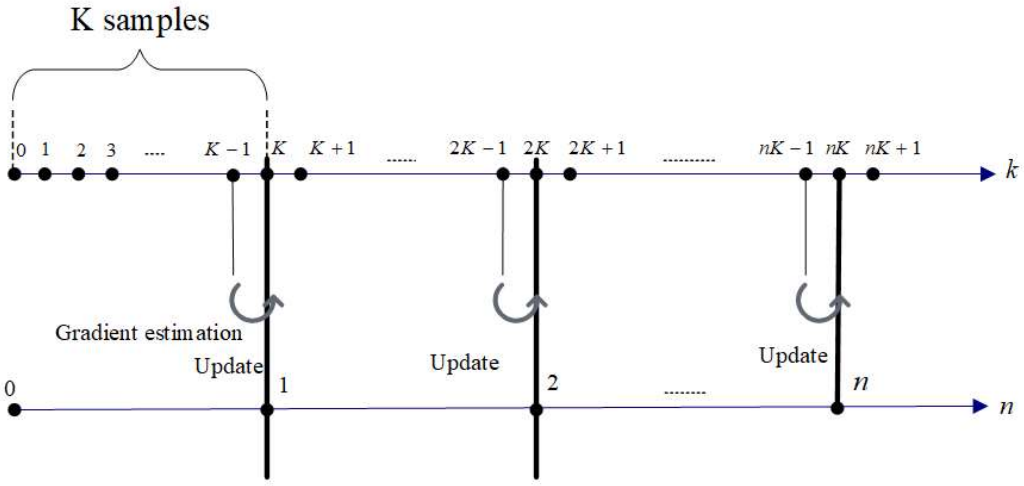

k :Discrete time processing index

n :Batch processing index

Figure 6-8: The dither time duration and equivalent sampling numbers

In other words, the gradient estimation problem (expressed in Eq. (6-21)) is converted to a signal processing problem which is implemented using the output phasor estimated by applying a discrete Fourier transform at the dither frequency (Eq. (6-19)). Furthermore, $\hat{H}$ operates as a dynamic compensator and compensates the phase shift caused by the output dynamics. The detailed information about designing the dynamic compensator will be discussed in section 5.2.

Then, the plant input N_0 is updated using the steepest descent algorithm, which is shown in Figure 6-1 as the learning law block [175]:

$$N_0[n+1] = N_0[n] - \mu\hat{G}[n] \tag{6-22}$$

The parameter μ denotes the scaling factor. For the sake of stability, when $t \to \infty$, $\mu \to 0$.

The initial value of pump speed ($N_0[0]$) can be estimated for a fixed condenser temperature ($T_{c,i}$) using the experimental data presented in Figure 6-4.

$$N_0[0] = F(T_{c,i}) \tag{6-23}$$

6.6.2. The discrete time dynamic model

The white noise signal $v[k]$ is added to the output of the discrete time non-linear plant to simulate the measured signal of $P_{e,m}[k]$.

$$P_{e,m}[k] = P_e[k] + v[k] \tag{6-24}$$

The system's dynamics are approximated using a Wiener-Hammerstein model. The input dynamics is negligible and not included in the non-linear dynamic model of the system. The input dynamics is related to the transient response of the pump when a step change is imposed to its speed. The pump transient response is quite fast and consequently it is not included in the system's dynamic model. While, the output dynamic model is presumed to be the first order discrete time model represented inside the output dynamics block in Figure 6-7. This assumption is made based on the developed dynamic model by the authors in their previous study. Regarding the dynamic model of ERS developed by Narimani et al. [182], the dynamic response of P_e in an ERS to a pump speed step change can be approximated by a first order model.

Since, the input dynamics is not included in the model, it is assumed that the internal variable Z is defined using the nonlinear static map, g, which is a function of the pump speed and condenser temperature:

$$Z[k] = g(N[k], T_{c,i}) \tag{6-25}$$

Thus, the output dynamics defined using a first order discrete time model:

$$P_e[k] = aP_e[k-1] + (1-a)Z[k-1] \tag{6-26}$$

where the parameter a, which characterizes the time response of the discrete time model, is defined as follows:

$$a = e^{-t_s/\tau} \tag{6-27}$$

The term τ (in seconds) denotes the time constant of the first order dynamic model. As a result, the transfer function of the output dynamics Eq. (6-26), based on the first order model (resulted from the ERS dynamic model [182]), is determined by Eq. (6-28):

$$F_O = \frac{P_e(z)}{Z(z)} = \frac{1-a}{z-a} \tag{6-28}$$

The complex gain of the transfer function (modulus and phase shift) at the pulsation of the dither, can be evaluated using Eq. (6-29).

$$F_O(e^{i\omega t_s}) = \frac{1-a}{e^{i\omega t_s}-a} \tag{6-29}$$

The steady state gain of the output dynamics (Eq. (6-29)) is equal to one ($|F_O(1)| = 1$), which is consistent with the principle of Wiener-Hammerstein model [172]. However, at the dither pulsation (ω), the modulus of the output transfer function is less than one ($\left|F_O\left(e^{i\omega\ s}\right)\right| < 1$), whereas its phase-shift depends on the dither frequency. For a low ω, the phase-shift is small enough (less than $\frac{\pi}{4}$) to be neglected. However, for a large ω , the phase shift can reach -π (if $\omega = 2\pi/(2t_s)$) and must not be ignored. Therefore, it is required to compensate the phase shift caused by the system's dynamics by dividing the output phasor A_p by $\widehat{H}$ in the gradient estimation. In the previous section, the use of a dynamic compensator was explained.

6.7. Estimation of the parameters of the BPESC

The performance of designed BPESC is strongly affected by the choice of its parameters including scaling factor (μ), dither frequency (f), its amplitude (A_d) and the number of the cycles of the dither per the batch time (N_{cycle}). The convergence rate of the algorithm is directly influence by scaling factor μ. To achieve the stability, μ should be relatively small but large enough to obtain the reasonable convergence rate, as mentioned by Koeln and Alleyne [127] and Krstić and Wang [89]. It was assumed that the largest possible value of μ can be defined according to Newton's method in optimization [183] [184] based on which new value of the input is evaluated using the following relation in discrete time:

$$N_0[n+1] = N_0[n] - \frac{\hat{G}[n]}{\hat{G}'[n]} \tag{6-30}$$

where the second derivative of the system's nonlinear map is evaluated using the relation of $G'(N_0) = \frac{\partial^2 g}{\partial N^2}\Big|_{N_0}$. Comparing the Newton method with Gradient Descent method, one can realize that $\mu_{crtical}$, which causes the algorithm to converge in one iteration, equals $\left|-1/G'\right|$. It means that μ should be less than $\mu_{crtical}$. In this study, the nonlinear map of the system defined using a third-order polynomial developed using the experimental data was applied as a replacement for the real experimental setup. The nonlinear static map of the system is approximated by fitting the experimental data into a third-order polynomial defined as follows:

$$P_e = g(N) = 20978.0065 - 38.035N + 2.304E-02N^2 - 4.646E-06N^3 \tag{6-31}$$

Hence, the second derivative of g is defined using Eq. (6-32):

$$G' = 4.608E-02 - 27.876E-06N \tag{6-32}$$

It was assumed that the value of μ is less than the inverse of second derivative of the non-linear map in the minimum point:

$$\mu < \frac{1}{\left|G'(N^*)\right|} \tag{6-33}$$

Krstić and Wang [89] mentioned that in the classical ESC, the perturbation frequency should be slower than the dynamics of the system. Koeln and Alleyne [127] also found that if the perturbation frequency is poorly chosen, e.g. it is too fast , then the ESC may converge to an input value far from the optimum.

In the present study, the cutoff frequency (f_{cf}) defined by Eq. (6-34) was used to define the criteria to determine the dither frequency. For $f<f_{cf}$ the phase shift is less than 1 rad/s ($\frac{\pi}{4}$), while for $f>f_{cf}$ there is a distinguishable phase shift more than 1 rad/s ($> \frac{\pi}{4}$).

$$f_{cf} = \frac{1}{2\pi\tau} \tag{6-34}$$

The τ is the time constant of the system and can be evaluated based on the experimental knowledge of the system or the dynamic models. According to the author's study on the

dynamics of an R245fa ERS [182], the dynamic response of P_e to a pump speed step change can be approximated by a first order model and it reaches 98% of its final value in about 90 s (4τ). Thus, τ and f_{cf} equal 22.5 s and 0.00707 Hz, respectively. On the other hand, the highest possible f equals $1/(2t_s)$.

It is assumed that the short convergence time is the main concern in estimating the parameters of the designed BPESC model. The desirable convergence time is considered to be approximately 30 minutes. To make an assumption of the convergence time, it was presumed that the condenser thermal fluid's inlet temperature is defined by environmental temperature. Thus, if the outside temperature changes 1 ℃ per 2 hours, then 30 minutes seems a reasonable criterion.

As a first step, the performance of BPESC was investigated without noise. Therefore, f was assumed to have the maximal allowable value of $1/(2t_s)$. Furthermore, the amplitude of the dither (A_d) was set to the least possible value, which is the pump resolution and equals 6 rpm and only one cycle of the dither ($N_{cycle} = 1$) was used to estimate gradient. The value of μ also was set on 400 based on Eq. (6-33). The results starting from three various initial values of the pump speed $N_0[0]$ are shown in Figure 6-1. According to Figure 6-9, the developed algorithm could efficiently track and find the optimal pump speed and minimum evaporating pressure in less than 2.5 minutes.

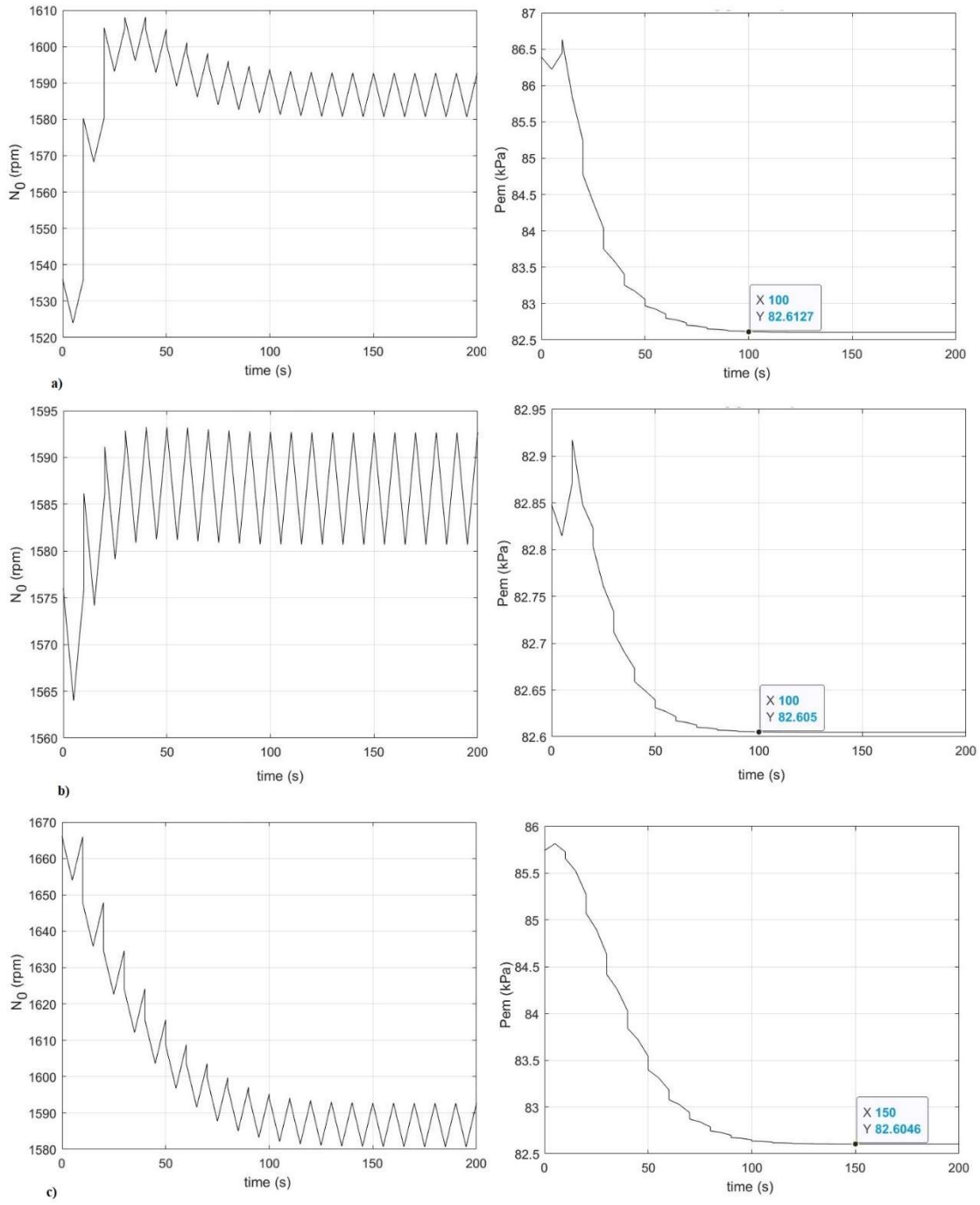

Figure 6-9: The BPESC convergence time of $P_{e,m}[k]$ without noise for three initial values of a) $N_0[0] = 1530rpm$ b)$N_0[0] = 1570rpm$ and c) $N_0[0] = 1660rpm$

In the second step, white noise is included in the simulation, with standard deviation of 0.5. The existence of the noise interferes with the designed algorithm operation. Therefore, the

parameters should be adjusted to simultaneously overcome the noise influence on the model and maintain the convergence time around 30 minutes. As a result, the dither frequency f is reduced to the cutoff frequency to overcome the noise influence. To improve the gradient estimation N_{cycle} is also raised to 2. The larger the N_{cycle}, the more accurate estimation of the gradient will be obtained. On the other hand, increasing the N_{cycle} will increase the time required for convergence. Thus, we only increased N_{cycle} to 2, which is adequate to estimate the gradient with fair accuracy.

The dither amplitude (A_d) (also known as the input phasor) is another important factor in designing PBESC. Koeln and Alleyne [127] mentioned that the larger the amplitude, the faster the algorithm would converge to the optimal input, although, it will also cause large perturbations close to the optimal point. However, we found out that A_d has a more significant effect on the reducing the fluctuations in the evaluated input and output signals, rather than on the convergence rate. In fact, the dither amplitude A_d must be augmented to make the output signal distinguishable above the noise, e.g. to improve the signal-noise ratio (SNR). Figure 6-10 shows the effect on the random fluctuation of $N_0[n]$ of increasing A_d after the convergence time.

Figure 6-10 demonstrates that after the convergence time (index n>5), the noise measurement on $P_{e,m}[k]$ causes a random fluctuation in the output phasor $A_p[n]$, which leads to a random fluctuation in the command $N_0[n]$ based on Eqs. (6-21) and (6-22). The random fluctuation in $N_0[n]$ results in the small random fluctuation in $g(N_0[n])$ at the optimal point, since the gradient is approximately 0. For low values of A_d, there are larger random fluctuations in the evaluated gradient and consequently larger fluctuations in $N_0[n]$. Increasing A_d improves the SNR, thus, it reduces the fluctuations in the estimated gradient and consequently in $N_0[n]$) and $g(N_0[n])$. Increasing A_d is preferred in designing the BPESC since the main goal of this model is to stay close to the optimal point during the operation. On the other hand, a large A_d reduces the accuracy of model in predicting the optimal output as can be seen in $A_d = 30rpm$ in Figure 6-10. As a result, we chose 18 rpm as a desirable value for A_d in the designed BPESC in this study.

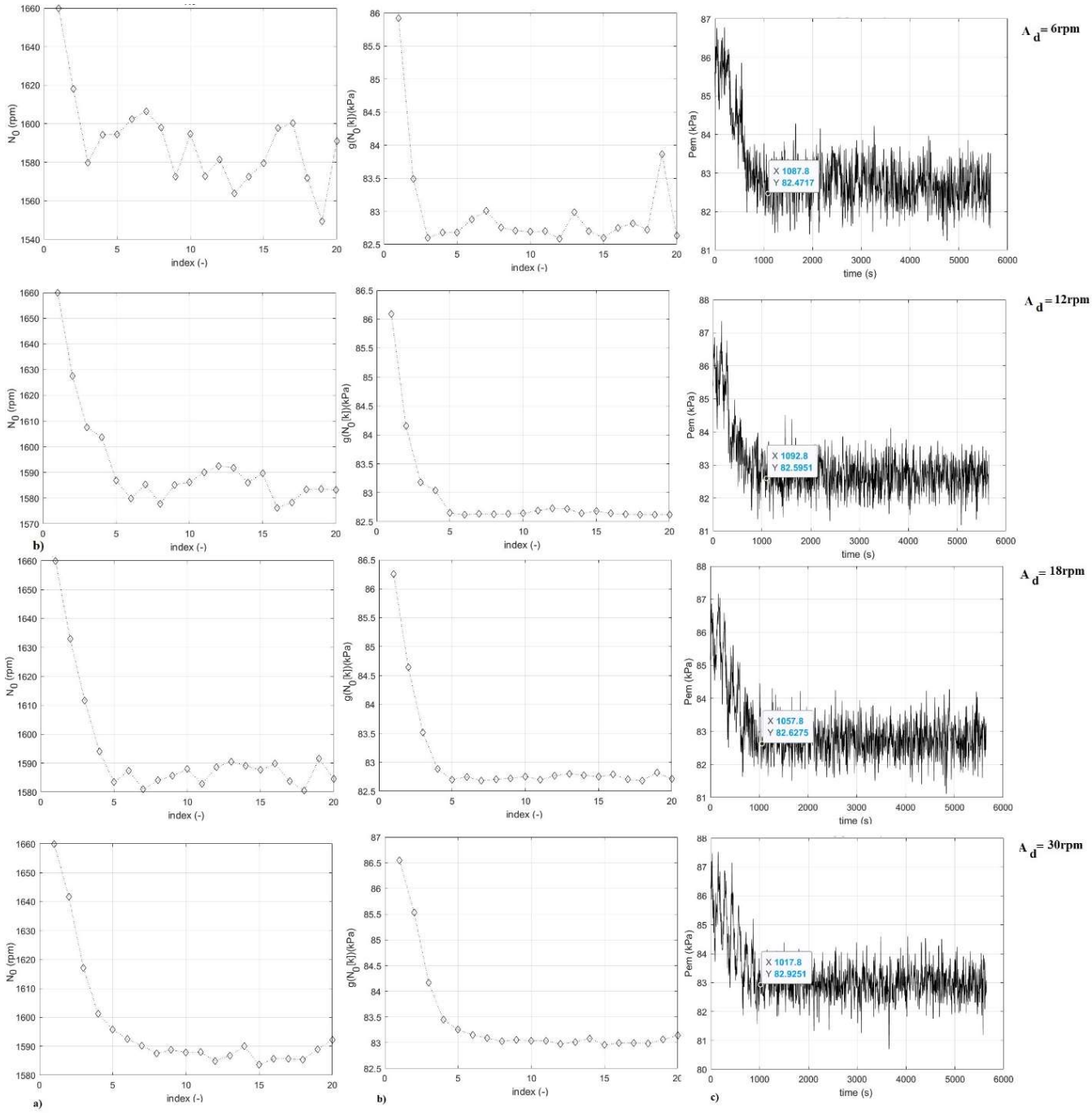

Figure 6-10: The influence of an increase in A_d on $a)N_0[k], b)g(N_0[k])$ and $c)$ $P_{e,m}[k]$

Furthermore, the system's dynamics, represented by the value of "a", must be considered to tune the BPESC parameters. The frequency response at the dither frequency (gain and phase lag shown by Eq. (6-29)) is defined based on "a", which is evaluated using Eq. (6-27) and equals 0.8.

The white noise is also calculated as the multiplication of the standard deviation (Std) of P_e and a random vector with size equals to *K*. The Std of P_e is defined using the experimental data presented in Figure 6-4. The parameters of BPESC used for the simulation are summarized in Table 6-2.

Table 6-2: BPESC controller parameters

Parameters (unit)	Values
a	0.8
f (Hz)	7.077E-03
A_d (rpm)	18
N_{cycle}	2
μ	400
Std (P_e), (kPa)	0.49
t_s (s)	5

6.8. Results and discussion

The proposed BPESC in the previous section is used to track the optimal pump speed (N^*) for fixed generator and evaporator inlet conditions (inlet temperatures of the thermal fluids).

The model was solved for $T_{c,i} = 18°C$ starting from three various initial values of the pump speed, including $N_0[0]$= 1530, 1620 and 1700 rpm. In Figure 6-11 the convergence rates of the proposed model to the optimal value have been compared for three cases in terms of the predicted optimal *N* and P_e.

Regarding Figure 6-11, the proposed BPESC model can seek the optimal values providing the parameters of the model, including the number of dither cycles, scaling factor, dither frequency and amplitude, can be efficiently tuned to overcome the noise influence on the solution. The convergence rates of the model for three different values of the initial pump speed are compared in Table 6-3. The slowest convergence time, which equals approximately 33 minutes, is related to the starting point located on the right side of the actual minimum point. It is due to the lower curvature of the nonlinear map. The BPESC

model could converge to the optimal value of P_e in three cases with errors not exceeding 0.21 %.

Table 6-3: The BPESC performance for various initial conditions with noise

N_0, rpm	1530	1620	1700
$P^*_{e,mod.}, [kPa]$	82.74	82.60	82.56
$t_{conv.}[s]$	348	413	2000
σ, [%]	0.21	0.036	0.012

$N^* = 1588.34\ rpm, P^*_e = 82.57\ kPa, \sigma = \left|\frac{(P^*_{e,mod.} - P^*_e)}{P^*_e}\right| 100$

According to Table 6-3, the performance of the BPESC for all three evaluated initial conditions are acceptable in terms of the convergence rates and predicted optimal values.

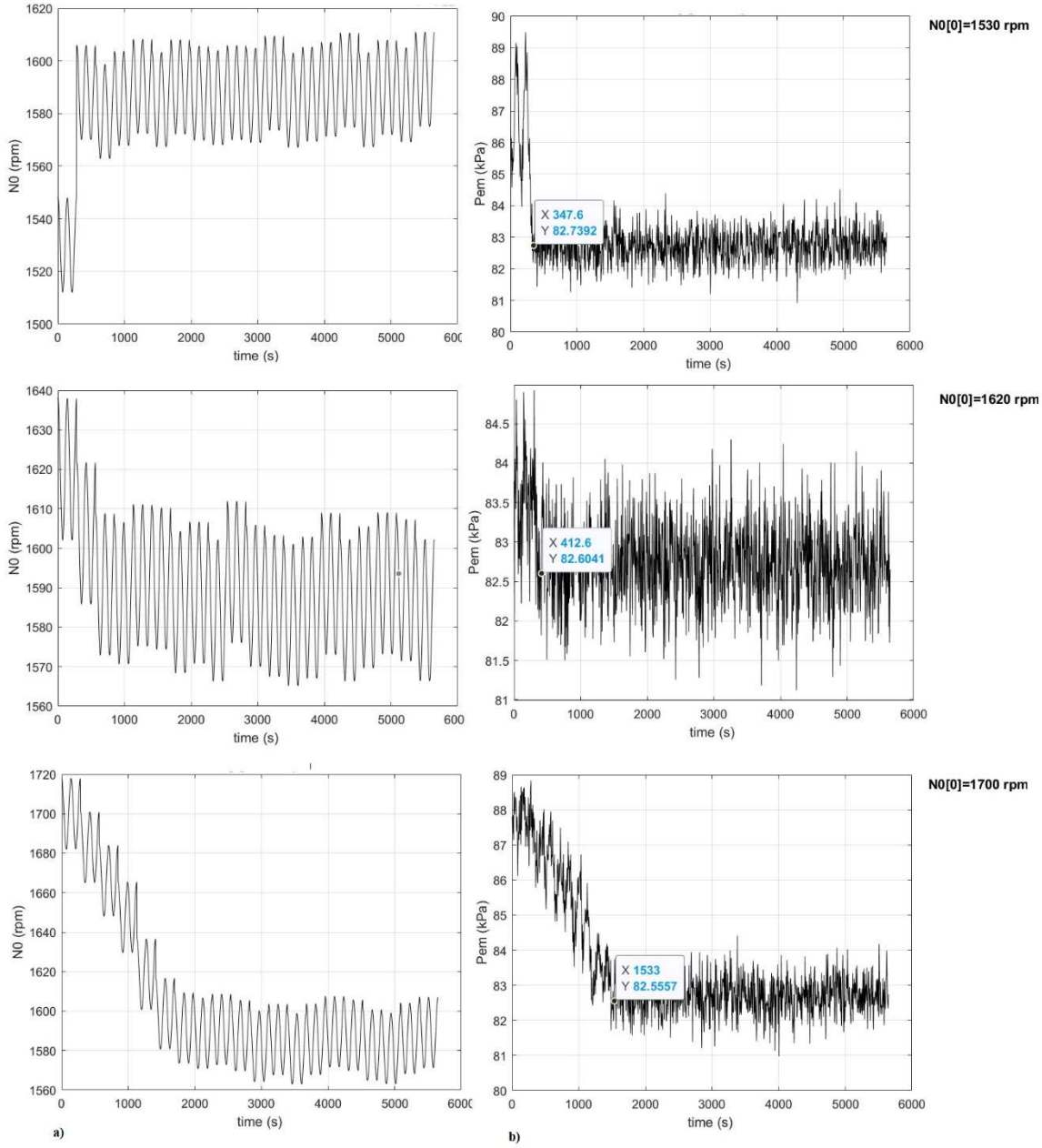

Figure 6-11: The convergence of BPESC for three values of $N_0[0]$ based on a)N_0 b)$P_{e,m}$

According to Table 6-3, the performance of BPESC for all the three various initial conditions are acceptable in terms of the convergence rate and predicted optimal values.

6.9. Conclusions

This paper provides a theoretical basis for developing the first control strategy for an R245fa ejector-based refrigeration system (ERS). A novel Extremum seeking control (ESC) model named batch phasor ESC, or BPESC, was proposed to minimize the evaporator pressure P_e (the output) of an ERS for fixed condenser thermal fluid inlet conditions. The main challenge of the control scheme was to appropriately manipulate the pump speed (the input) to minimize the target output, P_e. The BPESC model estimated the gradient by evaluating the phasor of the output in the batch time. The batch signal processing of captured data and the phasor approach could allow implementing and tuning of the extremal controller on the real process. The simulation studies conducted at three various initial conditions revealed that by defining the appropriate values of the parameters, the BPESC sought and found the optimum input values with fair accuracy, less than 0.21 % of the pump speed. The maximum convergence time was estimated to be 33.3 minutes for the three investigated cases. The results indicated that the applied BPESC model is a potential control strategy for maintaining the maximum achievable compression ratio Cr and exergy efficiency η_{II} in an ERS. It also has the advantage of being a simple and nearly model-free control model, requiring a very limited number of data measurements. The proposed BPESC model can be used to design a controller for an ERS in the future studies.

6.10. Acknowledgment

The authors wish to thank Hydro-Québec laboratory Shawinigan for their valuable contribution during this research study. This project is a part of the Collaborative Research and Development (CRD) Grants Program at the Université de Sherbrooke. The authors also acknowledge the support of the Natural Sciences and Engineering Research Council of Canada, Rio Tinto Alcan and CanmetEnergy Research Center of Natural Resources Canada.

6.11. Nomenclature

Table 6-4: Nomenclature

Latin	Definition
P	Pressure, [kPa]
Q	Heat load, [kW]
T	Temperature, [°C]
h	Specific enthalpy, [kJ/kg]
$\dot{m}$	Mass flow rate, [kg/s]
W	Pump work, [kW]
t	Time, [s]
f	Dither frequency, [Hz]
f_{cf}	cutoff frequency, [Hz]
A_d	Amplitude of the dither (input phasor), [rpm]
A_p	Output phasor
G	Gradient, [rpm^2]
$\hat{G}$	Gradient estimation, [rpm^2]
ω	Angular frequency (pulsation of the dither), [Hz Rad]
v	White noise
η_{II}	Exergy efficiency, [-]
μ	Scaling factor in the steepest decent method, [rpm^{-1}]
σ	Relative error, [%]
τ	Time constant of the first order model, [s]
Re	Real part of a complex number, [-]
N_{cycle}	Number of cycles of the sinusoidal dither
u	Input variable
u_0	Output of integrator
N	Pump speed (input variable), [rpm]
N_0	Output of the learning law block, [rpm]
N^*	Optimal pump speed, [rpm]
y_{ss}	Steady state output
t_b	Batch time, [s]
t_s	Sampling time, [s]
k	Discrete time processing index, [-]
n	Batch processing index, [-]

Z	Internal variable in BPESC model, [kPa]
F_i	Input dynamics, [rpm]
F_O	Output dynamics, [kPa]
Subscripts	
c	Condenser
e	Evaporator
g	Generator
i	Inlet
o	Outlet
0	Initial condition
p	Pump
P	Primary
d	Dither
s	Sampling
Superscripts	
*	Optimal value
m	Measured value
Abbreviation	
COP	Coefficient of performance
ERS	Ejector refrigeration system
Cr	Compression ratio
ESC	Extremum seeking Control
Er	Entrainment ratio of the ejector
Mod.	Model
Conv.	Convergence
SNR	Signal-noise ratio
STD	Standard deviation

CHAPTER 7 CONCLUSIONS AND RECOMMENDATIONS

7.1. Summary and conclusions

The ejector-based refrigeration systems (ERS) has the low performance efficiency compared to the conventional compressor-based refrigeration system, however, its sustainable operation due to the possibility of using waste heat or solar energy instead of electricity produced by fossil fuel has made ERS as one of the interesting research topics in the field of designing the cooling systems. Hence, the gab in the studies investigating the dynamic modeling and control strategies of the ERS on the one hand and the fast-growing interests in developing the environmentally friendly cooling systems on the other hand triggered this PhD research project.

In this PhD thesis, the effort has been made to design an optimal control model of ERS and develop a dynamic model explaining its dynamic behavior with changes in the system's disturbances. The detailed numerical and experimental analyses were conducted to investigate the impacts of operation parameters on the performance of the ejector and consequently on the performance of the system. Having defined the optimal operation condition of ERS, we focused on the development of dynamic and control models to derive the cycle towards its predetermined optimal operation condition.

First, the experimental study of ERS was carried out to investigate the influences of the operational parameters on the performance of ejector and the system. The experimental data was produced by the R245fa ERS experimental set-up located at Laboratoire des technologies de l'énergie of Hydro-Quebec. It was revealed that in a fixed condenser inlet condition, increasing the primary stream mass flow rate would raise the compression ratio (Cr) of the ejector and exergy efficiency (η_{II}) of the system to their maximum values before

decreasing. In the meantime, the evaporation pressure (P_e) decreases to a minimum value with an increase in the primary stream mass flow rate. This optimal point is crucial from the point of view of the ejector as it enables the ejector to operate at the higher back pressure in its optimal Cr in a fixed condenser inlet condition. Furthermore, in the optimal primary stream mass flow rate, ERS can operate with the highest thermal efficiency and the lowest irreversibility (maximum η_{II}). To explain this phenomenon, a 1-D thermodynamic model of the ejector plus the static models of the heat exchangers were developed. The steady-state models of the heat exchangers were developed based on $\varepsilon - NTU$ approach and using the switching moving boundary method.

The built thermodynamic model of the ejector and steady state models of the heat exchangers confirmed the occurrence of the optimum generating pressure (primary stream mass flow rate) in a fixed condenser inlet condition. The contribution of the developed ejector model to the literature studying ejector performance was its capability in the prediction of the ejector operation criteria. The developed ejector model implied that ejector operates in the single-choking mode when the generating pressure is lower than its optimum value, while it operates in the double-choking mode at generating pressures equal or greater than the optimum pressure.

The second step was related to the developing the dynamic model of the ERS to predict its transient behavior. The challenging task in development of the dynamic model of ERS was maintaining a balance between the high accuracy and low computation time of the developed model. To address this issue and regarding the fact that dominant dynamics of ERS belongs to the heat exchangers, the heat exchangers dynamic models were developed based on moving boundary approach. The other components were modeled by steady state models. The time derivatives of the inlet specific enthalpies of the generator and evaporator were included in the model using the assumption of the equality between the condenser outlet specific enthalpy and the generator and evaporator inlet specific enthalpies. This assumption was made based on the negligible enthalpy increase in the pump and isenthalpic expansion in the expansion valve. The transient responses of the system based on the pressures and outlet enthalpies of the generator, condenser and evaporator were simulated and measured experimentally against different values of the pump speed. The results of the validation study

revealed that the developed dynamic model of ERS can capture the relevant transient behavior qualitatively and quantitatively with the relative error less than 4 % for both the pressures and outlet enthalpies in the heat exchangers.

The third and last part of this PhD research project dealt with development of a control model for an ERS. The previous parts of this study proved the existence of an optimal primary stream mass flow rate which simultaneously maximizes the Cr and η_{II} and minimizes P_e in the fixed inlet condition of the condenser. Thus, a control scheme was required to drive the R245fa ERS towards this optimal operational condition. A novel scheme of Extremum seeking control (ESC) named batch phasor ESC was proposed to minimize P_e of the system. The suggested phasor-based ESC evaluated the gradient using the phasor of the output in the discrete time. A dynamic compensator was added to the gradient estimator which enabled the proposed model to cope with the phase lag resulted from the system's dynamic. The simulation results revealed that batch phasor ESC could seek the optimum values with good accuracy less than 0.21 % for the pump speed starting from the various initial conditions. The maximum convergence time of batch phasor ESC designed for an ERS was estimated to be about 33 minutes.

Regarding to the conclusions presented herein, it is possible to design a controller for real ERS to derive the system towards the highest Cr and η_{II} with manipulating the pump speed (the primary stream mass flow rate).

7.2. Limitations and recommendations for future studies

The present study is a primary step towards designing an optimal control model for the ERS with constant ejector geometry and constant heat exchangers inlet conditions. Despite the extensive experimental and numerical studies carried out in this PhD research project, it is still required to do more study to overcome the available limitations. In the remaining of the section, the limitations and the corresponding recommendations for future studies will be presented.

a) The control strategy using a batch phasor ESC was designed for an ERS to achieve the lowest P_e (as the control model output) which is equivalent to the highest Cr and

η_{II}. However, due to the limitations in the experimental set-up, the developed control model was not tested experimentally, and the study lacks the validation of the built control model. Therefore, in the future work, the control system can be designed and installed in ERS test rig at Laboratoire des technologies de l'énergie of Hydro-Quebec based on the outcomes and results of this PhD thesis.

b) The batch phasor ESC was designed for a fixed condenser inlet condition with the primary knowledge of the probable optimal pump speed obtained from the experimental data. However, the developed model was not investigated for the varying condenser inlet conditions. In the future study the proposed ESC model can be developed for varying condenser conditions with including the look-up table in the control model based on a learning algorithm such as neural network. At each condenser inlet condition, the ESC would find the optimal pump speed minimizing P_e and the optimal pump speed can be sent back to and saved in the look-up table. These values can be used to develop a learning scheme which is predicting the optimal pump speeds for various condenser conditions.

c) The experimental data was analyzed for a fixed geometry ejector to define the optimal operation condition and consequently the effects of the ejector sizing parameters was not investigated on obtaining the highest Cr and η_{II}. To overcome this limitation of the present study, the further studies are required to include the size of the ejector in designing the optimal control strategy for such a system.

d) The proposed control model in the present study was developed based on the constant inlet conditions of the heat exchangers among which the generator as heat source is believed to play a key role as its temperature can be among disturbances if the low-grade heat recourses would be applied. To overcome this limitation, it is recommended to conduct the future study in order to investigate the impact of varying generator inlet condition on the ERS performance and designing an optimal control strategy.

e) We developed a control strategy to obtain the maximum Cr and η_{II}, while the maximum COP was also another crucial parameter defining the operation performance of an ERS. In the future studies, the optimal control strategy can be

developed for an ERS to maximize its COP.

To sum up, regarding the results achieved in this thesis and the mentioned limitations and possible solutions presented previously, there still exists still a great research potential for the further investigation of ERS in order to develop the optimal control strategies.

7.3. Résumé et conclusions

Les systèmes de réfrigération à éjection (SRE) ont un rendement de performance faible comparé au système de réfrigération classique à compresseur. Cependant, son fonctionnement durable en raison de la possibilité d'utiliser de la chaleur perdue ou de l'énergie solaire a fait de le SRE l'un des sujets de recherche intéressants dans le domaine de la conception des systèmes de refroidissement. Ainsi, les études dans les études portant sur la modélisation dynamique et les stratégies de contrôle de le SRE, d'une part, et l'intérêt croissant pour le développement de systèmes de refroidissement respectueux de l'environnement, d'autre part, ont été à l'origine de ce projet de recherche.

Dans cette thèse, des efforts ont été déployés pour concevoir un modèle de contrôle optimal des SRE et pour développer un modèle dynamique expliquant son comportement dynamique en fonction de l'évolution des perturbations du système. Les analyses numériques et expérimentales détaillées ont été menées pour étudier l'impact des paramètres de fonctionnement sur les performances de l'éjecteur et, par conséquent, sur les performances du système. Après avoir défini les conditions de fonctionnement optimales de SRE, nous nous sommes concentrés sur le développement de modèles dynamiques et de modèles de contrôle permettant de dériver le cycle vers ses conditions de fonctionnement optimales prédéterminées.

Tout d'abord, une étude expérimentale sur le SRE a été réalisée pour étudier l'influence des paramètres opérationnels sur les performances de l'éjecteur et du système. Les données expérimentales ont été produites par le dispositif expérimental R245fa SRE situé au Laboratoire des technologies de l'énergie d'Hydro-Québec. Il a

été révélé que dans une condition d'entrée fixe du condenseur, l'augmentation du débit massique du flux primaire augmenterait le taux de compression (Cr) de l'éjecteur et l'efficacité exergétique (η_{II}) du système à leur valeur maximale avant de diminuer. Entretemps, la pression d'évaporation (P_e) diminue jusqu'à une valeur minimale lorsque le débit massique du flux primaire augmente. Ce point optimal est crucial du point de vue de l'éjecteur, car il permet à l'éjecteur de fonctionner à la contrepression plus élevée dans son Cr optimal dans des conditions d'admission fixes du condenseur. De plus, avec le débit massique optimal du flux primaire, le SRE peut fonctionner avec le rendement thermique le plus élevé et l'irréversibilité la plus faible (maximum η_{II}). Pour expliquer ce phénomène, un modèle thermodynamique 1-D de l'éjecteur ainsi que les modèles statiques des échangeurs de chaleur ont été développés. Les modèles statiques des échangeurs de chaleur ont été développés sur la base de l'approche ε-NTU et à l'aide de la méthode des limites mobiles à commutation.

Le modèle thermodynamique intégré de l'éjecteur et les modèles à l'état stationnaire des échangeurs de chaleur ont confirmé l'occurrence de la pression de production optimale (débit massique du flux primaire) dans une condition d'admission fixe du condenseur. La contribution du modèle d'éjecteur développé à la littérature sur les performances des éjecteurs réside dans sa capacité à prédire les critères de fonctionnement des éjecteurs. Le modèle d'éjecteur développé impliquait que l'éjecteur fonctionne en mode monoétouffement lorsque la pression générée est inférieure à sa valeur optimale, alors qu'il fonctionne en mode double étouffement pour générer des pressions égales ou supérieures à la pression optimale.

La deuxième étape était liée au développement du modèle dynamique du'SRE pour prédire son comportement transitoire. La tâche difficile dans le développement du modèle dynamique de SRE consistait à maintenir un équilibre entre la haute précision et le temps de calcul peu élevé du modèle développé. Pour résoudre ce problème et compte tenu du fait que la dynamique dominante de SRE appartient aux échangeurs de chaleur, les modèles dynamiques des échangeurs de chaleur ont été développés sur la base d'une approche par limites mobiles. Les autres composants ont été

modélisés par des modèles en régime permanent. Les dérivées temporelles des enthalpies spécifiques d'entrée du générateur et de l'évaporateur ont été incluses dans le modèle en utilisant l'hypothèse d'égalité entre l'enthalpie spécifique de la sortie du condenseur et les enthalpies spécifiques de l'entrée du générateur et de l'évaporateur. Cette hypothèse a été établie sur la base d'une augmentation enthalpique négligeable de la pompe et d'une expansion isenthalpique dans le détendeur. Les réponses transitoires du système basées sur les pressions et les enthalpies de sortie du générateur, du condenseur et de l'évaporateur ont été simulées et mesurées expérimentalement par rapport à différentes valeurs de la vitesse de la pompe. Les résultats de l'étude de validation ont révélé que le modèle dynamique de SRE développé peut capturer qualitativement et quantitativement le comportement transitoire pertinent, l'erreur relative étant inférieure à 4% pour les pressions et les enthalpies de sortie des échangeurs de chaleur.

La troisième et dernière partie de ce projet de recherche portait sur le développement d'un modèle de contrôle pour un SRE. Les parties précédentes de cette étude ont prouvé l'existence d'un débit optimal pour le flux primaire qui maximise simultanément le Cr et le η_{II} et minimise le P_e dans les conditions d'entrée fixe du condenseur. Ainsi, un schéma de contrôle était nécessaire pour amener le R245fa SRE vers cette condition opérationnelle optimale. Ce schéma novateur de commande extrêmale appelé BPESC (Batch Phasor ESC) a été proposé pour minimiser P_e du système. L'ESC basé sur le phraseur suggéré a évalué le gradient en utilisant le phraseur de l'entrée de la plante dans le temps discret. Une compensatrice dynamique a été ajoutée à l'estimateur de gradient, ce qui a permis au modèle proposé de traiter le retard de phase résultant de la dynamique du système.

Les résultats de la simulation ont révélé que le BPESC pouvait suivre les valeurs optimales avec une bonne précision inférieure à 0,21% pour la vitesse de la pompe à partir des différentes conditions initiales. Le temps de convergence maximum du BPESC conçu pour une ERS a été estimé à environ 33 minutes.

En ce qui concerne les conclusions présentées ici, il est possible de concevoir un contrôleur pour un SRE afin de dériver le système vers les plus hauts Cr et η_{II} en manipulant la vitesse de la pompe (le débit massique du flux primaire).

7.4. Limites et recommandations pour les études futures

La présente étude constitue une étape essentielle dans la conception d'un modèle de contrôle optimal pour le système ERS avec une géométrie d'éjecteur constante et des conditions d'entrée constantes pour les échangeurs de chaleur. Malgré les nombreuses études expérimentales et numériques réalisées dans le cadre de ce projet de recherche, il est nécessaire de poursuivre les études pour surmonter les limitations disponibles. Dans la suite de la section, les limites et les recommandations correspondantes pour les études futures seront présentées.

a) La stratégie de contrôle utilisant de commande extrêmale BPESC a été conçue pour qu'un SRE atteigne le plus bas P_e (en tant que sortie du modèle de contrôle), ce qui équivaut au plus haut Cr et η_{II}. Cependant, en raison des limites de la configuration expérimentale, le modèle de contrôle développé n'a pas été testé expérimentalement et l'étude ne dispose pas de la validation du modèle de contrôle construit. Par conséquent, dans les travaux futurs, le système de contrôle pourra être conçu et installé sur le banc d'essai SRE du Laboratoire des technologies de l'énergie d'Hydro-Québec en fonction des résultats de cette thèse.

b) Le BPESC a été conçu pour une condition d'admission fixe du condenseur avec la connaissance principale de la vitesse optimale probable de la pompe obtenue à partir des données expérimentales. Cependant, le modèle développé n'a pas été étudié pour les diverses conditions d'entrée du condenseur. À l'avenir, le modèle ESC proposé peut être développé pour diverses conditions de condenseur en incluant la table de consultation dans le modèle de contrôle basé sur un algorithme d'apprentissage. À chaque condition d'entrée du condenseur, le contrôleur suivra la vitesse optimale de la pompe en minimisant P_e et la vitesse optimale de la pompe peut être renvoyée et enregistrée dans la table de recherche. Ces valeurs peuvent être utilisées pour

développer un schéma d'apprentissage qui prédit les vitesses optimales de la pompe pour diverses conditions de condenseur.

c) Les données expérimentales ont été analysées pour un éjecteur à géométrie fixe afin de définir les conditions de fonctionnement optimales. Par conséquent, les effets des paramètres de dimensionnement de l'éjecteur n'ont pas été étudiés lors de l'obtention du Cr et du η_{II} les plus élevés. Pour surmonter cette limitation de la présente étude, il est nécessaire que les études ultérieures incluent la taille de l'éjecteur dans la conception de la stratégie de contrôle optimale pour un tel système.

d) Le modèle de contrôle proposé dans la présente étude a été développé sur la base des conditions d'entrée constantes des échangeurs de chaleur, parmi lesquelles le générateur en tant que source de chaleur jouerait un rôle essentiel, car sa température peut être un facteur perturbant si les appliqué. Pour surmonter cette limitation, il est recommandé de mener la future étude afin d'étudier l'impact de la variation des conditions d'entrée du générateur sur les performances du système SRE et de concevoir une stratégie de contrôle optimale.

e) Nous avons développé une stratégie de contrôle optimale pour obtenir le maximum de Cr et η_{II}, tandis que le maximum de COP était également un autre paramètre crucial définissant les performances de fonctionnement d'un SRE. Dans les études futures, la stratégie de contrôle optimale peut être développée pour un système de réhabilitation efficace afin de maximiser son COP.

En résumé, en ce qui concerne les résultats obtenus dans cette thèse, les limitations mentionnées et les solutions possibles présentées précédemment, il existe encore un grand potentiel de recherche pour la poursuite des recherches sur les SRE afin de développer des stratégies de contrôle optimales.

CHAPTER 8 APPENDIXES

8.1. Appendix A

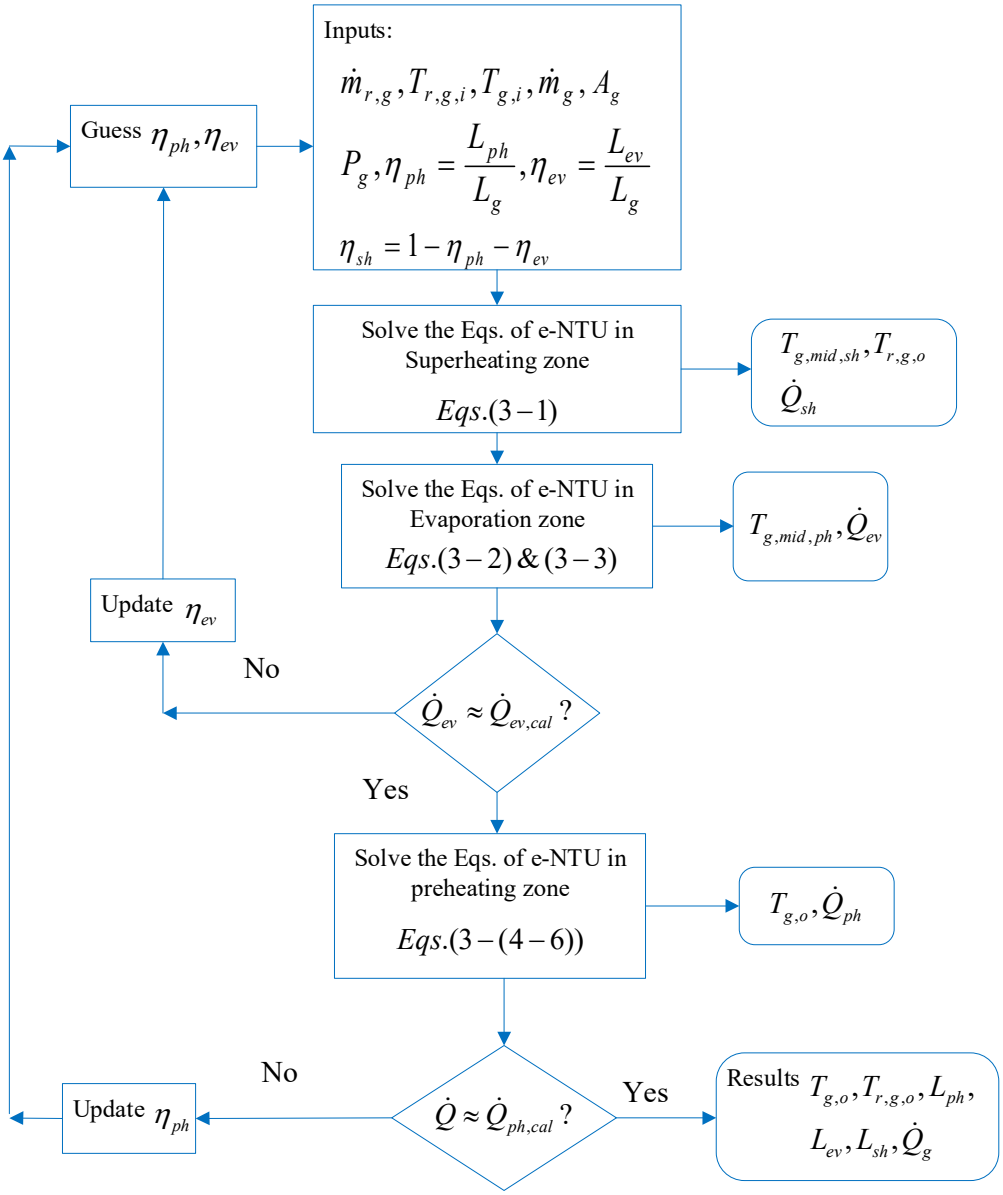

Figure 8-1: Solution algorithm flowchart for the generator steady state model (Appendix A)

8.2. Appendix B

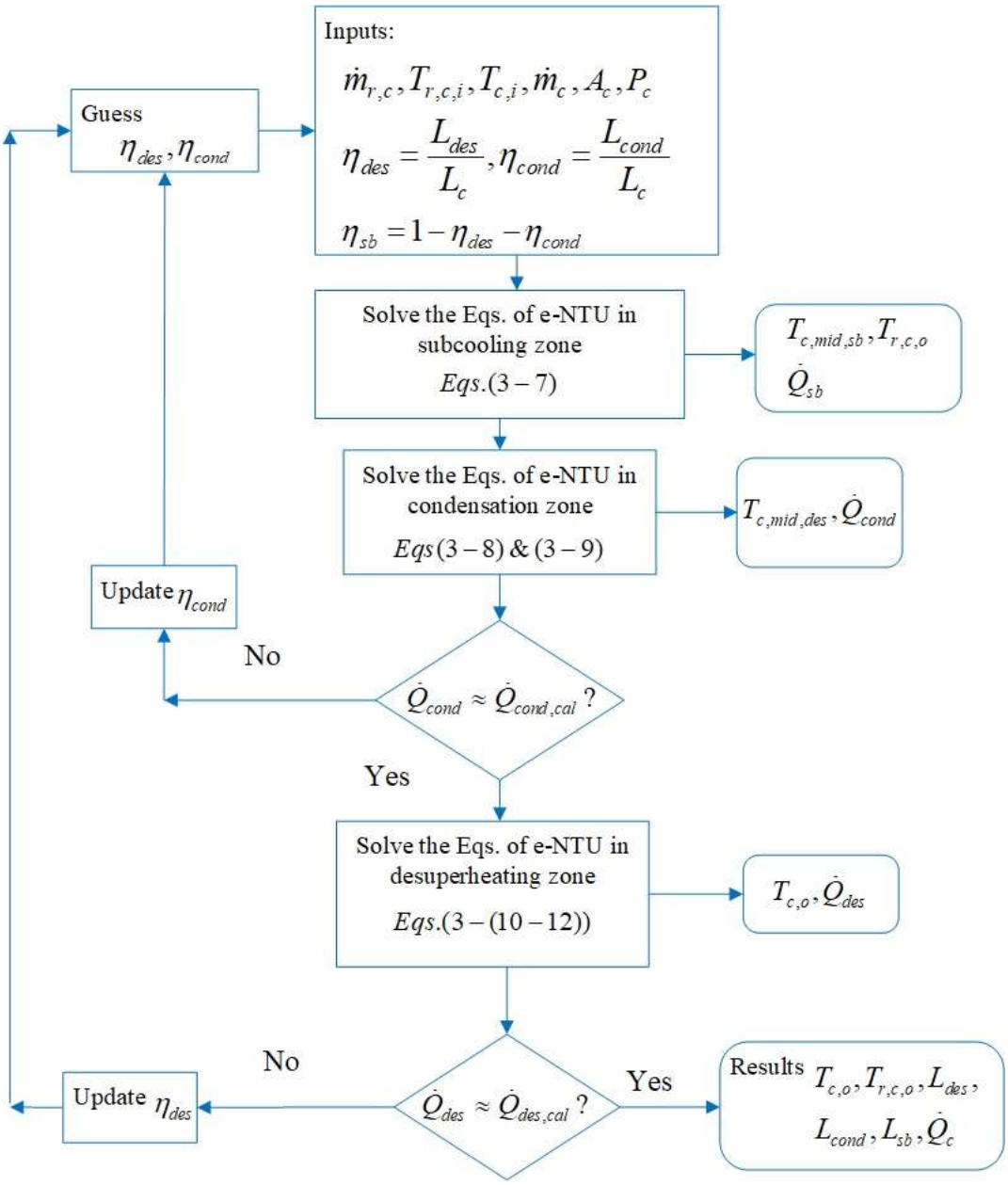

Figure 8-2: Solution algorithm flowchart for the condenser steady state model (Appendix B)

8.3. Appendix C

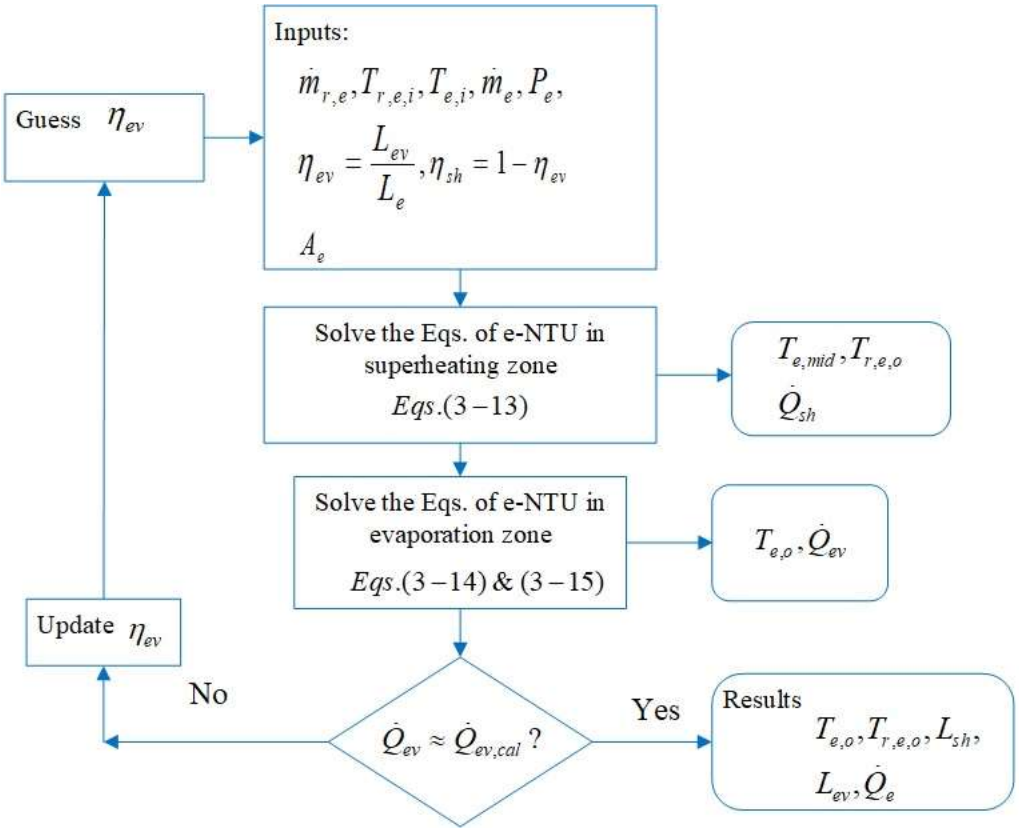

Figure 8-3: Solution algorithm flowchart for the evaporator steady state model (Appendix C)

8.4. Appendix D

Condenser model

The mass and energy conservation equations in superheating, two-phase and subcooling zones of the condenser are developed as follows:

$$[((\frac{\partial \rho_{c,1}}{\partial P_c}\bigg|_{h_{c,1}})+\frac{1}{2}(\frac{\partial \rho_{c,1}}{\partial h_{c,1}}\bigg|_{P_c})(\frac{dh_{c,g}}{dP_c})(h_{c,1}-h_{c,g})+\frac{1}{2}(\frac{dh_{c,g}}{dP_c})\rho_{c,1}-1]L_{c,1}A_{c,cs}\dot{P}_c$$
$$+\rho_{c,1}(h_{c,1}-h_{c,g})A_{c,cs}\dot{L}_{c,1}=\dot{m}_{c,r,i}(h_{c,i}-h_{c,g})+A_{c,1}\alpha_{c,r,1}(T_{c,w,1}-T_{c,r,1}) \quad (8\text{-}1)$$

$$[((\frac{\partial \rho_{c,1}}{\partial P_c}\bigg|_{h_{c,1}})+\frac{1}{2}(\frac{\partial \rho_{c,1}}{\partial h_{c,1}}\bigg|_{Pc})(\frac{dh_{c,g}}{dP_c}))h_{c,g}L_{c,1}+(\frac{d\rho_{c,f}h_{c,f}}{dP_c}(1-\overline{\gamma}_c)+\frac{d\rho_{c,g}h_{c,g}}{dP_c}\overline{\gamma}_c-1)L_{c,2}$$
$$+((\frac{\partial \rho_{c,3}}{\partial P_c}\bigg|_{h_{c,3}})+\frac{1}{2}(\frac{\partial \rho_{c,3}}{\partial h_{c,3}}\bigg|_{P_c})(\frac{dh_{c,f}}{dP_c}))h_{c,f}L_{c,3})]A_{c,cs}\dot{P}_c+\frac{1}{2}[(\frac{\partial \rho_{c,3}}{\partial h_{c,3}}\bigg|_{P_c})h_{c,f}L_{c,3}]A_{c,cs}\dot{h}_{c,o}+$$
$$+[(\rho_{c,g}h_{c,g}-\rho_{c,f}h_{c,f})\overline{\gamma}_c+(\rho_{c,f}-\rho_{c,3})h_{c,f}]A_{c,cs}\dot{L}_{c,2}+[\rho_{c,1}h_{c,g}-\rho_{c,3}h_{c,f}]A_{c,cs}\dot{L}_{c,1}=$$
$$\dot{m}_{c,r,i}h_{c,g}-\dot{m}_{c,r,o}h_{c,f}+A_{c,2}\alpha_{c,r,2}(T_{c,w,2}-T_{c,r,2}) \quad (8\text{-}2)$$

$$[((\frac{\partial \rho_{c,3}}{\partial P_c}\bigg|_{h_{c,3}})+\frac{1}{2}(\frac{\partial \rho_{c,3}}{\partial h_{c,3}}\bigg|_{P_c})(\frac{dh_{c,f}}{dP_c}))(h_{c,3}-h_{c,f})+\frac{1}{2}(\frac{dh_{c,f}}{dP_c})\rho_{c,3}-1]L_{c,3}A_{c,cs}\dot{P}_c$$
$$+\frac{1}{2}[(\frac{\partial \rho_{c,3}}{\partial h_{c,3}}\bigg|_{P_c})(h_{c,3}-h_{c,f})+\rho_{c,3}]L_{c,3}A_{c,cs}\dot{h}_{c,o}+\rho_{c,3}(h_{c,f}-h_{c,3})A_{c,cs}(\dot{L}_{c,1}+\dot{L}_{c,2})$$
$$=\dot{m}_{c,r,o}(h_{c,f}-h_{c,o})+A_{c,3}\alpha_{c,r,3}(T_{c,w,3}-T_{c,r,3}) \quad (8\text{-}3)$$

$$[((\frac{\partial \rho_{c,1}}{\partial P_c}\bigg|_{h_{c,1}})+\frac{1}{2}(\frac{\partial \rho_{c,1}}{\partial h_{c,1}}\bigg|_{P_c})(\frac{dh_{c,g}}{dP_c}))L_{c,1}+(\frac{d\rho_{c,f}}{dP_c}(1-\overline{\gamma}_c)+\frac{d\rho_{c,g}}{dP_c}\overline{\gamma}_c)L_{c,2}+((\frac{\partial \rho_{c,3}}{\partial P_c}\bigg|_{h_{c,3}})$$
$$+\frac{1}{2}(\frac{\partial \rho_{c,3}}{\partial h_{c,3}}\bigg|_{P_c})(\frac{dh_{c,f}}{dP_c}))L_{c,3}]A_{c,cs}\dot{P}_c+\frac{1}{2}[(\frac{\partial \rho_{c,3}}{\partial h_{c,3}}\bigg|_{P_c})L_{c,3}]A_{c,cs}\dot{h}_{c,o}+(\rho_{c,1}-\rho_{c,3})A_{c,cs}\dot{L}_{c,1}$$
$$+[(\rho_{c,g}-\rho_{c,f})\overline{\gamma}_c+(\rho_{c,f}-\rho_{c,3})]A_{c,cs}\dot{L}_{c,2}=\dot{m}_{c,r,i}-\dot{m}_{c,r,o} \quad (8\text{-}4)$$

The condenser wall equations are derived as follows:

$$\rho_w Cp_w A_w[\dot{T}_{c,w,1}L_{c,1} + (T_{c,w,1} - T_{c,w,2})\dot{L}_{c,1}] = \alpha_{c,r,1}A_{c,1}(T_{c,r,1} - T_{c,w,1}) - \dot{Q}_{c,th,1} \tag{8-5}$$

$$\rho_w Cp_w A_w \dot{T}_{c,w,2}L_{c,2} = \alpha_{c,r,2}A_{c,2}(T_{c,r,2} - T_{c,w,2}) - \dot{Q}_{c,th,2} \tag{8-6}$$

$$\rho_w Cp_w A_w[\dot{T}_{c,w,3}L_{c,3} + (T_{c,w,2} - T_{c,w,3})(\dot{L}_{c,1} + \dot{L}_{c,2})] = \alpha_{c,r,3}A_{c,3}(T_{c,r,3} - T_{c,w,3}) - \dot{Q}_{c,th,3} \tag{8-7}$$

$A_{c,1}$, $A_{c,2}$ and $A_{c,3}$ represents the heat transfer surface areas of each zone.

8.5. Appendix E

The mass and energy conservation equations of the evaporator are obtained as follows:

$$\begin{aligned}&[(\frac{d(\rho_{e,f}h_{e,f})}{dP_e} - \frac{d\rho_{e,f}}{dP_e}h_{e,g})(1-\overline{\gamma}_e) + (\frac{d(\rho_{e,g}h_{e,g})}{dP_e} - \frac{d\rho_{e,g}}{dP_e}h_{e,g})\overline{\gamma}_e + \rho_{e,f}(h_{e,g} \\ &-h_{e,f})(\frac{\partial\overline{\gamma}_e}{\partial P_e}\bigg|_{h_{e,i}}) - 1]A_{e,cs}L_{e,1}\dot{P}_e + \rho_{e,f}(h_{e,g} - h_{e,f})(\frac{\partial\overline{\gamma}_e}{\partial h_{e,i}}\bigg|_{P_e})A_{e,cs}L_{e,1}\dot{h}_{e,i} + \rho_{e,f}(h_{e,f} \\ &-h_{e,g})(1-\overline{\gamma}_e)A_{e,cs}\dot{L}_{e,1} = \dot{m}_{e,r,i}(h_{e,i} - h_{e,g}) + A_{e,1}\alpha_{e,r,1}(T_{e,w,1} - T_{e,r,1})\end{aligned} \tag{8-8}$$

$$\begin{aligned}&[((\frac{\partial\rho_{e,2}}{\partial P_e}\bigg|_{h_{e,2}}) + \frac{1}{2}(\frac{\partial\rho_{e,2}}{\partial h_{e,2}}\bigg|_{P_e})(\frac{dh_{e,g}}{dP_e}))(h_{e,2} - h_{e,g}) + \frac{1}{2}(\frac{dh_{e,g}}{dP_e})\rho_{e,2} - 1]L_{e,2}A_{e,cs}\dot{P}_e \\ &+\frac{1}{2}[(\frac{\partial\rho_{e,2}}{\partial h_{e,2}}\bigg|_{P_e})(h_{e,2} - h_{e,g}) + \rho_{e,2}]L_{e,2}A_{e,cs}\dot{h}_{e,o} + \rho_{e,2}(h_{e,g} - h_{e,2})A_{e,cs}\dot{L}_{e,1} \\ &= \dot{m}_{e,r,o}(h_{e,g} - h_{e,o}) + A_{e,2}\alpha_{e,r,2}(T_{e,w,2} - T_{e,r,2})\end{aligned} \tag{8-9}$$

$$[((\frac{\partial \rho_{e,2}}{\partial P_e}\bigg|_{h_{e,2}}) + \frac{1}{2}(\frac{\partial \rho_{e,2}}{\partial h_{e,2}}\bigg|_{P_e})(\frac{dh_{e,g}}{dP_e}))L_{e,2} + (\frac{d\rho_{e,f}}{dP_e}(1-\overline{\gamma}_e) + \frac{d\rho_{e,g}}{dP_e}\overline{\gamma}_e - (\rho_{e,f} - \rho_{e,g}) \tag{8-10}$$

$$(\frac{\partial \overline{\gamma}_e}{dP_e}\bigg|_{h_{e,i}})L_{e,1}]A_{e,cs}\dot{P}_e + \frac{1}{2}(\frac{\partial \rho_{e,2}}{\partial h_{e,2}}\bigg|_{P_e})A_{e,cs}L_2\dot{h}_{e,o} + (\rho_{e,g} - \rho_{e,f})(\frac{\partial \overline{\gamma}_e}{\partial h_{e,i}}\bigg|_{P_e})L_{e,1}A_{e,cs}\dot{h}_{e,i} +$$

$$[(\rho_{e,g} - \rho_{e,2}) + (\rho_{e,f} - \rho_{e,g})(1-\overline{\gamma}_e)]A_{e,cs}\dot{L}_{e,1} = \dot{m}_{e,r,i} - \dot{m}_{e,r,o}$$

The evaporator wall equations for two-phase and superheating zones are developed as follows:

$$\rho_w Cp_w A_w \dot{T}_{e,w,1} L_{e,1} = \alpha_{e,r,1} A_{e,1}(T_{e,r,1} - T_{e,w,1}) + \dot{Q}_{e,th,1} \tag{8-11}$$

$$\rho_w Cp_w A_w [\dot{T}_{e,w,2} L_{e,2} + (T_{e,w,1} - T_{e,w,2})\dot{L}_{e,1}] = \alpha_{e,r,2} A_{e,2}(T_{e,r,2} - T_{e,w,2}) + \dot{Q}_{e,th,2} \tag{8-12}$$

$A_{e,1}$, $A_{e,2}$ and $A_{e,3}$ represents the heat transfer surface areas of each zone.

REFERENCES

[1] J. Chen, S. Jarall, H. Havtun, B. Palm, A review on versatile ejector applications in refrigeration systems, Renew. Sustain. Energy Rev. 49 (2015) 67–90. doi:10.1016/j.rser.2015.04.073.

[2] ASHRAE, Steam-jet refrigeration equipment, Equipment Handbook, ASHRAE, Atlanta Georgia, 1979.

[3] G. Besagni, R. Mereu, F. Inzoli, Ejector refrigeration: A comprehensive review, Renew. Sustain. Energy Rev. 53 (2016) 373–407. doi:10.1016/j.rser.2015.08.059.

[4] J. Liu, L. Wang, L. Jia, Z. Li, H. Zhao, A control oriental model for combined compression-ejector refrigeration system, Energy Convers. Manag. 138 (2017) 538–546. doi:10.1016/j.enconman.2017.02.033.

[5] A. Thekdi, S.U. Nimbalkar, Industrial Waste Heat Recovery - Potential Applications, Available Technologies and Crosscutting R&D Opportunities, Oak Ridge, 2014. doi:10.2172/1185778.

[6] J.H. Keenan, F.L. Ernest Paul Neumann, An investigation of ejector design by analysis and experiment, Cambridge, Mass., 1948.

[7] D.-W. Sun, I.W. Eames, Recent developments in the design theories and applications of ejectors, J. Energy Inst. 68 (1995) 65–79. doi:10.1016/0140-6701(95)96874-C.

[8] S. He, Y. Li, R.Z. Wang, Progress of mathematical modeling on ejectors, Renew. Sustain. Energy Rev. 13 (2009) 1760–1780. doi:10.1016/j.rser.2008.09.032.

[9] B. Huang, J.M. Chang, C.P. Wang, V.A. Petrenko, A 1-D analysis of ejector performance, Int. J. Refrig. 22 (1999) 354–364. doi:10.1016/S0140-7007(99)00004-3.

[10] J.M. Cardemil, S. Colle, A general model for evaluation of vapor ejectors performance for application in refrigeration, Energy Convers. Manag. 64 (2012) 79–86. doi:10.1016/j.enconman.2012.05.009.

[11] N. Galanis, M. Sorin, Ejector design and performance prediction, Int. J. Therm. Sci. 104 (2016) 315–329. doi:http://dx.doi.org/10.1016/j.ijthermalsci.2015.12.022.

[12] M. Khennich, N. Galanis, M. Sorin, Effects of design conditions and irreversibilities on the dimensions of ejectors in refrigeration systems, Appl. Energy. 179 (2016) 1020–1031. doi:10.1016/j.apenergy.2016.07.053.

[13] E.D. Rogdakis, G.K. Alexis, Design and parametric investigation of an ejector in an air-conditioning system, Appl. Therm. Eng. 20 (2000) 213–226. doi:10.1016/S1359-4311(99)00013-7.

[14] S. Chen, G. Chen, L. Fang, An experimental study and 1-D analysis of an ejector with a

movable primary nozzle that operates with R236fa, Int. J. Refrig. 60 (2015) 19–25. doi:10.1016/j.ijrefrig.2015.08.011.

[15] H. Chen, D.Y. Goswami, E.K. Stefanakos, A review of thermodynamic cycles and working fluids for the conversion of low-grade heat, Renew. Sustain. Energy Rev. 14 (2010) 3059–3067. doi:10.1016/j.rser.2010.07.006.

[16] K. Cizungu, A. Mani, M. Groll, Performance comparison of vapour jet refrigeration system with environment friendly working fluids, Appl. Therm. Eng. 21 (2001) 585–598.

[17] R. Roman, J.I. Hernandez, Performance of ejector cooling systems using low ecological impact refrigerants, Int. J. Refrig. 34 (2011).

[18] P.R. Pereira, S. Varga, A.C. Oliveira, J. Soares, Development and Performance of an Advanced Ejector Cooling System for a Sustainable Built Environment, Front. Mech. Eng. 1 (2015) 1–12. doi:10.3389/fmech.2015.00007.

[19] J. Chen, Investigation of Vapor Ejectors in Heat Driven Ejector Refrigeration Systems, 2014.

[20] J. Chen, H. Havtun, B. Palm, Investigation of ejectors in refrigeration system: Optimum performance evaluation and ejector area ratios perspectives, Appl. Therm. Eng. 64 (2014) 182–191. doi:10.1016/j.applthermaleng.2013.12.034.

[21] R. Yapici, H.K. Ersoy, A. Aktoprakoğlu, H.S. Halkaci, O. Yiğit, Experimental determination of the optimum performance of ejector refrigeration system depending on ejector area ratio, Int. J. Refrig. 31 (2008) 1183–1189. doi:10.1016/j.ijrefrig.2008.02.010.

[22] T. Thongtip, S. Aphornratana, An experimental analysis of the impact of primary nozzle geometries on the ejector performance used in R141b ejector refrigerator, Appl. Therm. Eng. 110 (2017) 89–101. doi:10.1016/j.applthermaleng.2016.08.100.

[23] K. Chunnanond, S. Aphornratana, An experimental investigation of a steam ejector refrigerator: The analysis of the pressure profile along the ejector, Appl. Therm. Eng. 24 (2004) 311–322. doi:10.1016/j.applthermaleng.2003.07.003.

[24] D.-W. Sun, Variable geometry ejectors and their applications in ejector refrigeration, Energy. 21 (1996) 919–929.

[25] S.B. Riffat, S.A. Omer, CFD modelling and experimental investigation of an ejector refrigeration system using methanol as the working fluid, Int. J. Energy Res. 25 (2001) 115–128.

[26] K. Pianthong, W. Seehanam, M. Behnia, T. Sriveerakul, S. Aphornratana, Investigation and improvement of ejector refrigeration system using computational fluid dynamics technique, Energy Convers. Manag. 48 (2007) 2556–2564. doi:10.1016/j.enconman.2007.03.021.

[27] T. Thongtip, S. Aphornratana, An alternative analysis applied to investigate the ejector performance used in R141b jet-pump refrigeration system, Int. J. Refrig. 53 (2015) 20–33. doi:https://doi.org/10.1016/j.ijrefrig.2015.01.017.

[28] I.W. Eames, S. Aphornratana, H. Haider, A Theoretical and Experimental Study of a small sclae steam jet refrigerator, Int. J. Refrig. 18 (1995) 378–386.

[29] B.J. Huang, C.B. Jiang, F.L. Hu, Ejector Performance Characteristics and Design Analysis

of Jet Refrigeration System, J. Eng. Gas Turbines Power. 107 (1985) 792. doi:10.1115/1.3239802.

[30] M. Hamzaoui, H. Nesreddine, Z. Aidoun, M. Balistrou, Experimental study of a low grade heat driven ejector cooling system using the working fluid R245fa, Int. J. Refrig. 86 (2018) 388–400. doi:10.1016/j.ijrefrig.2017.11.018.

[31] T.L. McKinley, A.G. Alleyne, An advanced nonlinear switched heat exchanger model for vapor compression cycles using the moving-boundary method, Int. J. Refrig. 31 (2008) 1253–1264. doi:10.1016/j.ijrefrig.2008.01.012.

[32] E. Rodriguez, B. Rasmussen, A comparison of modeling paradigms for dynamic evaporator simulations with variable fluid phases, Appl. Therm. Eng. 112 (2017) 1326–1342. doi:10.1016/j.applthermaleng.2016.10.131.

[33] R.N.N. Koury, R.N. Faria, R.O. Nunes, K.A.R. Ismail, L. Machado, Dynamic model and experimental study of an air-water heat pump for residential use, Int. J. Refrig. 36 (2013) 674–688. doi:10.1016/j.ijrefrig.2012.11.006.

[34] D. Leducq, J. Guilpart, G. Trystram, Non-linear predictive control of a vapour compression cycle, Int. J. Refrig. 29 (2006) 761–772. doi:10.1016/j.ijrefrig.2005.12.005.

[35] H. Li, S.K. Jeong, J.I. Yoon, S.S. You, An empirical model for independent control of variable speed refrigeration system, Appl. Therm. Eng. 28 (2008) 1918–1924. doi:10.1016/j.applthermaleng.2007.12.008.

[36] J. Navarro-Esbrí, V. Berbegall, G. Verdu, R. Cabello, R. Llopis, A low data requirement model of a variable-speed vapour compression refrigeration system based on neural networks, Int. J. Refrig. 30 (2007) 1452–1459. doi:10.1016/j.ijrefrig.2007.03.007.

[37] J.A. Romero, J. Navarro-Esbrí, J.M. Belman-Flores, A simplified black-box model oriented to chilled water temperature control in a variable speed vapour compression system, Appl. Therm. Eng. 31 (2011) 329–335.

[38] S. Wang, Dynamic Simulation of a Building Central Chilling System and Evaluation of EMCS On-Line Control Strategies, Build. Environ. 33 (1998) 1–20. doi:10.1016/S0360-1323(97)00019-X.

[39] D. Shiming, A dynamic mathematical model of a direct expansion (DX), Build. Environ. 35 (2000) 603–613.

[40] M.W. Browne, P.K. Bansal, Transient simulation of vapour-compression packaged liquid chillers, Int. J. Re. 25 (2002) 597–610.

[41] Z. Lei, M. Zaheeruddin, Dynamic simulation and analysis of a water chiller refrigeration system, Appl. Therm. Eng. 25 (2005) 2258–2271. doi:10.1016/j.applthermaleng.2005.01.002.

[42] R. Llopis, R. Cabello, E. Torrella, A dynamic model of a shell-and-tube condenser operating in a vapour compression refrigeration plant, Int. J. Therm. Sci. 47 (2008) 926–934. doi:10.1016/j.ijthermalsci.2007.06.021.

[43] T. Pfafferott, G. Schmitz, Modelling and transient simulation of CO2-refrigeration systems with Modelica, Int. J. Refrig. 27 (2004) 42–52. doi:10.1016/S0140-7007(03)00098-7.

[44] R. Shi, D. Fu, Y. Feng, J. Fan, S. Mijanovic, Dynamic Modeling of CO2 Supermarket Refrigeration System, in: Proc. Int. Refrig. Air Cond. Conf., Purdue, 2010: pp. 2442:1-2442:8. http://docs.lib.purdue.edu/iracc/1127.

[45] Y. Yao, M. Huang, J. Chen, State-space model for dynamic behavior of vapor compression liquid chiller, Int. J. Refrig. 36 (2013) 2128–2147. doi:10.1016/j.ijrefrig.2013.05.006.

[46] S. Bendapudi, J.E. Braun, A Review of Literature on Dynamic Models of Vapor Compression Equipment, 2002.

[47] S. Bendapudi, J.E. Braun, E.A. Groll, A comparison of moving-boundary and finite-volume formulations for transients in centrifugal chillers, Int. J. Refrig. 31 (2008) 1437–1452. doi:10.1016/j.ijrefrig.2008.03.006.

[48] H. Pangborn, A.G. Alleyne, N. Wu, A comparison between finite volume and switched moving boundary approaches for dynamic vapor compression system modeling Une comparaison entre le volume fini et les approches par res mobiles pour la mod e lisation des interversion des fronti, 3 (2015).

[49] A. Desideri, B. Dechesne, J. Wronski, M. Van Den Broek, S. Gusev, V. Lemort, S. Quoilin, Comparison of moving boundary and finite-volume heat exchanger models in the Modelica language, Energies. 9 (2016) 1–18. doi:10.3390/en9050339.

[50] Y. Yao, W. Wang, M. Huang, A state-space dynamic model for vapor compression refrigeration system based on moving-boundary formulation, Int. J. Refrig. 60 (2015) 174–189. doi:10.1016/j.ijrefrig.2015.07.027.

[51] J. Bonilla, S. Dormido, F.E. Cellier, Switching moving boundary models for two-phase flow evaporators and condensers, Commun. Nonlinear Sci. Numer. Simul. 20 (2015) 743–768. doi:10.1016/j.cnsns.2014.06.035.

[52] D. Kim, D. Ziviani, J.E. Braun, E.A. Groll, A Moving Boundary Modeling Approach for Heat Heat Exchangers with Binary Mixtures, Energy Procedia. 129 (2017) 466–473. doi:10.1016/j.egypro.2017.09.161.

[53] X. Xue, X. Feng, J. Wang, F. Liu, Modeling and simulation of an air-cooling condenser under transient conditions, Procedia Eng. 31 (2012) 817–822. doi:10.1016/j.proeng.2012.01.1106.

[54] W.J. Zhang, C.L. Zhang, A generalized moving-boundary model for transient simulation of dry-expansion evaporators under larger disturbances, Int. J. Refrig. 29 (2006) 1119–1127. doi:10.1016/j.ijrefrig.2006.03.002.

[55] H. Qiao, C.R. Laughman, V. Aute, An advanced switching moving boundary heat exchanger model with pressure drop, Int. J. Refrig. 65 (2016) 154–171.

[56] N. Liang, S. Shao, C. Tian, Y. Yan, Dynamic simulation of variable capacity refrigeration systems under abnormal conditions, Appl. Therm. Eng. 30 (2010) 1205–1214. doi:10.1016/j.applthermaleng.2010.01.038.

[57] S. Bendapudi, J.E. Braun, E.A. Groll, A Dynamic Model Of A Vapor Compression Liquid Chiller, Int. Refrig. Air Cond. Conf. (2002) 568.

[58] M. Willatzen, N. Pettit, L. Ploug-Sørensen, A general dynamic simulation model for evaporators and condensers in refrigeration. Part I: moving-boundary formulation of two-

phase flows with heat exchange, Int. J. Refrig. 21 (1998) 398–403. http://www.sciencedirect.com/science/article/pii/S0140700797000911.

[59] E.W. Grald, J.W. MacArthur, A moving-boundary formulation for modeling time-dependent two-phase flows, Int. J. Heat Fluid Flow. 13 (1992) 266–272.

[60] Y. Xu, X. Fang, Correlations of void fraction for two-phase refrigerant flow in pipes, Appl. Therm. Eng. 64 (2014) 242–251. doi:10.1016/j.applthermaleng.2013.12.032.

[61] L. Zheng, J. Deng, Y. He, P. Jiang, Dynamic model of a transcritical CO2 ejector expansion refrigeration system, Int. J. Refrig. 60 (2015) 247–260.

[62] B.P. Rasmussen, A.G. Alleyne, Dynamic Modeling and Advanced Control of Air Conditioning and Refrigeration Systems, Urbana, 2006. https://www.mendeley.com/catalogue/dynamic-modeling-advanced-control-air-conditioning-refrigeration-systems/.

[63] X.-D. He, S. Liu, H.H. Asada, Modeling of Vapor Compression Cycles for Multivariable Feedback Control of HVAC Systems, J. Dyn. Syst. Meas. Control. 119 (1997) 183. doi:10.1115/1.2801231.

[64] J.B. Marcinichen, T.N. Holanda, C. Melo, A Dual Siso Controller for a Vapor Compression Refrigeration System, in: Int. Refrig. Air Cond. Conf., 2008.

[65] Y. Shen, W.-J. Cai, S. Li, Normalized decoupling control for high-dimensional MIMO processes for application in room temperature control HVAC systems, Control Eng. Pract. 18 (2010) 652–664.

[66] N.L. Ricker, Predictive hybrid control of the supermarket refrigeration benchmark process, Control Eng. Pract. 18 (2010) 608–617.

[67] D. Sarabia, F. Capraro, L.F.S. Larsen, C. de Prada, Hybrid NMPC of supermarket display cases, Control Eng. Pract. 17 (2009) 428–441.

[68] L.C. Schurt, C.J.L. Hermes, A.T. Neto, A model-driven multivariable controller for vapor compression refrigeration systems, Int. J. Refrig. 32 (2009) 1672–1682. doi:10.1016/j.ijrefrig.2009.04.004.

[69] L.C. Schurt, C.J.L. Hermes, A.T. Neto, Assessment of the controlling envelope of a model-based multivariable controller for vapor compression refrigeration systems, Appl. Therm. Eng. 30 (2010) 1538–1546.

[70] L. Larsen, J. Holm, Modelling and Multi-variable Control of Refrigeration Systems, in: Ecos 2003, 2003. http://forskningsbasen.deff.dk/Share.external?sp=S0b6129a0-9c2d-11db-8ed6-000ea68e967b&sp=Saau.

[71] J.A. Alfaya, G. Bejarano, M.G. Ortega, F.R. Rubio, Controllability analysis and robust control of a one-stage refrigeration system, Eur. J. Control. 26 (2015) 53–62.

[72] G. Bejarano, J.A. Alfaya, M.G. Ortega, F.R. Rubio, Multivariable analysis and H∞ control of a one-stage refrigeration cycle, Appl. Therm. Eng. 91 (2015) 1156–1167.

[73] N. Jain, Thermodynamics-based optimization and control of integrated energy systems, University of Illinois at Urbana-Champaign, 2013.

[74] N. Jain, A. Alleyne, Exergy-based optimal control of a vapor compression system, Energy Convers. Manag. 92 (2015) 353–365. doi:10.1016/j.enconman.2014.12.014.

[75] M. Leblanc, Sur l'electri"cation des chemins de fer au moyen de courants alternatifs de frequence elevee, Rev. Gen. l'Electricite. (1922).

[76] Y. Tan, W.H. Moase, C. Manzie, D. Nešić, I.M.Y. Mareels, Extremum seeking from 1922 to 2010, in: 29th Chinese Control Conf., 2010: pp. 14–26.

[77] K.B. Ariyur, M. Krstić, Real-time optimization by extremum-seeking control., John Wiley & Sons Inc, New York, NY, 2003.

[78] V.V.Kazakevich, Technique of automatic control of different processes to maximum or to minimum, 66335, 1943.

[79] V.V.Kazakevich, On extremum seeking, Moscow High Technical University, 1944.

[80] C.S. Draper, Y.T. Li, Principles of optimalizing control systems and an application to the internal combustion engine, American Society of Mechanical Engineers, 1951.

[81] I.S. Morosanov, Method of extremum control, Autom. Remote Control. 18 (1957) 1077–1092.

[82] I. I. Ostrovskii, Extremum regulation, Autom. Remote Control. 18 (1957) 900–907.

[83] S.M. Meerkov, Asymptotic methods for investigating a class offorced states in extremal systems, Autom. Remote Control. 12 (1967) 1916–1920.

[84] S.M. Meerkov, Asymptotic methods for investigating quasi-stationary states in continuous systems of automatic optimization, Autom. Remote Control. 11 (1967) 1726–1743.

[85] C.S. Draper, Y.T. Li, Principles of optimalizing control systems and an application to the internal combustion engine, in: Optim. Self-Optimizing Control, The M.I.T. Press, Boston, MA, 1951.

[86] V.K. Obabkov, Theory of multichannel extremal control systems with sinusoidal probe signals, Autom. Remote Control. 28 (1967) 48–54.

[87] J. of P.-H.C.S.C. Luxat, L.H. Lees, Stability of Peak-Holding Control Systems, IEEE Trans. Ind. Electron. Control Instrum. IECI-18 (1971) 11–15. doi:10.1109/TIECI.1971.230455.

[88] K.J. Astrom, B.Wittenmark, Adaptive control, second, Addison-Wesley, 1995.

[89] Krstic M., Wang H.-H., Stability of extremum seeking feedback for general nonlinear dynamic systems, Automatica. 36 (2000) 595–601. doi:10.1016/S0005-1098(99)00183-1.

[90] Y. Tan, D. Nešić, I.M.Y. Mareels, On non-local stability properties of extremum seeking control, Automatica. 42 (2006) 889–903. doi:10.1016/j.automatica.2006.01.014.

[91] S.-J. Liu, M. Krstic, Stochastic Averaging and Stochastic Extremum Seeking, Springer, London, 2012.

[92] James C Spall, Multivariate stochastic approximation using a simultaneous perturbation gradient approximation, in: IEEE Trans. Automat. Contr., 1992: pp. 332–341.

[93] J.C. Spall, A one-measurement form of simultaneous perturbation stochastic approximation, Automatica. 33 (1997) 109–112. doi:10.1016/S0005-1098(96)00149-5.

[94] J.C. SPALL, Implementation of the Simultaneous Perturbation Algorithm for Stochastic Optimization, IEEE Trans. Aerosp. Electron. Syst. 34 (1998) 817–823.

[95] A.R. Teel, D. Popovic, Solving smooth and nonsmooth multivariable extremum seeking problems by the methods of nonlinear programming, in: Proc. Am. Control Conf., Arlington, 2001: pp. 2394–2399. doi:10.1109/acc.2001.946111.

[96] K.B. Ariyur, M. Krstić, Multivariable Extremum Seeking Feedback: Analysis and Design, in: Proc. Am. Control Conf., Anchorage, 2002: pp. 2903–2908.

[97] A. Banaszuk, Y. Zhang, C.A. Jacobson, Adaptive control of combustion instability using extremum-seeking, in: Proc. Am. Control Conf., Chicago, Illinois, 2002: pp. 416–422 vol.1. doi:10.1109/acc.2000.878934.

[98] A. Banaszuk, K.. Ariyur, M. Krstic, C.A. Jacobson, An adaptive algorithm for control of combustion instability, Automatica. 40 (2004) 1965–1972. doi:10.1016/j.automatica.2004.06.008.

[99] M. Krstic, A. Banaszuk, Multivariable adaptive control of instabilities arising in jet engines, Control Eng. Pract. 14 (2006) 833–842. doi:10.1016/j.conengprac.2005.04.006.

[100] W.H. Moase, C. Manzie, M.J. Brear, Newton-like extremum-seeking for the control of thermoacoustic instability, IEEE Trans. Automat. Contr. 55 (2010) 2094–2105. doi:10.1109/TAC.2010.2042981.

[101] J.P. Moeck, M.R. Bothien, C.O. Paschereit, G. Gelbert, R. King, Two-Parameter Extremum Seeking for Control of Thermoacoustic Instabilities and Characterization of Linear Growth, in: 45th Aerosp. Sci. Meet. Exhipit, 2007: pp. 1416–1433. doi:https://doi.org/10.2514/6.2007-1416.

[102] K.S. Peterson, A.G. Stefanopoulou, Extremum seeking control for soft landing of an electromechanical valve actuator, Automatica. 40 (2004) 1063–1069. doi:10.1016/j.automatica.2004.01.027.

[103] I. Haskara, G.G. Zhu, J. Winkelman, Multivariable EGR/spark timing control for IC engines via extremum seeking, in: Proc. 2006 Am. Control Conf., 2006: pp. 1173–1178. doi:10.1109/acc.2006.1656376.

[104] N.J. Killingsworth, S.M. Ceves, D.L. Flowers, F. Espinosa-loza, Miroslav Krstic, HCCI Engine Combustion-Timing Control : Optimizing Gains and Fuel Consumption Via Extremum Seeking, IEEE Trans. Control Syst. Technol. 17 (2009) 1350–1361. doi:10.1109/TCST.2008.2008097.

[105] D. Popović, M. Janković, S. Magner, A.R. Teel, Extremum seeking methods for optimization of variable cam timing engine operation, IEEE Trans. Control Syst. Technol. 14 (2006) 398–407. doi:10.1109/TCST.2005.863660.

[106] S. Sugihira, K. Ichikawa, Hiromitu Ohmori, Starting Speed Control of SI Engine Based on Extremum Seeking Control, in: SICE Annu. Conf., Kagawa University, 2007: pp. 1036–1041. doi:10.3182/20080706-5-kr-1001.00177.

[107] Y.A. Chang, S.J. Moura, Air flow control in fuel cell systems: An extremum seeking approach, in: Proc. Am. Control Conf., St. Louis, 2009: pp. 1052–1059. doi:10.1109/ACC.2009.5160016.

[108] L. Henning, R. Becker, G. Feuerbach, R. Muminovic, R. King, A. Brunn, W. Nitsche, Extensions of adaptive slope-seeking for active flow control, Proc. Inst. Mech. Eng. Part I J. Syst. Control Eng. 222 (2008) 309–322. doi:10.1243/09596518JSCE490.

[109] K. Kim, C. Kasnakoglu, A. Serrani, M. Samimy, Extremum-Seeking Control of Subsonic Cavity Flow, AIAA J. 47 (2008) 195–205. doi:10.2514/1.38180.

[110] R. King, R. Petz, Olaf Lemke, Adaptive flow control using slope seeking, in: 14th Mediterr. Conf. Control Autom., 2006. doi:10.1109/MED.2006.328753.

[111] P. Binetti, K.B. Ariyur, M. Krstic, F. Bernelli, Control of formation flight via extremum seeking, in: Proc. Am. Control Conf., Anchorage, 2002: pp. 2848–2853.

[112] D.F. Chichka, J.L. Speyer, C.G. Park, Peak-seeking control with application to formation flight, in: Proc. 38th Conf. Decis. Control, Phoenix, Arizona, 1999: pp. 2463–2470. doi:10.1109/cdc.1999.831295.

[113] X. Feng, Z. Ximing, R. Fierro, M. Motter, Autopilot-based nonlinear UAV formation controller with extremum-seeking, in: Proc. 44th IEEE Conf. Decis. Control. Eur. Control Conf., Seville, 2005: pp. 4933–4938. doi:10.1109/CDC.2005.1582943.

[114] X.T. Zhang, D.M. Dawson, W.E. Dixon, B. Xian, Extremum-Seeking Nonlinear Controllers for a Human Exercise Machine, IEEE/ASME Trans. MECHATRONICS,. 11 (2006) 233–240. doi:10.1109/TPAMI.2012.125.

[115] L. Gurvich, Fuzzy logic base extremum seeking control system, in: 23rd IEEE Conv. Electr. Electron. Eng. Isr., 2004: pp. 18–21. doi:10.1109/eeei.2004.1361077.

[116] Y. Hu, B. Zuo, X. Li, The Application of an Annealing Recurrent Neural Network for Extremum Seeking Algorithm to Optimize UAV Tight Formation Flight, in: IMACS Multiconference "Computational Eng. Syst. Appl., 2006: pp. 613–620.

[117] P.M. Dower, P.M. Farrell, D. Nešić, Extremum seeking control of cascaded Raman optical amplifiers, in: IEEE Trans. Control Syst. Technol., 2008: pp. 396–407. doi:10.1109/TCST.2007.903056.

[118] N. Hudon, M. Guay, M. Perrier, D. Dochain, Adaptive extremum seeking control of a tubular reactor with limited actuation, in: Am. Control Conf., Portland, 2005: pp. 4563–4568. doi:10.1109/acc.2005.1470715.

[119] A.A. Krasovski, Problems of continuous systems theory of extremal control of industrial processes, IFAC Proc. Vol. 1 (1963) 519–526. doi:https://doi.org/10.1016/S1474-6670(17)69685-X.

[120] V. Tyagi, H. Sane, S. Darbha, An extremum seeking algorithm for determining the set point temperature for condensed water in a cooling tower, in: Proc. 2006 Am. Control Conf., Minneapolis,Minnesota, 2006: pp. 1127–1131. doi:10.1109/acc.2006.1656368.

[121] N. Araki, T. Sato, Y. Kumamoto, Y. Iwai, Y. Konishi, Design of Weigh Feeder Control System using Extremum-Seeking Method, in: Proc. 7th Asian Control Conf., Hong Kong, 2009: pp. 250–255.

[122] T. Cooler, Y. Li, M.A. Rotea, G.T. Chiu, L.G. Mongeau, I. Paek, Extremum Seeking Control of Tunable Thermoacoustic Cooler, IEEE Trans. Control Syst. Technol. 13 (2005) 527–536.

[123] P. Li, Y. Li, J.E. Seem, Efficient Operation of Air-Side Economizer Using Extremum Seeking Control, J. Dyn. Syst. Meas. Control. 132 (2010) 031009-1-031009–10. doi:10.1115/1.4001216.

[124] X. Li, Y. Li, J.E. Seem, P. Li, Dynamic modeling and self-optimizing operation of chilled water systems using extremum seeking control, Energy Build. 58 (2013) 172–182. doi:10.1016/j.enbuild.2012.12.010.

[125] D.J. Burns, W.K. Weiss, M. Guay, Realtime setpoint optimization with time-varying extremum seeking for vapor compression systems, in: Proc. Am. Control Conf., Chicago, 2015: pp. 974–979. doi:10.1109/ACC.2015.7170860.

[126] D.J. Burns, C. Laughman, Extremum Seeking Control for Energy Optimization of Vapor Compression Systems, in: Int. Refrig. Air Cond. Conf., Purdue, 2012: pp. 1–7.

[127] J.P. Koeln, A.G. Alleyne, Optimal subcooling in vapor compression systems via extremum seeking control : Theory and experiments, 3 (2014).

[128] B. Hu, Y. Li, F. Cao, Z. Xing, Extremum seeking control of COP optimization for air-source transcritical CO2 heat pump water heater system, Appl. Energy. 147 (2015) 361–372. doi:10.1016/j.apenergy.2015.03.010.

[129] S. Aphornratana, S. Chungpaibulpatana, P. Srikhirin, Experimental investigation of an ejector refrigerator: Effect of mixing chamber geometry on system performance, Int. J. Energy Res. 25 (2001) 397–411. doi:10.1002/er.689.

[130] I.W.Eames, S.Aphornratana, H.Haider, A theoretical and experimental study of a small scale steam jet refrigerator, Int. J. Refrig. 18 (1995) 378–386. doi:10.1016/0140-7007(95)98160-M.

[131] W. Chen, C. Shi, S. Zhang, H. Chen, D. Chong, J. Yan, Theoretical analysis of ejector refrigeration system performance under overall modes, Appl. Energy. (2016) 1–11. doi:10.1016/j.apenergy.2016.01.103.

[132] W.M. Kays, A.L. London, Compact Heat Exchangers, Third, Krieger Publishing Company, 1997.

[133] J. Liu, W. Wei, G. Ding, C. Zhang, M. Fukaya, K. Wang, T. Inagaki, A general steady state mathematical model for fin-and-tube heat exchanger based on graph theory, Int. J. Refrig. 27 (2004) 965–973. doi:10.1016/j.ijrefrig.2004.06.008.

[134] M.L.M. Costa, J.A.R. Parise, A THREE-ZONE SIMULATION MODEL FOR AIR-COOLED CONDENSERS, 13 (1993) 97–113.

[135] Y.T. Ge, R. Cropper, Performance evaluations of air-cooled condensers using pure and mixture refrigerants by four-section lumped modelling methods, Appl. Therm. Eng. 25 (2005) 1549–1564. doi:10.1016/j.applthermaleng.2004.10.001.

[136] G. liang Ding, Recent developments in simulation techniques for vapour-compression refrigeration systems, Int. J. Refrig. 30 (2007) 1119–1133. doi:10.1016/j.ijrefrig.2007.02.001.

[137] G. Bejarano, J.A. Alfaya, M.G. Ortega, M. Vargas, On the difficulty of globally optimally controlling refrigeration systems, Appl. Therm. Eng. 111 (2017) 1143–1157. doi:10.1016/j.applthermaleng.2016.10.007.

[138] SEYFETTİN YILDIZ, Design and Simulation of a Vapor Compression Refrigeration Cycle for a Micro Refrigerator a Thesis Submitted To the Graduate School of Natural and Applied Sciences of Middle East Technical University By Seyfettİ N Yildiz in Partial Fullfillment of the Re, Middle East Technical University, 2010.

[139] D.M. Admiraal, C.W. Bullard, Heat Transfer in Refrigerator Condensers and Evaporators, Illinois, Urbana, 1993.

[140] V.S. Gullapalli, Estimation of Thermal and Hydraulic Characteristics of Compact Brazed Plate Heat Exchangers, PhD Lund. (2013). http://lup.lub.lu.se/record/3799250/file/3799358.pdf.

[141] E. 98005. ESDU, Design and Performance Evaluation of Heat Exchangers: The Effectiveness – NTU Method, London, England, 1998.

[142] M.H. Eldakamawy, M. V Sorin, M. Brouillette, Energy and exergy investigation of ejector refrigeration systems using retrograde refrigerants, Int. J. Refrig. 78 (2017) 176–192. doi:10.1016/j.ijrefrig.2017.02.031.

[143] A. Selvaraju, A. Mani, Experimental investigation on R134a vapour ejector refrigeration system, Int. J. Refrig. 29 (2006) 1160–1166. doi:10.1016/j.ijrefrig.2006.01.004.

[144] Y. Jia, C. Wenjian, Area ratio effects to the performance of air-cooled ejector refrigeration cycle with R134a refrigerant, Energy Convers. Manag. 53 (2012) 240–246. doi:10.1016/j.enconman.2011.09.002.

[145] M.B. Demay, C.A. Flesch, R.C.C. Flesch, C.A. Penz, A.P. Rosa, Theoretical and Experimental Study of Signal Processing Techniques for Measuring Hermetic Compressor Speed through Pressure and Current Signals, in: Int. Compress. Eng. Conf., Purdue University Purdue e-Pubs, 2012.

[146] Samuel D. Streans, Ruth A. David, Signal Processing Algorithm, Prentice-Hall, Inc., New Jersey, n.d.

[147] S.W. Smith, Digital Signal Processing: A Practical Guide for Engineers and Scienctists, Elsevier Ltd, 2003.

[148] S. Liu, B. Dai, W. Zhang, X. Li, Experimental Study On R245fa Condensation Heat Transfer Properties In Horizontal Tube, Energy Procedia. 104 (2016) 419–424. doi:10.1016/j.egypro.2016.12.071.

[149] S.W. Smith, The Scientist and Engineer's Guide to Digital Signal Processing, 1999.

[150] S. Taslimi Taleghani, M. Sorin, S. Poncet, Modeling of two-phase transcritical CO2ejectors for on-design and off-design conditions, Int. J. Refrig. (2018) 1–15. doi:10.1016/j.ijrefrig.2017.10.025.

[151] B. Huang, A 1-D analysis of ejector performance, Int. J. Refrig. 22 (1999) 354–364. doi:10.1016/S0140-7007(99)00004-3.

[152] P.A. Thompson, Compressible Fluid Dynamics, McGraw-Hill, 1972.

[153] E. Narimani, M. Sorin, P. Micheau, H. Nesreddine, Numerical and experimental investigation of the influence of generating pressure on the performance of a one-phase ejector installed within an R245fa refrigeration cycle, Appl. Therm. Eng. 157 (2019).

doi:10.1016/j.applthermaleng.2019.04.064.

[154] W.R. Huster, Y. Vaupel, A. Mhamdi, A. Mitsos, Validated dynamic model of an organic Rankine cycle (ORC) for waste heat recovery in a diesel truck, Energy. 151 (2018) 647–661. doi:10.1016/j.energy.2018.03.058.

[155] B.A. Cullimore, T.J. Hendricks, Design and transient simulation of vehicle air conditioning systems, in: Veh. Therm. Manag. Syst. Conf. Exhib., Nashville,Tennessee, 2001. doi:https://doi.org/10.4271/2001-01-1692.

[156] J. Eborn, H. Tummescheit, K. Prölß, AirConditioning – a Modelica Library for Dynamic Simulation of AC Systems, in: Proc. 4th Int. Model. Conf. Hamburg, 2005: pp. 185–192. doi:10.1016/j.cep.2011.11.002.

[157] J.W. MacArthur, E.W. Grald, Unsteady compressible two-phase flow model for predicting cyclic heat pump performance and a comparison with experimental data, Int. J. Refrig. 12 (1989) 29–41. doi:10.1016/0140-7007(89)90009-1.

[158] B. Li, A.G. Alleyne, A dynamic model of a vapor compression cycle with shut-down and start-up operations, Int. J. Refrig. 33 (2010) 538–552. doi:10.1016/j.ijrefrig.2009.09.011.

[159] T.A. Horst, H.S. Rottengruber, M. Seifert, J. Ringler, Dynamic heat exchanger model for performance prediction and control system design of automotive waste heat recovery systems, Appl. Energy. 105 (2013) 293–303. doi:10.1016/j.apenergy.2012.12.060.

[160] J. Chen, J. Yu, Dynamic simulation of an air-source heat pump water heater using novel modified evaporator model, Appl. Therm. Eng. 144 (2018) 469–478. doi:10.1016/j.applthermaleng.2018.08.085.

[161] B. P. Rasmussen, R. Shah, A.B. Musser, A.G. Alleyne, P. C. W. Bullard, P.S. Hrnjak, N.R. Miller, Control-Oriented Modeling of Transcritical Vapor Compression Systems, 2002. doi:10.1115/1.1648312.

[162] J. Zhang, W. Zhang, G. Hou, F. Fang, Dynamic modeling and multivariable control of organic Rankine cycles in waste heat utilizing processes, Comput. Math. with Appl. 64 (2012) 908–921. doi:10.1016/j.camwa.2012.01.054.

[163] J. Zhang, Y. Zhou, R. Wang, J. Xu, F. Fang, Modeling and constrained multivariable predictive control for ORC (Organic Rankine Cycle) based waste heat energy conversion systems, Energy. 66 (2014) 128–138. doi:10.1016/j.energy.2014.01.068.

[164] J.I. Chowdhury, B.K. Nguyen, D. Thornhill, Dynamic Model of Supercritical Organic Rankine Cycle Waste Heat Recovery System for Internal Combustion Engine, Int. J. Automot. Technol. 18 (2017) 589–601. doi:10.1007/s12239.

[165] Radia Eldeeb, V. Aute, R. Radermacher, A survey of correlations for heat transfer and pressure drop for evaporation and condensation in plate heat exchangers, Int. J. Refrig. 65 (2016) 12–26. doi:10.1016/j.ijrefrig.2011.10.018.

[166] E.W. Lemmon, M.L. Huber, M.O. McLinden, NIST reference fluid thermodynamic and transport properties– REFPROP., (2013). https://www.nist.gov/programs-projects/reference-fluid-thermodynamic-and-transport-properties-database-refprop.

[167] N. Jain, A.G. Alleyne, Thermodynamics-based optimization and control of vapor-compression cycle operation:Optimization criteria, in: Am. Control Conf., San Francisco,

2011: pp. 1352–1357. doi:10.1115/DSCC2011-6088.

[168] L.S. Larsen, C. Thybo, Potential energy savings in refrigeration systems using optimal set-points, in: EEE Int. Conf. Control Appl., 2004: pp. 701–704. doi:10.1109/cca.2004.1387295.

[169] M. Salazar, F. Méndez, PID control for a single-stage transcritical CO 2 refrigeration cycle, Appl. Therm. Eng. 67 (2014) 429–438.

[170] Y.A. Çengel, M.A. Boles, Thermodynamics an Engineering Approach, 6th ed., 2011.

[171] Cecil L. Smith, ADVANCED PROCESS CONTROL Beyond Single-Loop Control, John Wiley & Sons, Inc. All, New Jersey, 2010.

[172] K.T. Atta, A. Johansson, T. Gustafsson, Extremum seeking control based on phasor estimation, Syst. Control Lett. 85 (2015) 37–45. doi:10.1016/j.sysconle.2015.08.010.

[173] M. Krsti, Performance Improvement and Limitations in Extremum Seeking Control, Syst. Control Lett. 39 (2000) 313–326.

[174] M. Chioua, B. Srinivasan, M. Guay, M. Perrier, Dependence of the Error in the Optimal Solution of Perturbation-Based Extremum Seeking Methods on the Excitation Frequency, Can. J. Chem. Eng. 85 (2008) 447–453. doi:10.1002/cjce.5450850407.

[175] J.A. Snyman, Practical Mathematical Optimization: An Introduction to Basic Optimization Theory and Classical and New Gradient- Based Algorithms, Springer, Berlin, 2005.

[176] A.A. Girgis, W. Bin Chang, Elham B. Makram, A Digital Recursive Measurement Scheme for On-Line Tracking of Power system Harmonics, IEEE Trans. Power Deliv. 6 (1991) 1153–1160. http://www.ncbi.nlm.nih.gov/pubmed/20952322.

[177] George E. P. Box, G.M. Jenkins, G.C. Reinsel, Time Series Analysis, Forecast and Control, Fourth, A JOHN WILEY AND SONS INC. PUBLICATION, New Jersey, 2008.

[178] G. Gelbert, J.P. Moeck, C.O. Paschereit, R. King, Advanced algorithms for gradient estimation in one- and two-parameter extremum seeking controllers, J. Process Control. 22 (2012) 700–709. doi:10.1016/j.jprocont.2012.01.022.

[179] L. Hardouin, P. Micheau, J. Tartarin, J. Laumonier, An anti-pulsatory device used as an active noise control system in a duct, Acta Acust. United with Acust. 1 (1993) 189–198.

[180] O. Trollberg, B. Carlsson, Elling W. Jacobsen, Extremum seeking control of the CANON process - existence of sub-optimal stationary solutions, J. Process Control. 24 (2014) 348–356.

[181] L. Tan, J. Jean, Digital Signal Processing Fundamentals and Applications, Third, Academic Press, 2019.

[182] E. Narimani, M. Sorin, P. Micheau, Hakim Nesreddine, Dynamic modeling of an R245fa ejector based refrigeration system, Int. J. Refrig. In press (2019).

[183] Bonnans J. Frédéric, J.C. Gilbert, Numerical optimization: Theoretical and practical aspects, Universite, Springer-Verlag, Berlin, 2006. doi:10.1007/978-3-540-35447-5.

[184] A. Mordecai, Nonlinear Programming: Analysis and Methods, Dover Publishing, 2003.